

# **FOURIER ACOUSTICS**

---

## **Sound Radiation and Nearfield Acoustical Holography**

Earl G. Williams  
Naval Research Laboratory  
Washington, D.C.



**ACADEMIC PRESS**  
San Diego London Boston New York  
Sydney Tokyo Toronto

This book is printed on acid-free paper

Copyright ©1999, by  
ACADEMIC PRESS

*All Rights Reserved*

No part of this publication may be reproduced or transmitted in any form  
or by any means, electronic or mechanical, including photocopy,  
recording, or any information storage and retrieval system,  
without permission in writing from the publisher

ISNG 0-12-753960-3

ACADEMIC PRESS  
24-28 Oval Road  
LONDON NW1 7DX  
<http://www.hbuk.co.uk/ap/>

ACADEMIC PRESS  
525 B Street, Suite 1900, San Diego,  
California 92101-4495, USA  
<http://www.apnet.com>

A catalogue record for this book is available from the British Library

Printed in the United Kingdom at the University Press, Cambridge  
99 00 01 02 03 04 CU 9 8 7 6 5 4 3 2 1

# Contents

<i>Preface</i>	<i>xi</i>
<b>1 Fourier Transforms &amp; Special Functions</b>	<b>1</b>
1.1 Introduction . . . . .	1
1.2 The Fourier Transform . . . . .	1
1.3 Fourier Series . . . . .	4
1.4 Fourier–Bessel (Hankel) Transforms . . . . .	5
1.5 The Dirac Delta Function . . . . .	6
1.6 The Rectangle Function . . . . .	7
1.7 The Comb Function . . . . .	8
1.8 Continuous Fourier Transform and the DFT . . . . .	8
1.8.1 Discretization of the Fourier Transform . . . . .	9
1.8.2 Discretization of the Inverse Fourier Transform . . . . .	11
1.8.3 Circumferential Transforms: Fourier Series . . . . .	12
Problems . . . . .	13
<b>2 Plane Waves</b>	<b>15</b>
2.1 Introduction . . . . .	15
2.2 The Wave Equation and Euler’s Equation . . . . .	15
2.3 Instantaneous Acoustic Intensity . . . . .	17
2.4 Steady State . . . . .	18
2.5 Time Averaged Acoustic Intensity . . . . .	19
2.6 Plane Wave Expansion . . . . .	20
2.6.1 Introduction . . . . .	20
2.6.2 Plane Waves . . . . .	21
2.6.3 Evanescent Waves . . . . .	24
2.7 Infinite Plate Vibrating in a Normal Mode . . . . .	26
2.8 Wavenumber Space: $k$ -space . . . . .	27
2.9 The Angular Spectrum: Fourier Acoustics . . . . .	31
2.9.1 Wave Field Extrapolation . . . . .	33
2.10 Derivation of Rayleigh’s Integrals . . . . .	34
2.10.1 The Velocity Propagator . . . . .	37
2.11 Farfield Radiation: Planar Sources . . . . .	38
2.11.1 Vibrators with Circular Symmetry . . . . .	40

2.11.2 Ewald Sphere Construction . . . . .	41
2.11.3 A Baffled Square Piston . . . . .	43
2.11.4 Baffled Square Plate with Traveling Wave . . . . .	46
2.11.5 Baffled Circular Piston . . . . .	48
2.11.6 First Product Theorem for Arrays . . . . .	49
2.12 Radiated Power . . . . .	52
2.12.1 Low Frequency Expansion . . . . .	55
2.13 Vibration & Radiation: Infinite Point-driven Plate . . . . .	56
2.13.1 Farfield Radiation . . . . .	60
2.14 Vibration & Radiation: Finite, Simply Supported Plate . . . . .	62
2.14.1 Rectangular Plate with Fluid Loading . . . . .	67
2.14.2 Radiation from Rectangular Plates: Radiation Impedance and Efficiency . . . . .	67
2.15 Supersonic Intensity . . . . .	77
2.15.1 Supersonic Intensity for a Point Source . . . . .	78
2.15.2 Supersonic Intensity of a Mode of a Simply Supported Plate . . . . .	81
Problems . . . . .	83
<b>3 The Inverse Problem: Planar NAH</b>	<b>89</b>
3.1 Introduction . . . . .	89
3.2 Overview of the Theory . . . . .	90
3.3 Presentation of Theory for a One-Dimensional Radiator . . . . .	91
3.4 Ill Conditioning Due to Measurement Noise . . . . .	93
3.5 The $k$ -space Filter . . . . .	94
3.5.1 Examples . . . . .	95
3.6 Modification of the Filter Shape . . . . .	97
3.7 Measurement Noise and the Standoff Distance . . . . .	98
3.8 Determination of the $k$ -space Filter . . . . .	100
3.9 Finite Measurement Aperture Effects . . . . .	103
3.10 Discretization and Aliasing . . . . .	105
3.11 Use of the DFT to Solve the Holography Equation . . . . .	107
3.12 Reconstruction of Other Quantities . . . . .	112
3.12.1 Time Domain . . . . .	113
Problems . . . . .	113
<b>4 Cylindrical Waves</b>	<b>115</b>
4.1 Introduction . . . . .	115
4.2 The Wave Equation . . . . .	115
4.2.1 Bessel Functions . . . . .	117
4.3 General Solution . . . . .	121
4.3.1 The Interior and Exterior Problems . . . . .	123
4.4 The Helical Wave Spectrum: Fourier Acoustics . . . . .	125
4.4.1 Evanescent Waves . . . . .	129
4.4.2 The Relationship Between Helical Wave Velocity and Pressure . . . . .	132
4.5 The Rayleigh-like Integrals . . . . .	133

4.5.1	Radiation from an infinite length cylinder with an arbitrary surface velocity distribution independent of $z$ . . . . .	134
4.5.2	Radiation from Infinite Cylinder with Standing Wave . . . . .	136
4.6	Farfield Radiation - Cylindrical Sources . . . . .	137
4.6.1	Stationary Phase Approximation . . . . .	137
4.6.2	Farfield of a General Velocity Distribution and $k$ -space . . . . .	140
4.6.3	Piston in a Cylindrical Baffle . . . . .	144
4.6.4	Radiation from a Confined Helical Wave in a Cylindrical Baffle . . . . .	146
4.7	Radiated Power . . . . .	147
Problems	. . . . .	148
<b>5</b>	<b>The Inverse Problem: Cylindrical NAH</b>	<b>149</b>
5.1	Introduction . . . . .	149
5.2	Overview of the Inverse Problem . . . . .	149
5.2.1	Resolution of the Reconstructed Image . . . . .	152
5.2.2	The $k$ -space Filter . . . . .	153
5.3	Computer Implementation of NAH . . . . .	154
5.3.1	Use of the Fast Fourier Transform (FFT) . . . . .	154
5.3.2	Errors Due to Discretization and Finite Scan Length . . . . .	156
5.4	Experimental Results . . . . .	160
5.4.1	Scanning Control and Data Acquisition . . . . .	160
5.4.2	Experimental Parameters . . . . .	160
5.4.3	Comparison to Other Techniques: Two-hydrophone Versus Cylindrical NAH . . . . .	162
5.4.4	Pressure, Velocity and Vector Intensity Reconstructions . . . . .	164
5.4.5	Comparisons with a Surface Accelerometer . . . . .	176
5.4.6	Helical Wave Spectrum Examples . . . . .	179
Problems	. . . . .	181
<b>6</b>	<b>Spherical Waves</b>	<b>183</b>
6.1	Introduction . . . . .	183
6.2	The Wave Equation . . . . .	183
6.3	The Angle Functions . . . . .	186
6.3.1	Legendre Polynomials . . . . .	186
6.3.2	Associated Legendre Functions . . . . .	187
6.3.3	Spherical Harmonics . . . . .	190
6.4	Radial Functions . . . . .	193
6.4.1	Spherical Bessel Functions . . . . .	193
6.5	Multipoles . . . . .	197
6.5.1	Monopoles . . . . .	198
6.5.2	Dipoles . . . . .	199
6.5.3	Quadrupoles . . . . .	202
6.6	Spherical Harmonic Directivity Patterns . . . . .	204
6.7	General Solution for Exterior Problems . . . . .	206
6.7.1	Spherical Wave Spectrum . . . . .	207
6.7.2	The Relationship Between Velocity and Pressure Spectra . . . . .	208

6.7.3	Evanescence Waves . . . . .	209
6.7.4	Boundary Value Problem with Specified Radial Velocity . . . . .	210
6.7.5	The Rayleigh-like Integrals . . . . .	210
6.7.6	Radiated Power . . . . .	211
6.7.7	Farfield Pressure . . . . .	211
6.7.8	Radiation from a Pulsating Sphere . . . . .	213
6.7.9	General Axisymmetric Source . . . . .	213
6.7.10	Circular Piston in a Spherical Baffle . . . . .	214
6.7.11	Point Source on a Baffle . . . . .	216
6.8	General Solution for Interior Problems . . . . .	217
6.8.1	Radial Surface Velocity Specified . . . . .	218
6.8.2	Pulsating Sphere . . . . .	219
6.9	Transient Radiation - Exterior Problems . . . . .	221
6.9.1	Radiation from an Impulsively Moving Sphere . . . . .	222
6.10	Scattering from Spheres . . . . .	224
6.10.1	Formulation . . . . .	224
6.10.2	Scattering from a Pressure Release Sphere . . . . .	227
6.10.3	Scattering from a Rigid Sphere . . . . .	228
6.10.4	Scattering from an Elastic Body . . . . .	231
	Problems . . . . .	232
<b>7</b>	<b>Spherical NAH</b>	<b>235</b>
7.1	Introduction . . . . .	235
7.2	Formulation of the Inverse Problem - Exterior Domain . . . . .	236
7.2.1	Tangential Components of Velocity . . . . .	237
7.2.2	Evanescence Spherical Waves . . . . .	238
7.3	Interior NAH . . . . .	238
7.3.1	Evanescence Spherical Waves . . . . .	238
7.3.2	Effect of Measurement Noise . . . . .	239
7.3.3	Plane Wave Example . . . . .	243
7.4	Scattering Nearfield Holography . . . . .	245
7.4.1	The Dual Surface Approach . . . . .	245
7.4.2	Holography Using an Intensity Probe . . . . .	248
	Problems . . . . .	249
<b>8</b>	<b>Green Functions &amp; the Helmholtz Integral</b>	<b>251</b>
8.1	Introduction . . . . .	251
8.2	Green's Theorem . . . . .	251
8.3	The Interior Helmholtz Integral Equation . . . . .	252
8.3.1	Example with Sphere . . . . .	257
8.4	HIE for Radiation Problems (Exterior Domain) . . . . .	260
8.5	HIE for Scattering Problems . . . . .	262
8.6	Green Functions & the Inhomogeneous Wave Equation . . . . .	264
8.6.1	Two-dimensional Free Space Green Function . . . . .	265
8.6.2	Conversion from Three Dimensions to Two Dimensions . . . . .	266
8.7	Simple Source Formulation . . . . .	267

8.7.1 Example . . . . .	270
8.8 The Dirichlet and Neumann Green Functions . . . . .	272
8.8.1 The Interior Neumann Green Function for the Sphere . . . . .	273
8.8.2 Equivalence to Scattering from a Point Source . . . . .	274
8.8.3 Neumann and Dirichlet Green Functions for a Plane . . . . .	275
8.8.4 Neumann Green Function for the Exterior Problem on a Sphere	277
8.9 Construction by Eigenfunction Expansion . . . . .	277
8.9.1 Example: Cylindrical Cavity . . . . .	279
8.10 Evanescent Neumann & Dirichlet Green Functions . . . . .	281
8.10.1 Cylindrical Cavity . . . . .	282
8.10.2 Forbidden Frequencies . . . . .	287
8.10.3 Interior Evanescent Neumann Green Function for a Cylindrical Cavity . . . . .	288
8.11 Arbitrarily Shaped Bodies . . . . .	288
8.11.1 The External Problem . . . . .	288
8.12 Conformal NAH for Arbitrary Geometry . . . . .	291
Problems . . . . .	293
<b>Index</b>	<b>296</b>

# Preface

This book is intended to serve both as a textbook and as a reference book. As a textbook it would be best suited for a graduate level course. In fact the book grew out of class notes written for a full year graduate course in radiation and scattering taught at The Catholic University of America. The reader need not have a background in acoustics, however. All of the necessary equations and concepts are included in an effort to make the text self-contained. It is assumed that the reader has good mathematical skills, especially a firm grounding in calculus, a knowledge of differential equations and a familiarity with the Fourier transform. Although an understanding of Fourier transforms is crucial, all the needed basic theorems are presented here, some with proof, some without. In fact, Chapter 1 covers a review of generalized functions, Fourier transforms, Fourier series and the discrete Fourier transform. Problems are included at the end of each chapter that test the material presented and provide additional concepts and theory.

How is this book different from the many books available in the field of acoustics? After thirty years of working in basic research in vibration, radiation and scattering of sound I have built my knowledge base not only from the standard acoustics textbooks, but also to a large extent from texts in other fields such as electromagnetism and optics. The integration of the materials from these different fields into my own research has led to a great deal of success. I hope that sharing this knowledge base will bring the reader a similar bonanza.

Chapter 2 begins with an overview of the basic and most important (at least for this book) equations of acoustics. The rest of the chapter discusses plane waves and how they can be used to derive some important theories of vibration and radiation. The initial material is presented quite simply, with illustrations to demonstrate the very physical concepts of plane and evanescent waves. Evanescent waves are emphasized, since they are rarely discussed in other books and because they are so important in the realm of underwater, structural acoustics. Expansions of plane and evanescent waves lead to the most important concept of the book: Fourier acoustics and the angular spectrum. The angular spectrum is used to derive some very powerful tools for the acoustician: the Rayleigh integrals, the Ewald sphere construction, plate radiation and supersonic intensity.

A similar approach is taken in Chapter 4 which deals with wave expansions in cylindrical coordinates and in Chapter 6 which presents spherical wave expansions. Thus some of the important theories discussed for plane waves in Chapter 2 are extended

to cylindrical and spherical coordinates. Additionally, spherical coordinates present an excellent forum for some additional concepts such as multipoles, transient radiation and scattering from spheres to be introduced. These concepts round out Chapter 6.

Although these chapters lead to some higher mathematical functions, such as Bessel functions and spherical harmonics, it is assumed the reader is not familiar with them, and thus they are discussed and plotted in great detail. This is done with all of the higher mathematical functions found in this book. I have too often found scientists somewhat timid when it comes to working with higher level functions, and thus have made a conscious effort here to emphasize their details, especially with visual help. Throughout my own research I have found that an essential ingredient for success has been mastering the mathematics and the mathematical functions presented here. I have attempted to be rigorous whenever possible, and precise in the symbolic conventions.

The use of the Fourier transform and Fourier series in the analysis in the three geometries presented in Chapters 2, 4 and 6 motivated the subtitle of the book, Fourier Acoustics.

Chapter 8 provides a detailed look at the Helmholtz integral equation (HIE), an essential tool for anyone working in acoustics. The HIE is truly a modern and popular tool, to which the many commercial computer codes predicting vibration and radiation on the market will attest. Detailed derivations of the HIE are presented for both interior and exterior radiation problems as well as the scattering problem. This chapter also presents Green functions in depth, providing formulas not usually found in acoustics texts. For example, the evanescent Green function is introduced. Dirichlet and Neumann Green functions are presented for various geometries which simplify the Helmholtz integral equation.

Now to explain Chapters 3, 5, 7 and the last section of Chapter 8. This book is aimed at both the theoretician and the experimentalist, although it is basically a theoretical text. My early background in experimental acoustics, coupled with the desire to understand in detail the physics of vibration and radiation of sound, led to the invention and development of more illuminating and more sophisticated experimental techniques, especially nearfield acoustical holography (NAH). NAH provides a solution to an inverse problem, backtracking the sound field in time and space. It requires mastery of theoretical concepts and mathematical methods (all presented in this book) for its successful implementation. Furthermore, this mastery is also necessary for the interpretation and understanding of the experimental results. It is the synergism between theory and experiment that gave birth to the materials presented in this book. The extraordinary power of the NAH technique has been proven by many researchers throughout the world. However, this is the first book presenting NAH in detail, including all of the basic theory needed to implement it not only in planar coordinates but also in other geometries. As Fourier optics is to optical holography, Fourier acoustics is to nearfield acoustical holography.

NAH is discussed in Chapters 3, 5, 7 and in the last section of Chapter 8, presenting the technique in planar, cylindrical and spherical coordinate systems and finally for an arbitrary geometry, respectively. The implementation of NAH is discussed thoroughly so that the reader has all the necessary information to apply NAH in his own work, if he or she should so desire. To demonstrate the power of NAH, actual experimental

results are shown from my own research for the cylindrical case.

Chapters 2, 4, 6 and 8 are completely self-consistent, that is, they do not rely on the NAH chapters, Chapters 3, 5 and 7, in any way. Thus, for the reader not interested in inverse problems, these latter chapters can be skipped without compromising the understanding of any of the material in the rest of the book. The inverse, however, is not true. Chapters 3, 5 and 7 rely heavily on the material in Chapters 2, 4 and 6.

I am indebted to many who have inspired me along the way, beginning with my PhD advisor at The Pennsylvania State University, Eugen Skudrzyk. Many enlightening discussions with Julian Maynard and Dean Aires followed in my postdoctoral work there. However, I am most indebted to an incredible research institution, the Naval Research Laboratory, which has allowed me to grow and mature through exciting and unperturbed basic research for the last sixteen years. This would not have been possible without the incredible support over these years of Joseph Bucaro, branch head, who also planted the idea and encouraged me to write a book on my work. And finally this work would have been possible without the support of a brilliant experimentalist, Brian Houston.

Great thanks go to my dedicated reviewers. To Joseph Kasper, who took such a serious interest and improved the work with his comments. To a close colleague, Anthony Romano, who also provided invaluable reviewing. To all my inquisitive students who sat through my lectures which formed the foundation of this book. And finally to my wonderful wife, Virginia, who has supported me throughout this task and who helped proofread the manuscript.

Dr. Earl G. Williams  
Naval Research Laboratory  
Washington D.C.  
1998

# Chapter 1

# Fourier Transforms & Special Functions

## 1.1 Introduction

At the heart of Fourier acoustics is the Fourier transform which includes the concepts of the Fourier series and the Hankel transform. We present in this chapter much of the prerequisite mathematics needed to understand the concepts presented in this book. Special functions, like the Dirac delta function, are crucial and provide an elegant shorthand in the mathematics. The rectangle and comb functions are invaluable in understanding the formulation of nearfield acoustical holography, especially in regard to discretization of the formulation for coding on a computer. Essential in this discretization is the relationship between the DFT (discrete Fourier transform) and the integral (continuous) Fourier transform.

## 1.2 The Fourier Transform

The Fourier transform,  $F(k_x)$  of a function  $f(x)$  throughout this work will be defined as

$$F(k_x) = \int_{-\infty}^{\infty} f(x)e^{-ik_x x} dx. \quad (1.1)$$

The following shorthand notation will be useful. Let  $\mathcal{F}_x$  represent the Fourier transform operator so that Eq. (1.1) becomes

$$\mathcal{F}_x[f(x)] \equiv F(k_x). \quad (1.2)$$

In this book we will use symbol  $\equiv$  to mean ‘definition of’ to differentiate from an equality defined with  $=$ . The inverse transform corresponding to Eq. (1.1) is

$$f(x) = \frac{1}{2\pi} \int_{-\infty}^{\infty} F(k_x)e^{ik_x x} dk_x, \quad (1.3)$$

and the shorthand notation for this equation is

$$\mathcal{F}_x^{-1}[F(k_x)] \equiv f(x). \quad (1.4)$$

Equation (1.3) is verified by inserting it into Eq. (1.1) and using the delta function relation, Eq. (1.36), written as

$$\delta(k_x - k'_x) = \frac{1}{2\pi} \int_{-\infty}^{\infty} e^{i(k'_x - k_x)x} dx. \quad (1.5)$$

Thus

$$F(k_x) = \frac{1}{2\pi} \int_{-\infty}^{\infty} dk'_x F(k'_x) \int_{-\infty}^{\infty} e^{i(k'_x - k_x)x} dx = F(k_x).$$

The spatial transform pair given in Eq. (1.1) and Eq. (1.3) is the counterpart to the time-frequency pair:

$$F(\omega) = \int_{-\infty}^{\infty} f(t) e^{i\omega t} dt \quad (1.6)$$

and

$$f(t) = \frac{1}{2\pi} \int_{-\infty}^{\infty} F(\omega) e^{-i\omega t} d\omega. \quad (1.7)$$

Notice a subtle difference, however. The sign of the exponential term is reversed. This is necessary, as will be discussed in Chapter 2, to retain the meaning of a plane wave given by  $\exp(i(k_x x + k_y y + k_z z - \omega t))$ . Thus a function of space and time when expanded with the inverse transforms is

$$f(x, t) = \frac{1}{4\pi^2} \int_{-\infty}^{\infty} \int_{-\infty}^{\infty} F(k_x, \omega) e^{ik_x x} e^{-i\omega t} dk_x d\omega. \quad (1.8)$$

It is simple to determine the Fourier transform of  $\frac{\partial f(x)}{\partial x}$  by taking the partial derivative of Eq. (1.3),

$$\frac{\partial f(x)}{\partial x} = \frac{1}{2\pi} \int_{-\infty}^{\infty} ik_x F(k_x) e^{ik_x x} dk_x \quad (1.9)$$

or

$$\frac{\partial f(x)}{\partial x} = \mathcal{F}_x^{-1}[ik_x F(k_x)],$$

from which we see, in view of Eq. (1.1), that

$$\mathcal{F}_x \left[ \frac{\partial f(x)}{\partial x} \right] = ik_x F(k_x). \quad (1.10)$$

There are several important theorems regarding the Fourier transform which we need to review.

- The shift theorem states that

$$\int_{-\infty}^{\infty} f(x - x') e^{-ik_x x} dx = F(k_x) e^{-ik_x x'}. \quad (1.11)$$

This theorem is easily proven by a change of variables.

- The convolution theorem is

$$\int_{-\infty}^{\infty} \left[ \int_{-\infty}^{\infty} f(x - x') g(x') dx' \right] e^{-ik_x x} dx = F(k_x) G(k_x). \quad (1.12)$$

Using the shift theorem the latter is proven:

$$\begin{aligned} & \int_{-\infty}^{\infty} \left[ \int_{-\infty}^{\infty} f(x - x') g(x') dx' \right] e^{-ik_x x} dx \\ &= \int_{-\infty}^{\infty} \left[ \int_{-\infty}^{\infty} f(x - x') e^{-ik_x x} dx \right] g(x') dx' \\ &= \int_{-\infty}^{\infty} \left[ F(k_x) e^{-ik_x x'} \right] g(x') dx' \\ &= F(k_x) \int_{-\infty}^{\infty} g(x') e^{-ik_x x'} dx' \\ &= F(k_x) G(k_x). \end{aligned}$$

In shorthand notion the convolution theorem is

$$\mathcal{F}_x [f(x) * g(x)] = F(k_x) G(k_x),$$

where the asterisk (\*) denotes convolution:

$$f(x) * g(x) \equiv \int_{-\infty}^{\infty} f(x - x') g(x') dx'. \quad (1.13)$$

Taking the inverse transform of both sides of Eq. (1.12) yields another form of the convolution theorem:

$$\mathcal{F}_x^{-1}[F(k_x) G(k_x)] = f(x) * g(x). \quad (1.14)$$

- The convolution theorem for a product of two spatial functions is

$$\int_{-\infty}^{\infty} f(x) g(x) e^{-ik_x x} dx = \frac{1}{2\pi} \int_{-\infty}^{\infty} F(k'_x) G(k_x - k'_x) dk'_x, \quad (1.15)$$

or

$$\mathcal{F}_x [f(x) g(x)] = \frac{1}{2\pi} F(k_x) * G(k_x).$$

Transition into two dimensions, dealing with functions of two variables, is straightforward. The two-dimensional function  $f(x, y)$  has the two-dimensional Fourier transform  $F(k_x, k_y)$ , satisfying the following relations:

$$F(k_x, k_y) = \int_{-\infty}^{\infty} \int_{-\infty}^{\infty} f(x, y) e^{-i(k_x x + k_y y)} dx dy \quad (1.16)$$

and

$$f(x, y) = \frac{1}{4\pi^2} \int_{-\infty}^{\infty} \int_{-\infty}^{\infty} F(k_x, k_y) e^{i(k_x x + k_y y)} dk_x dk_y. \quad (1.17)$$

If we define a two-dimensional convolution as

$$f(x, y) * * g(x, y) \equiv \int_{-\infty}^{\infty} \int_{-\infty}^{\infty} f(x - x', y - y') g(x', y') dx' dy', \quad (1.18)$$

then the two-dimensional convolution theorem is

$$\mathcal{F}_x \mathcal{F}_y [f(x, y) * * g(x, y)] = F(k_x, k_y) G(k_x, k_y), \quad (1.19)$$

or, equivalently,

$$f(x, y) * * g(x, y) = \mathcal{F}_x^{-1} \mathcal{F}_y^{-1} [F(k_x, k_y) G(k_x, k_y)]. \quad (1.20)$$

Similarly the transform of the product of two spatial functions becomes

$$\begin{aligned} & \int_{-\infty}^{\infty} \int_{-\infty}^{\infty} f(x, y) g(x, y) e^{-i(k_x x + k_y y)} dx dy \\ &= \frac{1}{4\pi^2} \int_{-\infty}^{\infty} \int_{-\infty}^{\infty} F(k'_x, k'_y) G(k_x - k'_x, k_y - k'_y) dk'_x dk'_y, \end{aligned} \quad (1.21)$$

or in shorthand

$$\mathcal{F}_x \mathcal{F}_y [f(x, y) g(x, y)] = \frac{1}{4\pi^2} F(k_x, k_y) * * G(k_x, k_y), \quad (1.22)$$

or, equivalently,

$$f(x, y) g(x, y) = \frac{1}{4\pi^2} \mathcal{F}_x^{-1} \mathcal{F}_y^{-1} [F(k_x, k_y) * * G(k_x, k_y)]. \quad (1.23)$$

### 1.3 Fourier Series

For problems in which the functions have circular symmetry, such as the vibrations of a circular plate or membrane, we will need the following relationships. The circular (polar) coordinates are given by  $\rho$  and  $\phi$ , so that a function  $f(\rho, \phi)$  can be represented in a Fourier series in the  $\phi$  coordinate as

$$f(\rho, \phi) = \sum_{n=-\infty}^{\infty} f_n(\rho) e^{in\phi} \equiv \mathcal{F}_{\phi}^{-1} [f_n(\rho)], \quad (1.24)$$

where the coefficient functions,  $f_n(\rho)$ , are given by

$$f_n(\rho) = \frac{1}{2\pi} \int_0^{2\pi} f(\rho, \phi) e^{-in\phi} d\phi \equiv \mathcal{F}_{\phi} [f(\rho, \phi)]. \quad (1.25)$$

Note that the  $1/2\pi$  could just as easily have been transferred to Eq. (1.24) instead of Eq. (1.25), but we use the former convention throughout this book.

The convolution relationship for Fourier series is easily derived given the completeness relationship<sup>1</sup> for the circumferential harmonics,

$$\frac{1}{2\pi} \sum_{n=-\infty}^{\infty} e^{in\phi} e^{-in\phi'} = \delta(\phi - \phi'). \quad (1.26)$$

Thus given the transforms,  $F_n$  and  $G_n$  of two functions  $f(\phi)$  and  $g(\phi)$ ,

$$F_n = \frac{1}{2\pi} \int_0^{2\pi} f(\phi) e^{-in\phi} d\phi,$$

$$G_n = \frac{1}{2\pi} \int_0^{2\pi} g(\phi) e^{-in\phi} d\phi,$$

we have

$$\begin{aligned} \sum_{n=-\infty}^{\infty} F_n G_n e^{in\phi} &= \frac{1}{4\pi^2} \int \int f(\phi') g(\phi'') \sum_n e^{in(\phi - \phi' - \phi'')} d\phi' d\phi'' \\ &= \frac{1}{2\pi} \int \int f(\phi') g(\phi'') \delta(\phi - \phi' - \phi'') d\phi' d\phi'' \\ &= \frac{1}{2\pi} \int_0^{2\pi} f(\phi') g(\phi - \phi') d\phi' \\ &= \frac{1}{2\pi} \int_0^{2\pi} f(\phi - \phi') g(\phi') d\phi'. \end{aligned} \quad (1.27)$$

We define as usual

$$f(\phi) * g(\phi) = \int_0^{2\pi} f(\phi') g(\phi - \phi') d\phi' = \int_0^{2\pi} f(\phi - \phi') g(\phi') d\phi',$$

so that Eq. (1.27) is

$$\mathcal{F}_\phi^{-1}[F_n G_n] \equiv \sum_{n=-\infty}^{\infty} F_n G_n e^{in\phi} = \frac{1}{2\pi} f(\phi) * g(\phi). \quad (1.28)$$

## 1.4 Fourier-Bessel (Hankel) Transforms

Hankel transforms arise in problems in polar coordinates, and the forward and inverse Hankel transforms are analogous to the forward and inverse Fourier transforms for rectangular coordinates. The  $n$ th order Hankel transform is defined as

$$F_n(k_\rho) = \int_0^\infty f_n(\rho) J_n(k_\rho \rho) \rho d\rho, \quad (1.29)$$

---

<sup>1</sup>For a discussion of completeness see J. D. Jackson (1975). *Classical Electrodynamics*, 2nd ed. Wiley & Sons, pp. 65–68.

where  $k_\rho$  is the transform variable and the relationship to rectangular coordinates is  $\rho = \sqrt{x^2 + y^2}$ .  $J_n$  is a Bessel function described in Section 4.2.1. We use the following shorthand notation for the Hankel transform:

$$\mathcal{B}_n[f_n(\rho)] \equiv F_n(k_\rho). \quad (1.30)$$

To derive the inverse Hankel transform we draw on an important integral for the Dirac delta function valid for all  $n$ :<sup>2</sup>

$$\frac{\delta(\rho - \rho')}{\rho} = \int_0^\infty J_n(k_\rho \rho') J_n(k_\rho \rho) k_\rho dk_\rho. \quad (1.31)$$

Multiply both sides of Eq. (1.29) by  $J_n(k_\rho \rho') k_\rho$  and integrate over  $k_\rho$ :

$$\int_0^\infty F_n(k_\rho) J_n(k_\rho \rho') k_\rho dk_\rho = \int_0^\infty \rho d\rho f_n(\rho) \int_0^\infty J_n(k_\rho \rho') J_n(k_\rho \rho) k_\rho dk_\rho.$$

Making use of Eq. (1.31) yields  $f_n(\rho')$  on the right hand side, and we arrive at (writing  $\rho$  for  $\rho'$ )

$$f_n(\rho) = \int_0^\infty F_n(k_\rho) J_n(k_\rho \rho) k_\rho dk_\rho, \quad (1.32)$$

the  $n$ th order inverse Hankel transform. We will use the shorthand notation

$$\mathcal{B}_n^{-1}[F_n(k_\rho)] \equiv \int_0^\infty F_n(k_\rho) J_n(k_\rho \rho) k_\rho dk_\rho \quad (1.33)$$

and  $\mathcal{B}_n[f_n(\rho)]$  for the forward Hankel transform. Note that Eqs (1.29) and (1.32) define an infinite set of Hankel transforms pairs, one for each order  $n$ . Most common in practice is the 0th order Hankel transform pair:

$$F(k_\rho) = \int_0^\infty f(\rho) J_0(k_\rho \rho) \rho d\rho, \quad (1.34)$$

or  $F[k_\rho] = \mathcal{B}[f(\rho)]$ , and

$$f(\rho) = \int_0^\infty F(k_\rho) J_0(k_\rho \rho) k_\rho dk_\rho, \quad (1.35)$$

or  $f(\rho) = \mathcal{B}^{-1}[F(k_\rho)]$ .

## 1.5 The Dirac Delta Function

The following are important properties of the delta function,  $\delta(x - x_0)$ , drawn from the theory of generalized functions:<sup>3</sup>

<sup>2</sup>J. D. Jackson (1975), *Classical Electrodynamics*, 2nd ed. Wiley & Sons, p. 110.

<sup>3</sup>M. J. Lighthill (1958). *Introduction to Fourier Analysis and Generalised Functions*, Cambridge University Press.

- An important integral relation for the delta function is

$$\delta(x - x_0) = \frac{1}{2\pi} \int_{-\infty}^{\infty} e^{ik_x(x-x_0)} dk_x. \quad (1.36)$$

Other integral relations for the Delta function will be given throughout this book.

- The sifting property is

$$\int_{-\infty}^{\infty} \delta(x - x_0) f(x) dx = f(x_0), \quad (1.37)$$

so that the area under the delta function is unity:

$$\int_{-\infty}^{\infty} \delta(x - x_0) dx = 1. \quad (1.38)$$

Equation (1.36) shows that  $\delta(x - x_0)$  is the inverse Fourier transform of  $e^{-ik_x x_0}$ :

$$\delta(x - x_0) = \mathcal{F}_x^{-1}(e^{-ik_x x_0}).$$

It follows from the forward Fourier transform that

$$\int_{-\infty}^{\infty} \delta(x - x_0) e^{-ik_x x} dx = e^{-ik_x x_0}, \quad (1.39)$$

or

$$e^{-ik_x x_0} = \mathcal{F}_x(\delta(x - x_0)).$$

For finite limits we have

$$\int_{-\infty}^{\xi} \delta(x - x_0) dx = \begin{cases} 0 & \xi < x_0 \\ \frac{1}{2} & \xi = x_0 \\ 1 & \xi > x_0 \end{cases}. \quad (1.40)$$

## 1.6 The Rectangle Function

The rectangle function is defined by

$$\Pi(x/L) = \begin{cases} 1 & |x| < L/2 \\ \frac{1}{2} & |x| = L/2 \\ 0 & |x| > L/2. \end{cases} \quad (1.41)$$

The Fourier transform of the rectangle function is

$$\int_{-\infty}^{\infty} \Pi(x/L) e^{-ik_x x} dx = \frac{L \sin(k_x L/2)}{(k_x L/2)} = L \text{sinc}(k_x L/2), \quad (1.42)$$

where

$$\text{sinc}(x) \equiv \sin(x)/x. \quad (1.43)$$

## 1.7 The Comb Function

The comb function is an infinite series of delta functions, and is defined as

$$\Pi(x/a) \equiv |a| \sum_{n=-\infty}^{\infty} \delta(x - na). \quad (1.44)$$

The Fourier transform of the comb function is another comb function,

$$\int_{-\infty}^{\infty} \Pi(x/a) e^{-ik_x x} dx = a \Pi\left(\frac{k_x}{2\pi/a}\right), \quad (1.45)$$

where, consistent with Eq. (1.44),

$$\Pi\left(\frac{k_x}{2\pi/a}\right) \equiv \frac{2\pi}{|a|} \sum_{n=-\infty}^{\infty} \delta\left(k_x - n(2\pi/a)\right). \quad (1.46)$$

Since  $\Pi(x/a)$  is a periodic function with period  $a$ , it can be expanded in a Fourier series which will lead us to an important formula. Following Eq. (1.24) and defining  $\phi \equiv 2\pi x/a$  and  $f(\rho, \phi) = f(\phi) = \Pi(x/a)$ , then

$$\Pi(x/a) = \sum_{m=-\infty}^{\infty} f_m e^{im(2\pi x/a)},$$

which reflects the period of  $x = a$ . The constants  $f_m$  are obtained from Eq. (1.25) with  $d\phi = \frac{2\pi}{a} dx$ :

$$f_m = \frac{1}{a} \int_0^a \Pi(x/a) e^{-im(2\pi x/a)} dx.$$

The delta functions at each end of the integration range contribute a factor of  $1/2$  (see Eq. (1.40)). Thus  $f_m = 1$ . Inserting this value in Eq. (1.7) leads to the important formula (called the Poisson sum formula)

$$\frac{1}{a} \Pi(x/a) \equiv \sum_{n=-\infty}^{\infty} \delta(x - na) = \frac{1}{a} \sum_{m=-\infty}^{\infty} e^{2\pi imx/a}. \quad (1.47)$$

The comb function is a dimensionless quantity.

## 1.8 Continuous Fourier Transform and the DFT

The discrete Fourier transform (DFT) is defined by the forward and inverse relations

$$F_m = \sum_{q=0}^{N-1} f_q e^{-2\pi i q m / N} \quad (1.48)$$

and

$$f_q = \frac{1}{N} \sum_{m=0}^{N-1} F_m e^{2\pi i q m / N}, \quad (1.49)$$

respectively. The equivalence between Eqs (1.48) and (1.49) can be proven with the following relation, the discrete analog of the Dirac delta function: Eq. (1.36),

$$\frac{1}{N} \sum_{m=0}^{N-1} e^{2\pi i m(q-q')/N} = \delta_{qq'} \quad \text{where } \begin{cases} \delta_{qq'} = 1 & \text{if } q = q' \\ \delta_{qq'} = 0 & \text{otherwise.} \end{cases} \quad (1.50)$$

### 1.8.1 Discretization of the Fourier Transform

We assume for the particular problem of interest that the infinite integral of the continuous Fourier transform can be approximated accurately by the finite integral:

$$F(k) = \int_{-\infty}^{\infty} f(x) e^{-ikx} dx \approx \int_{-L/2}^{L/2} f(x) e^{-ikx} dx. \quad (1.51)$$

(Finite aperture effects will be discussed in Section 3.9.)

This finite integral can be transformed to look like a DFT by using a simple rectangular integration rule to replace the integral with a summation. Discretize the function  $f(x)$  with equally spaced samples separated by  $\Delta x$  and let

$$x = q\Delta x, \quad q = -N/2, -N/2 + 1, \dots, N/2 - 1,$$

where  $N$  is the total number of samples, and the last sample is just shy of the right end of the interval as indicated in Eq. (1.51). We must have that

$$\Delta x = L/N. \quad (1.52)$$

At the same time assume that we are interested in the positive and negative wavenumbers of the continuous Fourier transform, which we also quantize as

$$k = m\Delta k, \quad m = -N/2, -N/2 + 1, \dots, N/2 - 1, \quad (1.53)$$

using the same number of points. In order to obtain a DFT we must restrict  $\Delta k$  to

$$\Delta k = 2\pi/L. \quad (1.54)$$

This is equivalent to one wavelength over the total extent of the aperture  $L$ .

With these relations the rectangular quadrature rule is used to approximate Eq. (1.51) to yield

$$\begin{aligned} F(m\Delta k) &\approx \sum_{q=-N/2}^{N/2-1} f(q\Delta x) e^{-imq\Delta x \Delta k} \Delta x \\ &= \frac{L}{N} \sum_{q=-N/2}^{N/2-1} f(q\Delta x) e^{-i2\pi mq/N}. \end{aligned} \quad (1.55)$$

To arrive at Eq. (1.48) we make the following change of indices:  $m' = m + N/2$  and  $q' = q + N/2$ , so that  $m' = 0, 1, \dots, N - 1$  and  $q' = 0, 1, \dots, N - 1$ , and substitute in Eq. (1.55):

$$\begin{aligned} F((m' - N/2)\Delta k) &\approx \frac{L}{N} \sum_{q'=0}^{N-1} f((q' - N/2)\Delta x) e^{-i2\pi(m'-N/2)(q'-N/2)/N} \\ &= (-1)^{m'} \frac{L}{N} \underbrace{\sum_{q'=0}^{N-1} (-1)^{q'} f((q' - N/2)\Delta x)}_{f_{q'}} e^{-i2\pi m' q'/N} e^{-i\pi N/2}. \end{aligned} \quad (1.56)$$

As indicated by the underbraces, this last expression is equivalent to Eq. (1.48) if we define

$$f_{q'} = (-1)^{q'} f((q' - N/2)\Delta x), \quad (1.57)$$

and

$$F((m' - N/2)\Delta k) = (-1)^{m'} \frac{L}{N} F_{m'}. \quad (1.58)$$

If we choose  $N$  to be a power of 2 (as in a fast Fourier transform (FFT) algorithm), then the term  $e^{-i\pi N/2} = 1$ . (For all practical purposes  $N$  is greater than 2.) Equations (1.57) and (1.58) provide the recipe for using the forward DFT to approximate a forward continuous Fourier transform, Eq. (1.51).

As an example consider the DFT of a rectangle function  $\Pi(x/L)$  with  $N = 8$  shown on the left of Fig. 1.1. On the right is shown the modification necessary to construct the

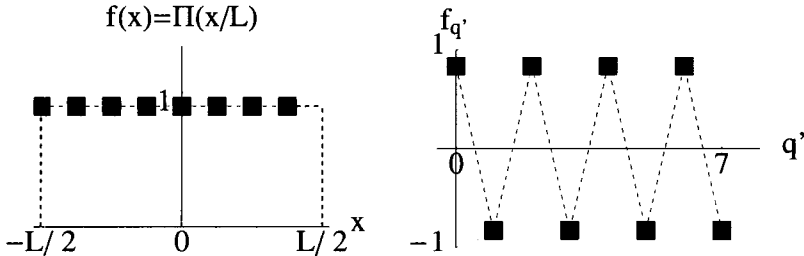


**Figure 1.1:** Left: Sampled version of  $\Pi(x/L)$ , with  $N = 8$ . Right: Modification for the DFT according to Eq. (1.57). Note that  $(-1)^{q'}$  creates the sawtooth effect.

series  $f_{q'}$ . Note the oscillation due to the multiplication by  $(-1)^{q'}$ . The result from the DFT is shown in Fig. 1.2. The left plot results from the FFT algorithm (an optimized coding of the DFT for computations),<sup>4</sup> implementing Eq. (1.48) with  $m' = m = 0, \dots, 7$ . The continuous transform produces the result on the right of the figure, which when sampled at intervals of  $\Delta k = 2\pi/L$  exactly equals the FFT result. One obtains exact agreement, according to the Shannon sampling theorem,<sup>5</sup> when the Fourier transform

<sup>4</sup>E. Oran Brigham (1974). *The Fast Fourier Transform*, Prentice-Hall, N. J.

<sup>5</sup>A. Papoulis (1962). *The Fourier Integral and its Applications*, McGraw-Hill, N.Y., p. 50.

of the function  $f(x)$  is zero above a specific frequency  $k_s$ , that is, when

$$F(k) = 0 \quad \text{for } k \geq |k_s|. \quad (1.59)$$

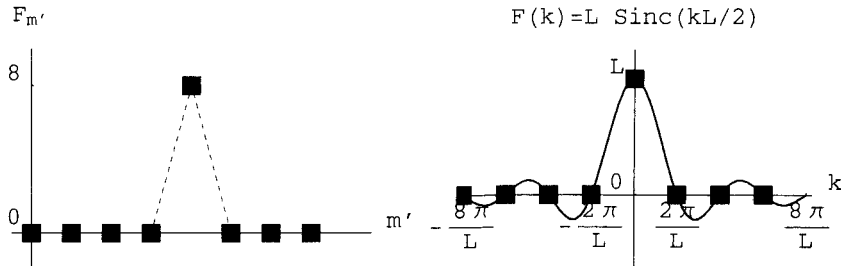


**Figure 1.2:** Left: Result from the FFT. Only point  $m' = 4$  is nonzero. Right: Continuous Fourier transform of the rectangle function with sample interval shown. Since  $\Delta k = 2\pi/L$  then the sinc function is sampled exactly at the zero crossings and the FFT provides an errorless result.

### 1.8.2 Discretization of the Inverse Fourier Transform

Using the identical quantization scheme and derivation, we will obtain the approximation of the continuous inverse Fourier transform using the DFT. Again we assume that the infinite limits can be replaced with finite ones without appreciable error:

$$f(x) = \frac{1}{2\pi} \int_{-\infty}^{\infty} F(k) e^{ikx} dk \approx \frac{1}{2\pi} \int_{-k_m}^{k_m} e^{ikx} dk, \quad (1.60)$$

where  $k_m$  represents the maximum wavenumber provided by Eqs (1.52–1.54),

$$k_m = (N/2)\Delta k = \pi N/L = \pi/\Delta x, \quad (1.61)$$

that is, one wavelength over two spatial samples. Inserting the quantizations given above into Eq. (1.60) leads to

$$\begin{aligned} f(q\Delta x) &\approx \frac{1}{2\pi} \sum_{m=-N/2}^{N/2-1} F(m\Delta k) e^{imq\Delta x \Delta k} \Delta k \\ &= \frac{1}{L} \sum_{m=-N/2}^{N/2-1} F(m\Delta k) e^{i2\pi mq/N}. \end{aligned} \quad (1.62)$$

Making the same change of indices given in the last section in order to obtain the form of the inverse DFT, Eq. (1.49), we obtain

$$\begin{aligned} f((q' - N/2)\Delta x) &\approx \frac{1}{L} \sum_{m'=0}^{N-1} F((m' - N/2)\Delta k) e^{i2\pi(m' - N/2)(q' - N/2)/N} \\ &= (-1)^{q'} \frac{N}{L} \underbrace{\frac{1}{N} \sum_{m'=0}^{N-1} \underbrace{(-1)^{m'} F((m' - N/2)\Delta k)}_{F_{m'}} e^{i2\pi m' q'/N}}_{f_{q'}} e^{i\pi N/2}, \end{aligned}$$

which is related to Eq. (1.49) by equating

$$F_{m'} = (-1)^{m'} F((m' - N/2)\Delta k) \quad (1.63)$$

and (again  $e^{i\pi N/2} = 1$ )

$$f((q' - N/2)\Delta x) = (-1)^{q'} \frac{N}{L} f_{q'}. \quad (1.64)$$

Equations (1.63) and (1.64) provide the recipe for the approximation of the inverse Fourier transform using the DFT.

### 1.8.3 Circumferential Transforms: Fourier Series

The inverse and forward relations which make up the Fourier series are, respectively,

$$f(\phi) = \sum_{m=-\infty}^{\infty} F(m) e^{im\phi} \quad (1.65)$$

and

$$F(m) = \frac{1}{2\pi} \int_{-\pi}^{\pi} f(\phi) e^{-im\phi} d\phi, \quad (1.66)$$

where  $f(\phi)$  is a cyclic function with period  $2\pi$ .

Results identical to the Fourier transform discretization are obtained in this case noting that

$$L = 2\pi$$

and  $x \rightarrow \phi$  (where  $-\pi \leq \phi \leq \pi$ ),  $k \rightarrow m$ ,  $\Delta k = 1$ ,  $\Delta x = 2\pi/N$ , except that the  $\frac{1}{2\pi}$  normalization is included with the forward transform instead of the inverse, which leads to an extra factor of  $2\pi$  dividing Eq. (1.57) and the same factor multiplying Eq. (1.64).

## Problems

**1.1** Carry out the integration

$$\int_{-\infty}^{\infty} f(t') \delta(t - t' + t_0) dt'.$$

**1.2** If  $\mathcal{F}_x[f(x)] = J_1(\beta k_x)$ , then what is  $\mathcal{F}_x[f(x-a)]$ ?

**1.3** Let the complex function  $f(x)$  be written as a sum of an even  $e(x)$  and an odd function  $o(x)$ . Prove that if  $F(k_x) = E(k_x) + O(k_x)$  is the Fourier transform of  $f(x)$  with even and odd parts given by  $E$  and  $O$ , respectively, then

$$E(k_x) = \mathcal{F}_x[e(x)].$$

Note that  $e^{-ik_x x}$  can be written as a sum of an even and an odd function in  $x$ .

**1.4** Write the convolution theorem for  $\frac{1}{2\pi} \int_{-\infty}^{\infty} F(k_x)G(k_x)H(k_x)e^{ik_x x} dk_x$ .

**1.5** The zero-order Hankel transform and its inverse are given by

$$F(k_\rho) = \mathcal{B}[f(\rho)] \equiv \int_0^\infty f(\rho) J_0(k_\rho \rho) \rho d\rho$$

and

$$f(\rho) = \int_0^\infty F(k_\rho) J_0(k_\rho \rho) k_\rho dk_\rho.$$

Prove the following Hankel transform relationships:

(a) If  $f(\rho) = \delta(\rho - \rho_0)$  and  $\rho_0 \geq 0$ , then

$$\mathcal{B}[f(\rho)] = \rho_0 J_0(k_\rho \rho_0).$$

(b) If  $f(\rho) = 1$  for  $0 \leq a \leq \rho \leq 1$  and zero otherwise, then

$$\mathcal{B}[f(\rho)] \propto \frac{J_1(k_\rho) - a J_1(k_\rho a)}{k_\rho}.$$

(c) If  $\mathcal{B}[f(\rho)] = F(k_\rho)$  then

$$\mathcal{B}[f(ak_\rho)] = F(k_\rho/a)/a^2.$$

# Chapter 2

## Plane Waves

### 2.1 Introduction

In this chapter we present the foundations of Fourier acoustics—plane wave expansions. This material is presented in depth to provide a firm foundation for the rest of the book, introducing important concepts like wavenumber space and the extrapolation of wavefields from one surface to another. Fourier acoustics is used to derive some famous tools for the radiation from planar sources: the Rayleigh integrals, the Ewald sphere construction of farfield radiation, the first product theorem for arrays, vibrating plate radiation, and radiation classification theory. Finally, a new tool called supersonic intensity is introduced which is useful in locating acoustic sources on vibrating structures. We begin the chapter with a review of some fundamentals: the wave equation, Euler's equation, and the concept of acoustic intensity.

### 2.2 The Wave Equation and Euler's Equation

Let  $p(x, y, z, t)$  be an infinitesimal variation of acoustic pressure from its equilibrium value which satisfies the acoustic wave equation

$$\nabla^2 p - \frac{1}{c^2} \frac{\partial^2 p}{\partial t^2} = 0 \quad (2.1)$$

for a homogeneous fluid with no viscosity.  $c$  is a constant and refers to the speed of sound in the medium. At 20°C  $c = 343$  m/s in air and  $c = 1481$  m/s in water. The right hand side of Eq. (2.1) indicates that there are no sources in the volume in which the equation is valid. In Cartesian coordinates

$$\nabla^2 \equiv \frac{\partial^2}{\partial x^2} + \frac{\partial^2}{\partial y^2} + \frac{\partial^2}{\partial z^2}.$$

A second equation which will be used throughout this book is called Euler's equation,

$$\rho_0 \frac{\partial \vec{v}}{\partial t} = -\vec{\nabla} p, \quad (2.2)$$

where  $\vec{v}$  (Greek letter upsilon) represents the velocity vector with components  $\dot{u}$ ,  $\dot{v}$ ,  $\dot{w}$ ;

$$\vec{v} = \dot{u}\hat{i} + \dot{v}\hat{j} + \dot{w}\hat{k}, \quad (2.3)$$

where  $\hat{i}$ ,  $\hat{j}$ , and  $\hat{k}$  are the unit vectors in the  $x$ ,  $y$ , and  $z$  directions, respectively, and the gradient is defined in terms of the unit vectors as

$$\vec{\nabla} \equiv \frac{\partial}{\partial x}\hat{i} + \frac{\partial}{\partial y}\hat{j} + \frac{\partial}{\partial z}\hat{k}. \quad (2.4)$$

We use the convention of a dot over a displacement quantity to indicate velocity as is done in Junger and Feit.<sup>1</sup> The displacements in the three coordinate directions are given by  $u$ ,  $v$ , and  $w$ .

The derivation of Eq. (2.2) is useful in developing some understanding of the physical meaning of  $p$  and  $\vec{v}$ . Let us proceed in this direction.

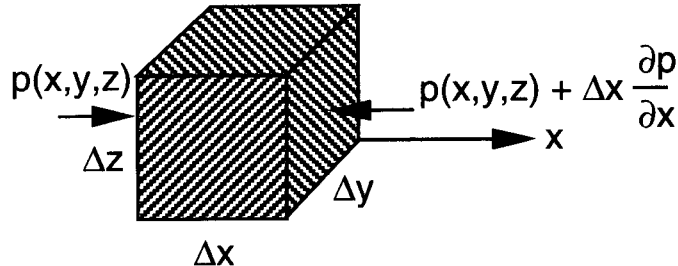


**Figure 2.1:** Infinitesimal volume element to illustrate Euler's equation.

Figure 2.1 shows an infinitesimal volume element of fluid  $\Delta x \Delta y \Delta z$ , with the  $x$  axis as shown. All six faces experience forces due to the pressure  $p$  in the fluid. It is important to realize that pressure is a scalar quantity. There is no direction associated with it. It has units of force per unit area, N/m<sup>2</sup> or Pascals. The following is the convention for pressure,

$$\begin{aligned} p &> 0 \rightarrow \text{Compression} \\ p &< 0 \rightarrow \text{Rarefaction}. \end{aligned}$$

At a specific point in a fluid, a positive pressure indicates that an infinitesimal volume surrounding the point is under compression, and forces are exerted *outward* from this volume. It follows that if the pressure at the left face of the cube in Fig. 2.1 is positive, then a force will be exerted in the positive  $x$  direction of magnitude  $p(x, y, z)\Delta y \Delta z$ . The pressure at the opposite face  $p(x + \Delta x, y, z)$  is exerted in the negative  $x$  direction. We expand  $p(x + \Delta x, y, z)$  in a Taylor series to first order, as shown in the figure. Note that the force arrows indicate the direction of force for positive pressure. Given the directions of force shown, the total force exerted on the volume in the  $x$  direction is

$$(p(x, y, z) - p(x + \Delta x, y, z))\Delta y \Delta z = -\Delta x \Delta y \Delta z \frac{\partial p}{\partial x}.$$

---

<sup>1</sup>M. C. Junger and D. Feit (1986). *Sound, Structures, and Their Interaction*. 2nd ed. MIT Press, Cambridge, MA.

Now we invoke Newton's equation,  $f = ma = m\frac{\partial \dot{u}}{\partial t}$ , where  $f$  is the force,  $m = \rho_0 \Delta x \Delta y \Delta z$  and  $\rho_0$  is the fluid density, yielding

$$\rho_0 \frac{\partial \dot{u}}{\partial t} = -\frac{\partial p}{\partial x}.$$

Carrying out the same analysis in the  $y$  and  $z$  directions yields the following two equations:

$$\rho_0 \frac{\partial \dot{v}}{\partial t} = -\frac{\partial p}{\partial y}$$

and

$$\rho_0 \frac{\partial \dot{w}}{\partial t} = -\frac{\partial p}{\partial z}.$$

We combine the above three equations into one using vectors yielding Eq. (2.2) above, Euler's equation.

## 2.3 Instantaneous Acoustic Intensity

It is critical in the study of acoustics to understand certain energy relationships. Most important is the acoustic intensity vector. In the time domain it is called the instantaneous acoustic intensity and is defined as

$$\vec{I}(t) = p(t)\vec{v}(t), \quad (2.5)$$

with units of energy per unit time (power) per unit area, measured as (joules/s)/m<sup>2</sup> or watts/m<sup>2</sup>.

The acoustic intensity is related to the energy density  $e$  through its divergence,

$$\frac{\partial e}{\partial t} = -\vec{\nabla} \cdot \vec{I}, \quad (2.6)$$

where the divergence is

$$\vec{\nabla} \cdot \vec{I} \equiv \frac{\partial I_x}{\partial x} + \frac{\partial I_y}{\partial y} + \frac{\partial I_z}{\partial z}. \quad (2.7)$$

The energy density is given by

$$e = \frac{1}{2}\rho_0|\vec{v}(t)|^2 + \frac{1}{2}\kappa p(t)^2 \quad (2.8)$$

where  $\kappa$  is the fluid compressibility,

$$\kappa = \frac{1}{\rho_0 c^2}. \quad (2.9)$$

Equation (2.6) expresses the fact that an increase in the energy density at some point in the fluid is indicated by a negative divergence of the acoustic intensity vector; the intensity vectors are pointing into the region of increase in energy density. Figure 2.2 should make this clear.

If we reverse the arrows in Fig. 2.2, a positive divergence results and the energy density at the center must decrease, that is,  $\frac{\partial e}{\partial t} < 0$ . This case represents an apparent source of energy at the center.

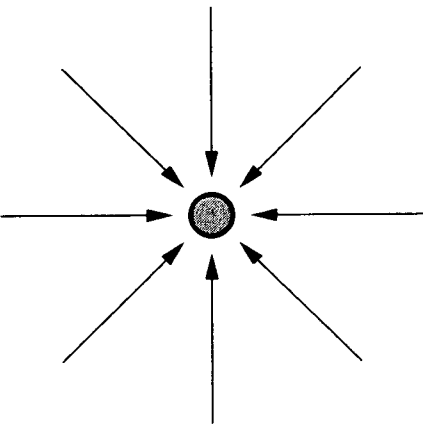


**Figure 2.2:** Illustration of negative divergence of acoustic intensity. The region at the center has an increasing energy density with time, that is, an apparent sink of energy.

## 2.4 Steady State

To consider phenomena in the frequency domain, we obtain the steady state solution through Fourier transforms

$$p(t) = \frac{1}{2\pi} \int_{-\infty}^{\infty} \bar{p}(\omega) e^{-i\omega t} d\omega \quad (2.10)$$

leading to the steady state solution

$$\bar{p}(\omega) = \int_{-\infty}^{\infty} p(t) e^{i\omega t} dt. \quad (2.11)$$

Equation (2.10) can be differentiated with respect to time to yield the important relationship

$$\frac{\partial p(t)}{\partial t} = \frac{1}{2\pi} \int_{-\infty}^{\infty} -i\omega \bar{p}(\omega) e^{-i\omega t} d\omega,$$

so that

$$\mathcal{F}\left(\frac{\partial p(t)}{\partial t}\right) = -i\omega \bar{p}(\omega), \quad (2.12)$$

where the calligraphic letter  $\mathcal{F}$  represents the Fourier transform operation defined in Eq. (2.11).

Equation (2.12) can be used to compute the Fourier transform of the time domain wave equation, Eq. (2.1), yielding the Helmholtz equation

$$\nabla^2 \bar{p} + k^2 \bar{p} = 0, \quad (2.13)$$

where the acoustic wavenumber is  $k = \omega/c$ , the frequency is given by  $2\pi f = \omega$ , and  $\bar{p}$  is the function  $\bar{p}(x, y, z, \omega)$ . For simplicity of notation we drop the bar above the variable. It will be clear from the context of the discussion if the quantity is in the frequency or

in the time domain. The Fourier transform of Euler's equation, Eq. (2.2), becomes, in the frequency domain

$$i\omega\rho_0\vec{v} = \vec{\nabla}p, \quad (2.14)$$

where Eq. (2.12) has been used again for the time derivative.

## 2.5 Time Averaged Acoustic Intensity

Now consider the intensity relationship for steady state fields. This is defined as the average of the instantaneous intensity over a period  $T$ , where  $T = 1/f$  and  $f$  is the excitation frequency:

$$\vec{I}(\omega) = \frac{1}{T} \int_0^T p(t)\vec{v}(t) dt. \quad (2.15)$$

Using complex variable notation this relationship becomes

$$\vec{I}(\omega) = \frac{1}{2} \text{Re}(p(\omega)\vec{v}(\omega)^*), \quad (2.16)$$

where  $*$  stands for complex conjugate and  $\text{Re}$  for the real part. The one-half results from the time average process.  $\vec{I}$  is the average power over one period passing through unit area. For example, the  $x$  component of this flow  $I_x$  represents the power passing through an element of area  $\Delta y \Delta z$ .

Important in this chapter is the radiation from planar radiators. Of particular interest is the power flow crossing an infinite plane. For example, consider the total power crossing the coordinate plane  $z = 0$ , a quantity expressed in watts or joules per second. We use the symbol  $\Pi(\omega)$  to represent the total power in watts crossing the boundary:

$$\Pi(\omega) = \int_{-\infty}^{\infty} \int_{-\infty}^{\infty} I_z(x, y, 0) dx dy. \quad (2.17)$$

If there are no sources in the upper half space, then  $\Pi$  is the total power radiated to the farfield ( $z \rightarrow \infty$ ). Besides the plane at  $z = 0$ , every other plane defined by  $z = z_0$  has the same power passing through it, since there is no absorption in the fluid and there are no sources above the boundary.

The equation of continuity, Eq. (2.6), becomes

$$\frac{1}{T} \int_0^T \frac{\partial e}{\partial t} dt = \frac{e(T) - e(0)}{T} = -\vec{\nabla} \cdot \vec{I}(\omega). \quad (2.18)$$

By the definition of steady state the energy density at time  $T$  is the same as the density at time 0, so that we have

$$\vec{\nabla} \cdot \vec{I}(\omega) = 0. \quad (2.19)$$

This means that in a source-free field the divergence of the time averaged acoustic intensity must always be zero. The only way the intensity field can have a non-zero divergence is if there are sources or sinks of energy within the medium, or losses in the medium.

## 2.6 Plane Wave Expansion

We turn now to plane wave solutions of the wave equation, seeking solutions of the Helmholtz equation, Eq. (2.13), in the frequency domain.

### 2.6.1 Introduction

Our concern in this chapter is with solutions of the wave equation in Cartesian coordinates. These solutions will be useful in the study of sources which are planar (or nearly planar) in geometry such as vibrating plates. We note that Eq. (2.1) is very similar to the equation for a vibrating string:

$$\frac{\partial^2 w}{\partial x^2} - \frac{1}{c_s^2} \frac{\partial^2 w}{\partial t^2} = 0, \quad (2.20)$$

where  $w$  is normal displacement of the string, and  $c_s$  is the wave speed, a constant. A solution to this equation is given by

$$w(x, t) = Ae^{i(k_x x - \omega t)} + Be^{i(-k_x x - \omega t)}, \quad (2.21)$$

where  $A$  and  $B$  are arbitrary constants. For this solution to satisfy Eq. (2.20) we must have

$$k_x = \omega/c_s. \quad (2.22)$$

We introduce the string solution to understand the plane wave solutions of Eq. (2.1). In Eq. (2.21)  $k_x$  is called the wavenumber in the  $x$  direction.

Consider the phase term in Eq. (2.21) given by  $\phi(x, t) = k_x x - \omega t$ . We track the crest of a wave traveling down the string by choosing a constant value of phase and then following it as a function of position and time. The position of the crest, choosing  $\phi = 0$  arbitrarily, is given by  $x = \omega t/k_x = c_s t$ . Thus,  $c_s$  is the velocity of the crest in the positive  $x$  direction and is called the phase velocity of the wave. The solution corresponding to the second term in Eq. (2.21) is a wave traveling in the negative  $x$  direction. At a fixed time the phase repeats over a distance  $\Delta x = \lambda_x$ . Over this distance the phase term in Eq. (2.21) changes by  $2\pi$ , giving  $2\pi = k_x \Delta x = k_x \lambda_x$ , leading to the important relationship

$$k_x = 2\pi/\lambda_x. \quad (2.23)$$

$\lambda_x$  is the wavelength in the  $x$  direction and is the distance over which the phase of the wave changes by  $2\pi$  when time is held constant.

One final note on the reality of Eq. (2.21). Motions of strings and pressure waves in a fluid are never complex quantities, although we represent them with complex numbers. They must always be real, as no microphone or accelerometer provides a complex signal voltage in the process of measurement. To simulate the actual motion of the string, say with a graphics program on a computer, we must choose either the real or the imaginary part of Eq. (2.21). Choosing the real part we would use  $\cos(k_x x - \omega t)$  to represent a wave traveling to the right.

## 2.6.2 Plane Waves

We now consider the general solution of Eq. (2.13), the Helmholtz equation, in three dimensions. Consider the following solution for  $\bar{p}(\omega)$

$$p(\omega) = A(\omega)e^{i(k_x x + k_y y + k_z z)}, \quad (2.24)$$

where  $A(\omega)$  is an arbitrary constant. This equation satisfies Eq. (2.13) as long as

$$k^2 = k_x^2 + k_y^2 + k_z^2. \quad (2.25)$$

Since  $k$  is a constant the three wavenumbers are not independent of one another. We can choose a maximum of two as independent variables, the third being dependent. Throughout this work we will use  $k_z$  as the dependent variable so that

$$k_z^2 = k^2 - k_x^2 - k_y^2.$$

Note that there is no restriction on the values of  $k_x$  and  $k_y$ ; they can extend over all real numbers from  $-\infty$  to  $+\infty$ .

Equation (2.24) represents a plane wave solution to the wave equation, although the time dependence is not indicated. To demonstrate this time dependence we must consider what we mean by a plane wave. It has meaning only for a single frequency, that is, in the steady state. Mathematically, writing the arbitrary constant in Eq. (2.24) as

$$A(\omega) = 2\pi B(\omega)\delta(\omega - \omega_0),$$

then

$$p(\omega) = 2\pi B\delta(\omega - \omega_0)e^{i(k_x x + k_y y + k_z z)}, \quad (2.26)$$

where the delta function expresses the monochromatic nature of the time dependence. To arrive at the plane wave we take the inverse Fourier transform given in Eq. (2.10) above. This yields the final result, a plane wave at the frequency  $\omega_0$ :

$$p(t) = Ae^{i(k_x x + k_y y + k_z z - \omega_0 t)}, \quad (2.27)$$

where  $k = \omega_0/c$ . Now we will study the nature of plane waves in more detail.

Consider the pressure in the infinite  $x, z$  coordinate plane at  $y = 0$ . The phase term is given by (including the time dependent part, but dropping the zero subscript for simplicity)

$$\phi = (k_x x + k_z z - \omega t). \quad (2.28)$$

This term looks like the string expression given in the introduction above if we plot it along each of the coordinate axes. That is, along the  $x$  axis ( $z = 0$ ) the phase expression is  $k_x x - \omega t$  and the wavelength in the  $x$  direction is  $\lambda_x = 2\pi/k_x$ .  $\lambda_x$  is called the trace wavelength in the  $x$  direction and  $k_x$  the trace wavenumber in the  $x$  direction. As the plane wave travels through space, there is a trace wave along the  $x$  axis moving with a phase speed  $c_x = \omega/k_x$ . Similarly along the  $z$  axis the phase speed of the trace wave is  $c_z = \omega/k_z$ . To determine the direction of the plane wave consider Fig. 2.3.

For this example assume that  $k_y = 0$ , that is, there is no variation of pressure in the  $y$  direction. The sinusoidal variation of pressure along the two axes is shown gray scale

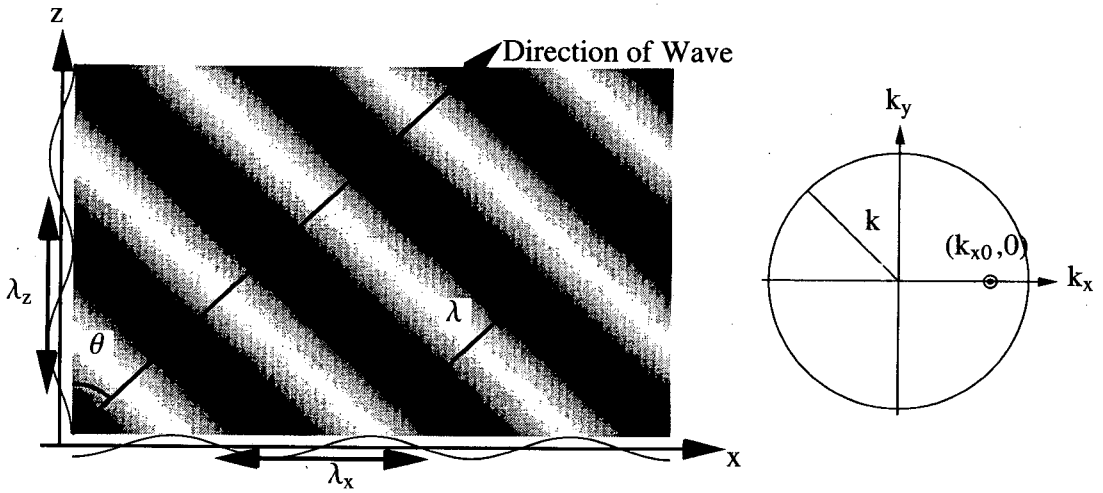


**Figure 2.3:** Plane wave illustration showing trace matching. Snapshot at  $t = 0$ . The insert on the right shows the equivalent  $k$ -space representation. The trace wave is supersonic, and lies within the radiation circle of radius  $k$ .

coded, with white-gray representing positive pressure and black-gray negative pressure. Since pressure must be continuous throughout space (no sources), adjacent regions along the two axes must have the same pressure. These regions are separated by diagonal lines of constant gray scale, as shown, which are called wavefronts. In this example the trace wavelengths in the vertical and horizontal directions are equal;  $k_z = k_{z0} = k_x = k_{x0}$ . This figure must reflect the relationship  $k^2 = k_x^2 + k_z^2$ , where the acoustic wavelength  $\lambda$  is shown along the direction of travel of the wave (perpendicular to the wavefronts; the lines of constant phase). The wave propagates in the direction given by  $\theta$ , as shown in Fig. 2.3. Thus the following must be true:

$$\begin{aligned}
 \lambda_x \sin \theta &= \lambda \\
 \lambda_z \cos \theta &= \lambda \\
 k_x &= k \sin \theta \\
 k_z &= k \cos \theta \\
 k_x^2 + k_z^2 &= k^2.
 \end{aligned} \tag{2.29}$$

The insert on the right in Fig. 2.3 shows a  $k$ -space diagram that displays the wavenumbers which exist in the  $(x, y)$  plane. In this example only one wavenumber exists,  $(k_{x0}, 0)$ , corresponding to a single plane wave. The large circle is called the radiation circle and has a radius  $k$ . In this example we have  $k_{x0} = k_{z0}$  so that  $k_{x0} = k/\sqrt{2}$ , the latter determining the location of the plane wave wavenumber on the  $k$ -space diagram—shown in the small circle in the figure.

If we form the vector  $\vec{k} = k_x \hat{i} + k_z \hat{k}$ , where  $|\vec{k}| = k$ ; then, since  $k_x = k \sin \theta$  and  $k_z = k \cos \theta$ ,  $\vec{k}$  points in the direction of propagation of the plane wave. This result is completely general; the direction of any plane wave is given by  $\vec{k} = k_x \hat{i} + k_y \hat{j} + k_z \hat{k}$ .

Since  $k = \omega/c$  and  $k_x = k \sin \theta$ , then

$$\begin{aligned} c_x &= c/\sin \theta, \\ c_z &= c/\cos \theta. \end{aligned} \quad (2.30)$$

The trace velocities along the coordinate axes are greater than the speed of sound. In fact, when  $\lambda_x \rightarrow \infty$  then  $c_x \rightarrow \infty$  ( $\lambda_x = c_x/f$ ) and the crest of the wave moves at infinite speed along the  $x$  axis. Since both  $c_x$  and  $c_z$  are greater than  $c$ , the trace waves are classified as supersonic waves. Note that nothing (especially energy) actually travels at this speed—we are only looking at the projection of the wave on the coordinate axes as it travels through space.

A plane wave can be represented using condensed notation;

$$e^{i(k_x x + k_y y + k_z z)} = e^{i(\vec{k} \cdot \vec{r})}, \quad (2.31)$$

where  $\vec{r} = x\hat{i} + y\hat{j} + z\hat{k}$  represents the position vector to the observation point in the sound field, and  $\vec{k}$  gives the direction of the wave.

Returning to Fig. 2.3 we can see that as the wave turns towards the normal to the  $(x, y)$  plane ( $\theta = 0$ ), then  $k_x \rightarrow 0$  and  $k_z \rightarrow k$ . This case is illustrated in Fig. 2.4. Here the wavelength along the  $x$  axis is infinite, and the wavefronts are planes parallel to the  $(x, y)$  plane. The  $k$ -space diagram on the right indicates that this plane wave is represented by a point at the origin ( $k_{x0} = 0$ ).

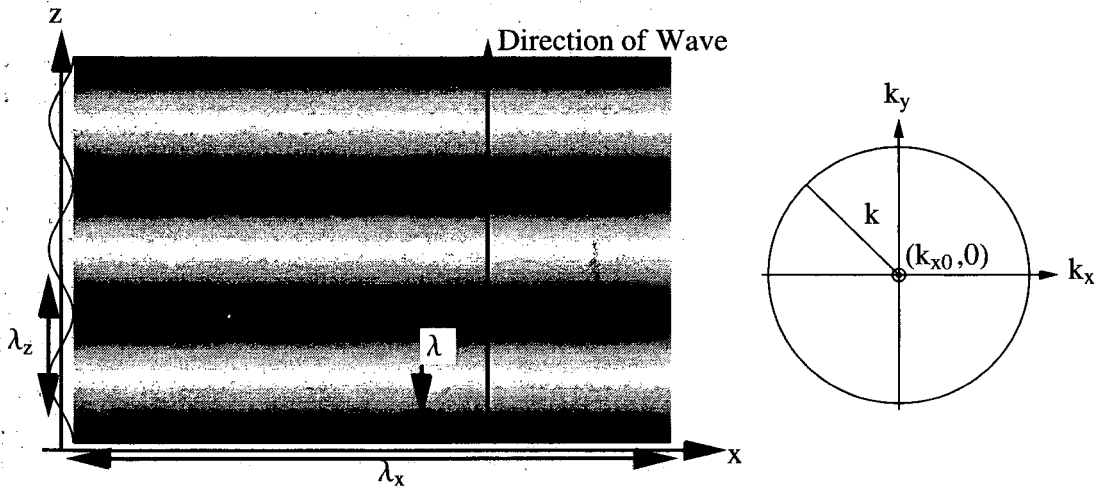


**Figure 2.4:** Plane wave traveling normal to  $x$  axis. In  $k$ -space this wave appears as a dot at the origin, as shown on the right.

Figure 2.5 presents the case in which the wavelength in the vertical direction is infinite. In this case we see that wave propagation is in the  $x$  direction ( $\theta = \pi/2$ ) along the  $x$  axis and  $c_x = c$ . In  $k$ -space this wave is represented by a single dot located on the radiation circle.

Consider now the average intensity vector for plane waves. First we must determine the velocity associated with a plane wave. This is given by inserting Eq. (2.24) into

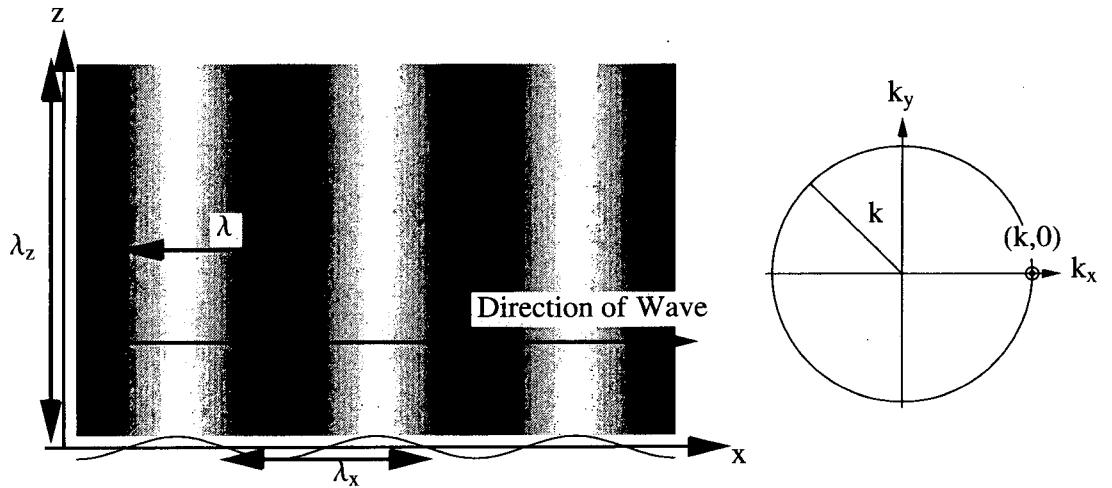


**Figure 2.5:** Plane wave traveling parallel to  $x$  axis, infinite wavelength in the vertical direction. In  $k$ -space the wave falls on the radiation circle as shown.

Eq. (2.14):

$$\vec{v}(\omega) = \frac{1}{\omega\rho_0} (k_x \hat{i} + k_y \hat{j} + k_z \hat{k}) p(\omega). \quad (2.32)$$

Thus Eq. (2.16) yields

$$\vec{I} = \frac{|A|^2}{2\omega\rho_0} (k_x \hat{i} + k_y \hat{j} + k_z \hat{k}). \quad (2.33)$$

Clearly the direction of the power flow is given by the last part of this expression, or

$$\vec{k} = (k_x \hat{i} + k_y \hat{j} + k_z \hat{k}),$$

where the direction of  $\vec{k}$  is the direction of the plane wave and the length of this vector satisfies Eq. (2.25).

### 2.6.3 Evanescent Waves

Figures 2.3 and 2.4 illustrate the conditions for wave propagation away from the  $(x, y)$  plane. In Fig. 2.5 the wave does not propagate away from the  $(x, y)$  plane but travels parallel to it with wavefronts in vertical planes parallel to the  $(y, z)$  plane. Looking again at Eq. (2.25) we have

$$k_z = \pm \sqrt{k^2 - k_x^2 - k_y^2}, \quad (2.34)$$

so that Fig. 2.5 corresponds to the case, since  $k_y = 0$ , where the argument of the square root vanishes ( $k_z = 0$ ). Particle motion is now only in the  $x$  direction.

It is important to realize that the plane wave solution still satisfies the wave equation, Eq. (2.13), when  $k_x$  or  $k_y > k$ , a condition under which the plane waves turn into evanescent waves. Note that Eq. (2.34) becomes

$$k_z = \pm i \sqrt{k_x^2 + k_y^2 - k^2} = \pm i k'_z \quad (2.35)$$

where  $k'_z$  is real and the plane wave, turned evanescent, has the form

$$p = Ae^{\mp k'_z z} e^{i(k_x x + k_y y)}. \quad (2.36)$$

If the sources exist in the half space defined by  $z < 0$ , then the  $e^{+k'_z z}$  solution to the wave equation is non-physical, since it blows up at  $+\infty$ , and we restrict our solution to the decaying term (Sommerfeld radiation condition [see Chapter 8]):

$$p = Ae^{-k'_z z} e^{i(k_x x + k_y y)}. \quad (2.37)$$

This is the form of an evanescent wave, decaying in amplitude in the  $z$  direction. We illustrate this case in Fig. 2.6 below, again for the case where  $k_y = 0$ . Since  $k_x > k$  we see that the trace velocity of the wave along the  $x$  axis is less than the sound speed, since  $c_x < c$ . As a result, this wave is called a subsonic wave in contrast to the nonevanescent waves discussed above which resulted in supersonic trace velocities. Also since  $k_x > k$ , then  $\lambda_x < \lambda$  and the trace wavelengths are less than the acoustic wavelength. In  $k$ -space, shown on the right in Fig. 2.6, the wavenumber is outside the radiation circle—always the case for evanescent waves.

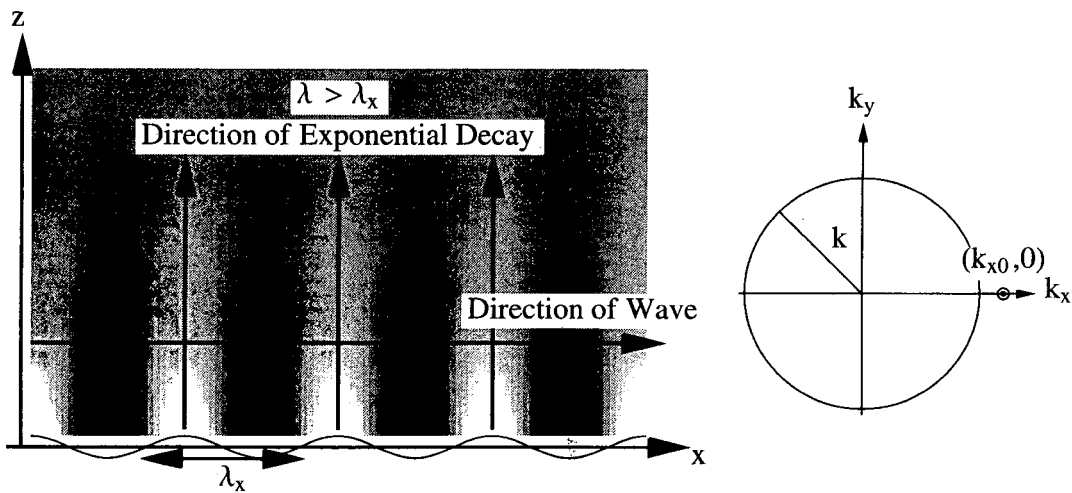


**Figure 2.6:** Evanescent wave traveling parallel to  $x$  axis, decaying exponentially in the vertical direction. In  $k$ -space this wave falls outside the radiation circle, as shown. All plane waves outside the radiation circle are subsonic.

From Eq. (2.14) the particle velocity associated with an evanescent wave is

$$\vec{v} = \frac{1}{\omega \rho_0} (k_x \hat{i} + k_y \hat{j} + ik'_z \hat{k}) p(\omega) \quad (2.38)$$

so that the intensity is

$$\vec{I} = \frac{|A|^2 e^{-2k'_z z}}{2\omega \rho_0} (k_x \hat{i} + k_y \hat{j}). \quad (2.39)$$

From this it is clear that the power flows parallel to the  $(x, y)$  plane in the direction  $k_x \hat{i} + k_y \hat{j}$ , decaying exponentially in the  $z$  direction. The direction of the evanescent

wave is  $\vec{k}_{ev} = k_x \hat{i} + k_y \hat{j}$ . Note that this differs from the plane wave case, where  $k_z$  enters into the direction of the wave.

Evanescence waves are also called inhomogeneous waves. They have tremendous relevance in the studies of radiation from plates and wave reflection and transmission between two differing media. Also, they are important for any vibrating structure that supports subsonic waves (wavelength less than the wavelength in the medium) and we will meet them quite frequently throughout this book.

A mathematical particular is the need to select the correct branch of the square root function when the argument is complex. When sources are confined to the lower half space ( $z < 0$ ) and radiation is considered into the space  $z > 0$ , we must choose for the proper behavior of the evanescent waves

$$k_z = +i\sqrt{k_x^2 + k_y^2 - k^2}. \quad (2.40)$$

## 2.7 Infinite Plate Vibrating in a Normal Mode

In order to tie the concept of plane waves to a coupled vibration/radiation problem, we next consider the radiation from an infinite plate located in the  $z = 0$  plane, which is vibrating in a standing wave mode at a single frequency with normal surface velocity  $\eta$  given by

$$\eta(x, y) = \eta_0 \cos(k_{x0}x) \cos(k_{y0}y). \quad (2.41)$$

The distance between nodal lines on the plate in the  $x$  and  $y$  directions is given by

$$\begin{aligned} \lambda_{x0}/2 &= \pi/k_{x0}, \\ \lambda_{y0}/2 &= \pi/k_{y0}. \end{aligned}$$

We now specify the conditions needed to solve this boundary value problem, that is, to determine the pressure in the half-space above the plate. There are four conditions for the pressure  $p$  and fluid particle velocity  $\dot{w}$  which must be satisfied:

- (1)  $p$  must satisfy the Helmholtz equation, Eq. (2.13), for  $z \geq 0$ ,
- (2)  $\dot{w}$  and  $p$  must satisfy Euler's equation, Eq. (2.14),
- (3)  $\eta(x, y)$  must equal  $\dot{w}(x, y, z)$  at the interface,  $z = 0$ , and
- (4) there are no sources above ( $z > 0$ ) the plate.

The third condition implies that the fluid always stays in contact with the plate. The displacement of the fluid particles near the plate boundary and normal to the plate surface must be continuous. It is important to realize, however, that this continuity requirement is not imposed in the  $x$  and  $y$  directions. Thus if the plate undergoes motion in-plane, this motion need not be continuous with the fluid particle motion in the  $x$  and  $y$  directions. This implies that the plate is allowed to slip under the fluid, like a frictionless boundary. Because it is frictionless it cannot drag the fluid particles along with it. This results from our neglect of viscosity in the fluid.

We make an educated guess at the solution to Eq. (2.13), in view of Eq. (2.41):

$$p(x, y, z) = p_0 e^{ik_{z0}z} \cos(k_{x0}x) \cos(k_{y0}y), \quad (2.42)$$

and insert this result into conditions (1) and (2) above. Condition (1) yields

$$k_{z0} = \pm \sqrt{k^2 - k_{x0}^2 - k_{y0}^2}$$

and condition (4) eliminates the negative value of  $k_{z0}$ , since  $e^{-ik_{z0}z-i\omega t}$  is a wave traveling towards the plate which could only arise from a source above the plate (such as a reflecting boundary). As usual  $k = \omega/c$ , where  $\omega$  is the radian frequency of plate oscillation. Thus

$$k_{z0} = \sqrt{k^2 - k_{x0}^2 - k_{y0}^2}. \quad (2.43)$$

Inserting Eq. (2.42) into condition (2),

$$\dot{w}(x, y, 0) = \frac{1}{i\rho_0 c k} \frac{\partial p}{\partial z} \Big|_{z=0},$$

yields

$$\dot{w}(x, y, 0) = \frac{p_0 k_{z0}}{\rho_0 c k} \cos(k_{x0}x) \cos(k_{y0}y). \quad (2.44)$$

Imposing condition (3), that is,  $\dot{w}(x, y, 0) = \eta_0 \cos(k_{x0}x) \cos(k_{y0}y)$ , yields

$$p_0 = \frac{\eta_0 \rho_0 c k}{k_{z0}}$$

so that the final result is

$$p(x, y, z) = \frac{\eta_0 \rho_0 c k}{k_{z0}} e^{ik_{z0}z} \cos(k_{x0}x) \cos(k_{y0}y). \quad (2.45)$$

Equation (2.45) is the steady state pressure radiated from a vibrating plate with surface velocity given by Eq. (2.41).  $k_{x0}$  and  $k_{y0}$  are the given wavenumbers of the modal pattern of the plate, and  $k_{z0}$  is a function of them representing the variation of the pressure in the direction normal to the plate.

## 2.8 Wavenumber Space: *k*-space

Vibrations due to wave phenomena and resulting radiation can be represented in *k*-space. Often this presentation is extremely powerful in displaying the physics underlying the phenomena. We have already seen the *k*-space representations of various plane waves shown in Figs 2.3–2.6 and discussed in the captions. To illustrate further we continue with the infinite plate example of the last section.

We cast Eq. (2.45) in terms of the plane waves discussed earlier noting that

$$\cos(k_{x0}x) = \frac{1}{2}(e^{ik_{x0}x} + e^{-ik_{x0}x})$$

and

$$\cos(k_{y0}y) = \frac{1}{2}(e^{ik_{y0}y} + e^{-ik_{y0}y}),$$

so that the product of the two cosines results in four plane waves given by

$$e^{i(k_{z0}z \pm k_{x0}x \pm k_{y0}y)}.$$

The four plane waves can be illustrated by using a wavenumber space diagram ( $k$ -space) as shown in Fig. 2.7.

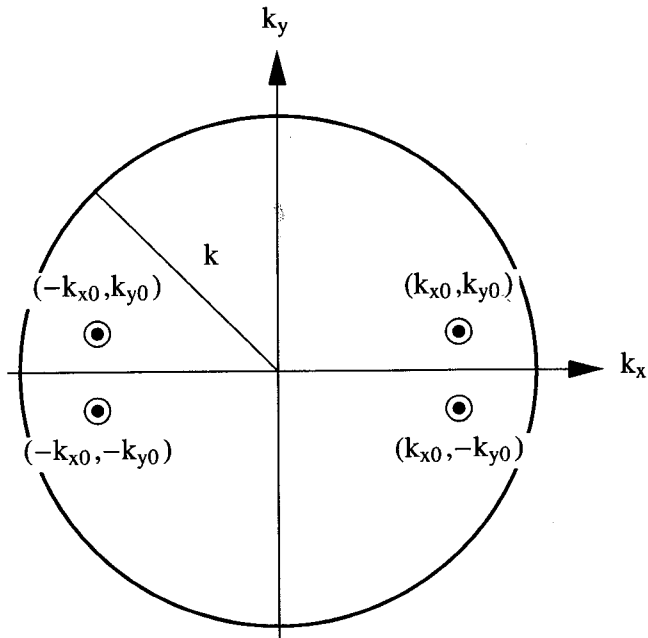


**Figure 2.7:**  $k$ -space diagram showing locations of 4 plane waves radiating from a vibrating plate with standing wave pattern given by  $k_{x0}$  and  $k_{y0}$ .

The small circles with dots indicate the location of the four plane wave components resulting from a standing wave on the plate. The large circle has a radius given by the acoustic wavenumber  $k$  and is called the radiation circle. The case illustrated here is for supersonic wavenumbers in the  $x$  and  $y$  directions; the components  $(\pm k_{x0}, \pm k_{y0})$  are all located within the radiation circle. In this case Eq. (2.43) dictates that  $k_{z0}$  is real and less than  $k$  in magnitude. The directions of the plane waves are given by  $\vec{k} = k_{x0}\hat{i} + k_{y0}\hat{j} + k_{z0}\hat{k}$ .

The directions of the plane waves can be illustrated using a hemisphere, with the  $k$ -space diagram shown in Fig. 2.7 in the equatorial plane, and the  $k_z$  axis as the polar axis. This is illustrated in Fig. 2.8.

We use a spherical coordinate system to describe the radiation. The spherical coordinates with polar angle  $\theta$  and azimuthal angle  $\phi$  are shown. The direction of the plane wave shown in the figure with the arrow labeled  $k$  is then, in spherical coordinates,

$$\vec{k} = k \cos \phi \sin \theta \hat{i} + k \sin \phi \sin \theta \hat{j} + k \cos \theta \hat{k}, \quad (2.46)$$

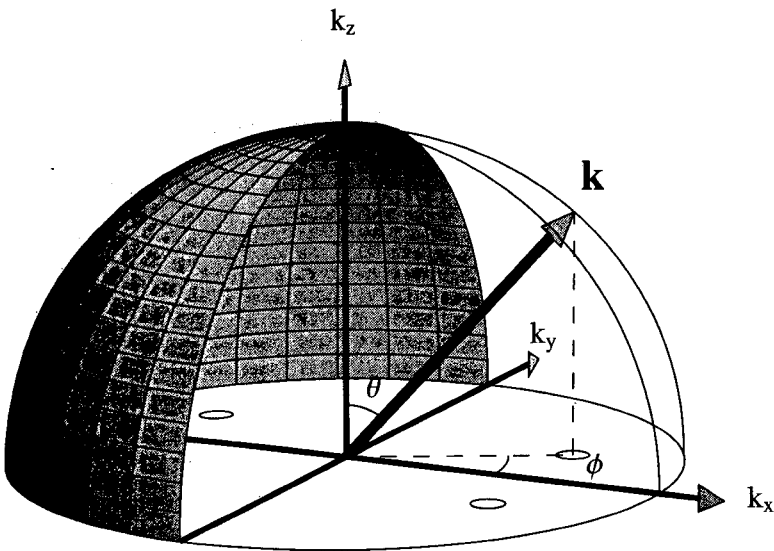


**Figure 2.8:** Radiation sphere in  $k$ -space. The  $k$ -space diagram of Fig. 2.7 is the equatorial plane. The direction of the plane wave with positive components  $(k_{x0}, k_{y0})$  is shown by the vector  $\vec{k}$ , with the spherical angles  $\theta$  and  $\phi$ . The radius of the hemisphere is  $k$ .

where we must have

$$\begin{aligned} k_{x0} &= k \cos \phi_0 \sin \theta_0 \\ k_{y0} &= k \sin \phi_0 \sin \theta_0 \\ k_{z0} &= k \cos \theta_0. \end{aligned} \quad (2.47)$$

This equation expresses the important inter-relationship between the wavenumbers on the plate and the direction of propagation of the radiated plane waves. For example, we can see that as the distance between the nodal lines (see Eq. (2.41)) on the plate increases, keeping the frequency fixed (as if we were making the plate stiffer), then  $k_{x0} \rightarrow 0$  and  $k_{y0} \rightarrow 0$ , then Eq. (2.47) shows that  $\theta \rightarrow 0$  and the plane wave travels in the direction of the  $z$  axis, normal to the plate.

The case illustrated above assumes that both  $k_{x0}$  and  $k_{y0}$  are supersonic, that is, both are less than or equal to  $k$ . However, if either wavenumber is greater than  $k$ , one of the components is subsonic ( $c_{x0}$  or  $c_{y0} < c$ ) and the square root in Eq. (2.43) becomes

$$k_{z0} = i \sqrt{k_{x0}^2 + k_{y0}^2 - k^2} = ik'_{z0}, \quad (2.48)$$

where the argument of the square root is now positive and  $k'_{z0}$  is real. The pressure above the plate, Eq. (2.45), now becomes

$$p(x, y, z) = \frac{-i\eta_0\rho_0ck}{k'_{z0}} e^{-k'_{z0}z} \cos(k_{x0}x) \cos(k_{y0}y), \quad (2.49)$$

decaying exponentially away from the plate boundary. Again because of the product of cosines in Eq. (2.49), this pressure is composed of four **evanescent** waves given by

$$e^{-k'_{z0}z} e^{i(\pm k_{x0}x \pm k_{y0}y)}$$

The  $k$ -space diagram (in this case  $c_{x0}$  and  $c_{y0}$  are both subsonic) is shown in Fig. 2.9. The four plane wave components fall outside the radiation circle. Clearly no radiation

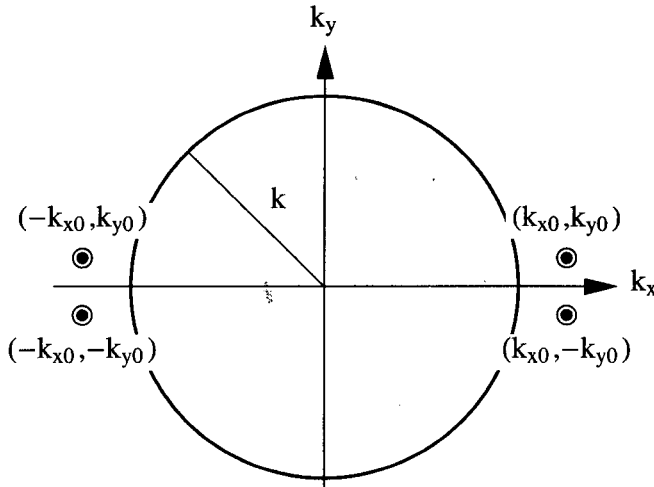


**Figure 2.9:**  $k$ -space diagram showing locations of 4 plane waves radiating from a vibrating plate with a subsonic standing wave pattern.

reaches the farfield in this case. In other words, an infinite plate with a subsonic wave component in either (or both) the  $x$  or  $y$  direction does not radiate to the farfield. Thus waves with  $k$ -space components outside the radiation circle do not radiate to the farfield.

Consider now the acoustic intensity for the evanescent case. The normal acoustic intensity (time averaged) at the plate surface is given by

$$I_z(x, y, 0) = \frac{1}{2} \operatorname{Re}(p(x, y, 0)\eta^*(x, y))$$

which we can compute from Eqs (2.49) and (2.41). We see that since  $p$  is purely imaginary and  $\eta$  is real, the time-averaged, normal acoustic intensity is identically zero;  $I_z(x, y, 0) = 0$ . This is a very important statement of the fact that there is no average power transfer from the plate to the fluid. In fact Eq. (2.17) gives the result  $\Pi(\omega) = 0$ ; there is no power radiated into the half-space  $z > 0$ , and thus no power radiated to the farfield. This happens when the nodal lines in either direction on the plate are separated by less than  $\lambda/2$  in the fluid. This condition is often referred to as a hydrodynamic short circuit, alluding to the fact that adjacent regions of negative and positive velocity tend to cancel one another as they push against the fluid in an effort to launch radiation into the farfield. This condition is illustrated in Fig. 2.10 below.

Equation (2.49) also indicates that as the nodal line separation gets smaller and smaller, then  $k'_{z0} \rightarrow \infty$  and the pressure at the surface of the plate diminishes to zero;

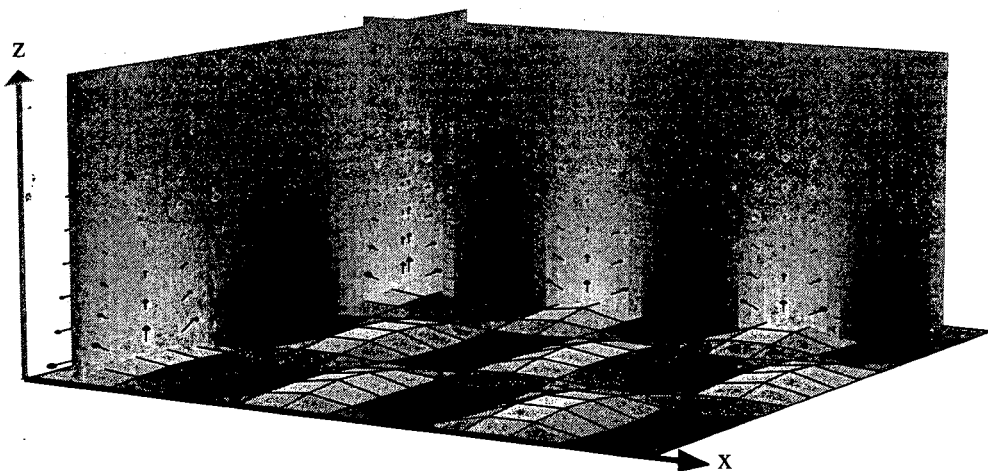


**Figure 2.10:** Hydrodynamic short circuit occurring when adjacent regions on the plate push fluid into one another, canceling any radiation from the plate. The arrows show the magnitude and direction of the velocity of the fluid above the plate, revealing the circulation of energy in the nearfield. The vertical planes provide a gray scale mapping of the fluid pressure, illustrating the exponential decay of the sound field resulting from the hydrodynamic short circuit.

another indication of the effect of the hydrodynamic short circuit. Notice there appears to be a problem when  $k_{z0} = 0$ , when the plate turns from supersonic to subsonic (called coincidence), and the plane waves excited travel parallel to the surface of the plate extending without decay to infinity. The zero in the denominator of Eq. (2.49) then implies an infinite pressure above the plate. This impossible condition results from a violation of condition (3) above, which requires the normal velocity of the plate to be continuous with the fluid velocity in contact with it. However, a plane wave traveling parallel to the plate has only a fluid velocity parallel to the plate (in the direction of travel) and zero normal velocity. The contradiction in our problem is expressed in the mathematics by the appearance of an infinity.

This completes our discussion of the radiation from an infinite plate with a given modal pattern of vibration. We included this example to build up our understanding of plane and evanescent waves, critical to the analysis which we are about to present. In a more general way than was presented in the plate problem above, we now show how any arbitrary pressure distribution in a source-free half space can be decomposed into plane and evanescent waves.

## 2.9 The Angular Spectrum: Fourier Acoustics

Consider a general unknown, steady state pressure distribution  $p(x, y, z)$  in a source-free half space,  $z > 0$ . This pressure can be expressed uniquely and completely by a sum of plane and evanescent waves of the form discussed above. We must keep in mind that  $k_x$  and  $k_y$  are independent variables, and that  $k_z$  depends upon them. Each of

the plane/evanescent waves which make up  $p$  may have different amplitudes and phases which we account for by using a multiplying coefficient term  $P(k_x, k_y)$  which depends on the two wavenumbers. That is, we expect any pressure distribution in a source-free region to be expressible as a wave sum such as

$$p(x, y, z) = \sum_{k_x} \sum_{k_y} P(k_x, k_y) e^{i(k_x x + k_y y + k_z z)}$$

where we recognize the exponential term as a plane/evanescent wave. This is similar in concept to the result from the plate example presented above in which four plane or evanescent wave components were needed to solve for the pressure field for a given plate velocity. In this case, the sums above would only contain two terms each ( $\pm k_{x0}$  and  $\pm k_{y0}$ ) and, as Eq. (2.45) shows,

$$P(k_x, k_y) = \frac{\eta_0 \rho_0 c k}{4k_{z0}}.$$

For a general problem, because of the infinite extent in the  $x$  and  $y$  directions, we expect a continuum of possible wavenumbers so that the sums above have to be represented by integrals to accommodate the continuum of values. Thus the pressure field can be written in general as

$$p(x, y, z) = \frac{1}{4\pi^2} \int_{-\infty}^{\infty} dk_x \int_{-\infty}^{\infty} dk_y P(k_x, k_y) e^{i(k_x x + k_y y + k_z z)}. \quad (2.50)$$

The introduction of the arbitrary constant  $1/4\pi^2$  is for purposes which will become clear later. This equation is extremely important and central to this book. The integrals are over all values, supersonic and subsonic, of the wavenumbers and, as before,

$$k_z = \sqrt{k^2 - k_x^2 - k_y^2}.$$

Note that only positive  $k_z$  values are taken from the square root. This expresses the fact that we are dealing with a half-space problem, that is, the sources are confined to  $z \leq 0$  and thus no plane waves can travel in the negative  $z$  direction.

Now consider the interpretation of the complex quantity  $P(k_x, k_y)$ . If  $z = 0$  in Eq. (2.50) we have

$$p(x, y, 0) = \frac{1}{4\pi^2} \int_{-\infty}^{\infty} dk_x \int_{-\infty}^{\infty} dk_y P(k_x, k_y) e^{i(k_x x + k_y y)}. \quad (2.51)$$

This equation is an expression for the pressure in the infinite plane at  $z = 0$ . Comparing this to Eq. (1.17) reveals that the integrals represent two inverse Fourier transforms in  $k_x$  and  $k_y$ , respectively. Thus, in view of Eq. (1.17), the complex amplitude  $P(k_x, k_y)$  is given by the corresponding two-dimensional Fourier transform:

$$P(k_x, k_y) = \int_{-\infty}^{\infty} dx \int_{-\infty}^{\infty} dy p(x, y, 0) e^{-i(k_x x + k_y y)}. \quad (2.52)$$

The Fourier transform guarantees that *any* pressure distribution,  $p(x, y, 0)$  can be represented by Eq. (2.51).  $P(k_x, k_y)$  is called the angular spectrum.<sup>2</sup>

---

<sup>2</sup>J. Goodman (1968). *Introduction to Fourier Optics*. McGraw-Hill, New York.

### 2.9.1 Wave Field Extrapolation

This analysis leads us to a significant result which forms the backbone of Fourier acoustics (as well as Fourier optics). Once  $P(k_x, k_y)$  is known, computed from the pressure in the plane  $z = 0$ , then we can use Eq. (2.50) to compute the pressure field over the three-dimensional volume from  $z = 0$  to infinity, without any more information. We will see that this ability to extrapolate fields from one plane to another in such simple fashion will provide powerful tools for numerical and experimental applications, and forms the foundation of nearfield acoustical holography.

Another way to express this extrapolation is to note that the Fourier transform of the pressure in a plane  $z = \text{constant}$  is related to the transform of the pressure in the plane  $z = 0$  by

$$\mathcal{F}_x \mathcal{F}_y [p(x, y, z)] \equiv P(k_x, k_y, z) = P(k_x, k_y) e^{ik_z z}, \quad (2.53)$$

so that the plane wave amplitudes only undergo a phase change (for  $k_z$  real) from one horizontal plane to another. For example, if  $k_x = k_y = 0$ , then  $k_z = k$  and  $P(0, 0) e^{ik_z} = P(0, 0, z)$  and  $e^{ik_z}$  is the phase change of a plane wave traveling in the  $z$  direction (normal). The general expression then to extrapolate the angular spectrum in the plane  $z = z'$  to a plane  $z = z$  is

$$P(k_x, k_y, z) = P(k_x, k_y, z') e^{ik_z(z-z')}. \quad (2.54)$$

Note that the evanescent waves are also included in this expression. When  $k_z$  is purely imaginary then

$$P(k_x, k_y, z) = P(k_x, k_y, z') e^{-|k_z|(z-z')}. \quad (2.55)$$

Note the following definition has been assumed,

$$P(k_x, k_y) \equiv P(k_x, k_y, 0). \quad (2.56)$$

Very simple algebraic equations also exist relating the  $k$ -space velocity and the  $k$ -space pressure. These are derived from a two-dimensional Fourier transform of Euler's equation, Eq. (2.14). Let the transform of the normal velocity be

$$\dot{W}(k_x, k_y, z) \equiv \mathcal{F}_x \mathcal{F}_y [\dot{w}(x, y, z)]. \quad (2.57)$$

Similarly, the Fourier components of the other velocity components are  $\dot{U}(k_x, k_y, z)$  and  $\dot{V}(k_x, k_y, z)$ . From Eq. (2.54)

$$\mathcal{F}_x \mathcal{F}_y \left[ \frac{\partial p(x, y, z)}{\partial z} \right] = \frac{\partial P(k_x, k_y, z)}{\partial z} = ik_z P(k_x, k_y, z') e^{ik_z(z-z')}, \quad (2.58)$$

and, given Eq. (1.10), the Fourier transform of Euler's equation is

$$\dot{U}(k_x, k_y, z) \hat{i} + \dot{V}(k_x, k_y, z) \hat{j} + \dot{W}(k_x, k_y, z) \hat{k} = \frac{1}{\rho_0 c k} (k_x \hat{i} + k_y \hat{j} + k_z \hat{k}) P(k_x, k_y, z). \quad (2.59)$$

Note that the partial differentiation operations of the gradient have been replaced with a multiplication by  $ik_x$  and  $ik_y$ . This formula makes the rather significant statement

that from a knowledge of the angular spectrum of the pressure in a plane, one can easily determine the three angular spectrum components of the vector velocity.

In particular, we can use Eq. (2.54) to relate the velocity to the pressure in a different plane;

$$\begin{aligned} & \dot{U}(k_x, k_y, z)\hat{i} + \dot{V}(k_x, k_y, z)\hat{j} + \dot{W}(k_x, k_y, z)\hat{k} \\ = & \frac{1}{\rho_0 c k} (k_x \hat{i} + k_y \hat{j} + k_z \hat{k}) P(k_x, k_y, z') e^{ik_z(z-z')}. \end{aligned} \quad (2.60)$$

Thus, the normal component of velocity is

$$\dot{W}(k_x, k_y, z) = \frac{k_z}{\rho_0 c k} P(k_x, k_y, z') e^{ik_z(z-z')}. \quad (2.61)$$

This important equation relates the angular spectrum components of normal velocity in one plane to components of pressure in a different plane.

$\hat{z}$

## 2.10 Derivation of Rayleigh's Integrals

We will now use the angular spectrum to derive some rather famous integrals. It is a tribute to the angular spectrum approach that we are able to proceed in this direction. The following integrals were developed using a different approach by Rayleigh.<sup>3</sup> First, we will derive his second integral formula (also called the second diffraction formula). Start with the inverse Fourier transform of Eq. (2.54):

$$p(x, y, z) = \frac{1}{4\pi^2} \int_{-\infty}^{\infty} \int_{-\infty}^{\infty} P(k_x, k_y, z') e^{ik_z(z-z')} e^{i(k_x x + k_y y)} dk_x dk_y.$$

Note that this integral is the product of two Fourier transforms. In shorthand notation this equation is,

$$p(x, y, z) = \mathcal{F}_x^{-1} \mathcal{F}_y^{-1} [P(k_x, k_y, z') e^{ik_z(z-z')}].$$

If we let  $F(k_x, k_y) = P(k_x, k_y, z')$  and  $G_p(k_x, k_y, z - z') \equiv e^{ik_z(z-z')}$  then we can use the convolution theorem, Eq. (1.20), in  $x$  and  $y$ :

$$f(x, y) * * g_p(x, y, z - z') = \mathcal{F}_x^{-1} \mathcal{F}_y^{-1} [F(k_x, k_y) G_p(k_x, k_y, z - z')],$$

to arrive at

$$p(x, y, z) = \iint p(x', y', z') g_p(x - x', y - y', z - z') dx' dy', \quad (2.62)$$

where the inverse transform of  $P(k_x, k_y, z')$  is  $p(x', y', z')$  and the inverse transform of  $G_p(k_x, k_y, z - z')$  is  $g_p(x - x', y - y', z - z')$ . To determine  $g_p(x - x', y - y', z - z')$  we note that

$$g_p(x, y, z - z') = \mathcal{F}_x^{-1} \mathcal{F}_y^{-1} [e^{ik_z(z-z')}],$$

---

<sup>3</sup>J. W. S. Rayleigh (1897). "On the passage of waves through apertures in plane screens, and allied problems", Philosophical Magazine, **43**, pp. 259–272.

so that, using the shift theorem,  $g_p(x - x', y - y', z - z')$  is given by the integral

$$g_p(x - x', y - y', z - z') = \frac{1}{4\pi^2} \int_{-\infty}^{\infty} \int_{-\infty}^{\infty} e^{i[k_x(x-x')+k_y(y-y')]} e^{i(z-z')\sqrt{k^2-k_x^2-k_y^2}} dk_x dk_y. \quad (2.63)$$

Note  $k_z$  has been written out in terms of  $k_x$  and  $k_y$ .

Now we will evaluate the integrals on the right. They can be cast in the form of a well known integral called Weyl's integral<sup>4</sup> as was pointed out by Lalor.<sup>5</sup> Weyl's integral provides the expansion of the free space Green function, which will be discussed in more detail in Section 6.5.1, in terms of plane waves:

$$\frac{e^{ik|\vec{r}-\vec{r}'|}}{|\vec{r}-\vec{r}'|} = \frac{i}{2\pi} \int_{-\infty}^{\infty} \int_{-\infty}^{\infty} e^{i[k_x(x-x')+k_y(y-y')]} \frac{e^{ik_z|z-z'|}}{k_z} dk_x dk_y, \quad (2.64)$$

where  $\vec{r} = (x, y, z)$ ,  $\vec{r}' = (x', y', z')$ , and

$$|\vec{r} - \vec{r}'| = \sqrt{(x - x')^2 + (y - y')^2 + (z - z')^2}.$$

Differentiating both sides of this integral with respect to  $z'$  and restricting  $z > z'$  yields,

$$\frac{\partial}{\partial z'} \left[ \frac{e^{ik|\vec{r}-\vec{r}'|}}{|\vec{r}-\vec{r}'|} \right] = -\frac{1}{2\pi} \int_{-\infty}^{\infty} \int_{-\infty}^{\infty} e^{i[k_x(x-x')+k_y(y-y')]} e^{ik_z(z-z')} dk_x dk_y. \quad (2.65)$$

Comparison with Eq. (2.63) gives

$$g_p(x - x', y - y', z - z') = -\frac{1}{2\pi} \frac{\partial}{\partial z'} \left[ \frac{e^{ik|\vec{r}-\vec{r}'|}}{|\vec{r}-\vec{r}'|} \right]. \quad (2.66)$$

Finally we insert this result into Eq. (2.62) to yield **Rayleigh's second integral formula**:

$$p(x, y, z) = -\frac{1}{2\pi} \int_{-\infty}^{\infty} \int_{-\infty}^{\infty} p(x', y', z') \frac{\partial}{\partial z'} \left[ \frac{e^{ik|\vec{r}-\vec{r}'|}}{|\vec{r}-\vec{r}'|} \right] dx' dy', \quad (2.67)$$

with  $z \geq z'$ . This formula relates the spatial pressure in one plane to the spatial pressure in another plane. It gives a forward propagation formula by convolving the pressure in the plane  $z' = \text{constant}$  with a propagator  $g_p$  projecting the field to a more distant plane ( $z > z'$ ). Later we will look at the inverse of this equation so that we can backpropagate the spatial acoustic pressure field.

When  $z = z'$  in Eq. (2.67) an identity arises and one can not solve for the pressure field. That is, when  $z = z'$  Eq. (2.63) yields, using the delta function relation Eq. (1.36),

$$g_p(x - x', y - y', 0) = \delta(x - x')\delta(y - y'),$$

so that Eq. (2.67) is simply

$$p(x, y, z') = \iint p(x', y', z') \delta(x - x')\delta(y - y') dx' dy',$$

<sup>4</sup>H. Weyl (1919). Ann. Physik, **60**, p. 481.

<sup>5</sup>E. Lalor (1968). "Inverse Wave Propagator", J. Math. Phys., **9**, p. 2001.

which reduces to an identity.

We will discuss Eq. (2.67) in more detail after we derive Rayleigh's first integral formula, which is better known than his second and is extensively used in the study of radiation from finite plates. Again we use the angular spectrum approach for the derivation. This formula relates the velocity on the surface to the pressure radiated and thus we look for the angular spectrum representation which relates normal velocity to pressure. This is given by Eq. (2.61), resulting from Euler's equation, which we rewrite as

$$P(k_x, k_y, z) = \rho_0 c k \dot{W}(k_x, k_y, z') \frac{e^{ik_z(z-z')}}{k_z}, \quad (2.68)$$

where we have interchanged  $z$  and  $z'$ , and assumed  $z \geq z'$ . We can now take the inverse Fourier transforms in  $k_x$  and  $k_y$  of both sides of this equation, using the convolution theorem, Eq. (1.20), again:

$$p(x, y, z) = \mathcal{F}_x^{-1} \mathcal{F}_y^{-1} [\dot{W}(k_x, k_y, z')] * * \mathcal{F}_x^{-1} \mathcal{F}_y^{-1} \left[ \frac{\rho_0 c k e^{ik_z(z-z')}}{k_z} \right]. \quad (2.69)$$

Defining the function  $g_v(x, y, z)$  as

$$g_v(x, y, z) \equiv \mathcal{F}_x^{-1} \mathcal{F}_y^{-1} \left[ \frac{\rho_0 c k e^{ik_z z}}{k_z} \right], \quad (2.70)$$

then by definition of convolution Eq. (2.69) becomes

$$p(x, y, z) = \iint \dot{w}(x', y', z') g_v(x - x', y - y', z - z') dx' dy'. \quad (2.71)$$

By the shift theorem,

$$g_v(x - x', y - y', z - z') = \mathcal{F}_x^{-1} \mathcal{F}_y^{-1} \left[ \rho_0 c k \frac{e^{-ik_x x'} e^{-ik_y y'} e^{ik_z(z-z')}}{k_z} \right], \quad (2.72)$$

that is,

$$g_v(x - x', y - y', z - z') = \frac{\rho_0 c k}{4\pi^2} \iint e^{i[k_x(x-x') + k_y(y-y')]} \frac{e^{ik_z(z-z')}}{k_z} dk_x dk_y. \quad (2.73)$$

The integral is recognized as Weyl's integral, Eq. (2.64), as long as  $z \geq z'$ ; thus

$$g_v(x - x', y - y', z - z') = -i \rho_0 c k \frac{e^{ik|\vec{r} - \vec{r}'|}}{2\pi |\vec{r} - \vec{r}'|}. \quad (2.74)$$

Substitution into Eq. (2.71) yields the final result, again for  $z \geq z'$ ,

$$p(x, y, z) = \frac{-i \rho_0 c k}{2\pi} \int_{-\infty}^{\infty} \int_{-\infty}^{\infty} \dot{w}(x', y', z') \frac{e^{ik|\vec{r} - \vec{r}'|}}{|\vec{r} - \vec{r}'|} dx' dy'. \quad (2.75)$$

This very important equation is **Rayleigh's first integral formula** and is used extensively in the literature in solving radiation problems from plates. Both of Rayleigh's formulas provide a means to compute the radiation into a half space ( $z \geq z'$ ) given either the pressure on a surface  $z = z'$ , Eq. (2.67), or the normal velocity on a surface  $z = z'$ , Eq. (2.75). These surface fields are convolved with a propagator, a process which implies that all the source points  $(x', y', z')$  contribute to the radiation at a single field point  $(x, y, z)$ .

The following figure should make clear the geometrical ramifications of Rayleigh's integral.

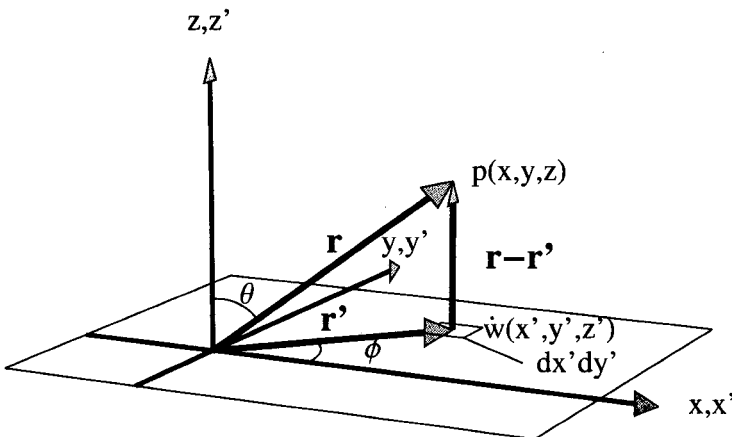


**Figure 2.11:** Geometric interpretation of Rayleigh's first integral formula. The small box represents an element of area  $dx'dy'$  with normal velocity  $\dot{w}$ . The integral indicates that for a fixed field point  $(x, y, z)$  this area sweeps over the complete  $(x', y')$  plane.

The normal velocity of the element of area  $dx'dy'$  on the surface radiates to the field point at  $(x, y, z)$  with an amplitude and phase given by the propagator. One must add the contributions of all of the area elements in the infinite plane to determine the pressure at a single field point.

### 2.10.1 The Velocity Propagator

The propagator  $g_v$  defined in Eq. (2.74) is called the velocity propagator since it determines the pressure radiated to an outward plane through convolution with the normal velocity distribution on a surface. This propagator is proportional to the pressure from a *baffled* point source located at  $(x', y', z')$ , as we will now show.

We can represent a baffled point source located at  $(x_0, y_0, 0)$  using delta functions:

$$\dot{w}(x', y', 0) = Q_h \delta(x' - x_0) \delta(y' - y_0). \quad (2.76)$$

$Q_h$  represents the strength of the source in the units of meters per second times area, or volume per unit time (cubic meters per second). This is the amount of fluid injected

into the medium per unit time. The angular spectrum is found by taking the Fourier transform of Eq. (2.76),

$$\dot{W}(k_x, k_y, 0) = Q_h e^{-ik_x x_0} e^{-ik_y y_0}.$$

The pressure spectrum associated with this is, from Eq. (2.61),

$$P(k_x, k_y, 0) = \frac{Q_h \rho_0 c k}{k_z} e^{-ik_x x_0} e^{-ik_y y_0},$$

which can be extended to a different value of  $z$  by multiplication by  $\exp(ik_z z)$ :

$$P(k_x, k_y, z) = \frac{Q_h \rho_0 c k}{k_z} e^{-ik_x x_0} e^{-ik_y y_0} e^{ik_z z}.$$

Review of Eq. (2.72) and Eq. (2.74) reveals that the inverse transform of this expression is

$$p(x, y, z) = \mathcal{F}_x^{-1} \mathcal{F}_y^{-1} [P(k_x, k_y, z)] = \frac{-i Q_h \rho_0 c k}{2\pi} \frac{e^{ik|\vec{r} - \vec{r}_0|}}{|\vec{r} - \vec{r}_0|}, \quad (2.77)$$

with  $z' = z_0 = 0$  and  $\vec{r}_0 = (x_0, y_0, 0)$ . This equation gives the pressure field radiated by a point source in a baffle<sup>6</sup> with source strength  $Q_h$ . This source is like a tiny dome loudspeaker (radius  $a$  and surface area  $2\pi a^2$ ) in an infinite baffle moving with a radial velocity  $\dot{w}_r$  so that

$$Q_h = 2\pi a^2 \dot{w}_r.$$

We will now show how we can use the Rayleigh integral to calculate the farfield radiation from planar sources.

## 2.11 Farfield Radiation: Planar Sources

Rayleigh's integral is the springboard for a very powerful formula which relates the farfield radiation from planar sources to the Fourier transform of the surface velocity. The reader with a strong background in Fourier transforms will find that he has a complementary knowledge of the farfield patterns for many kinds of planar sources.

To begin the derivation, we let the field point move far from the source plane in the  $z$  direction. We will assume that any given source distribution will always be confined to a finite area in the  $(x, y)$  plane, and that outside this area there is a rigid baffle extending to infinity. A rigid baffle is defined by vanishing normal velocity on its surface, that is, when  $(x', y')$  is on the baffle then  $\dot{w}(x', y', 0) = 0$ . If the surface velocity is contained within an area  $S$  then Rayleigh's integral has finite limits and becomes,

$$p(x, y, z) = \frac{-i \rho_0 c k}{2\pi} \iint_S \dot{w}(x', y', 0) \frac{e^{ik|\vec{r} - \vec{r}'|}}{|\vec{r} - \vec{r}'|} dx' dy'. \quad (2.78)$$

For  $\vec{r}'$  in  $S$  ( $z' = 0$ ) the definition of the farfield (see Fig. 2.11) is  $r >> r'$ , where

$$r \equiv |\vec{r}| \text{ and } r' \equiv |\vec{r}'|.$$

---

<sup>6</sup>L. E. Kinsler and A. R. Frey (1962). *Fundamentals of Acoustics*. Wiley & Sons, New York, 2nd ed., p. 165.

Under these conditions,

$$\begin{aligned} |\vec{r} - \vec{r}'| &= ((x - x')^2 + (y - y')^2 + z^2)^{1/2} \\ &\approx r \left( 1 - \frac{x}{r}x' - \frac{y}{r}y' \right). \end{aligned} \quad (2.79)$$

Define a vector  $\vec{k} = k_x \hat{i} + k_y \hat{j} + k_z \hat{k}$  in the same direction as  $\vec{r}$  so that

$$\frac{\vec{k}}{k} = \frac{\vec{r}}{r},$$

that is, the unit vectors point in the same direction. Thus  $\frac{x}{r} = \frac{k_x}{k}$  and  $\frac{y}{r} = \frac{k_y}{k}$ , and

$$\frac{e^{ik|\vec{r}-\vec{r}'|}}{|\vec{r}-\vec{r}'|} \approx \frac{e^{ikr}}{r} e^{-i(k_x x' + k_y y')}.$$
 (2.80)

Note that whereas one can replace  $|\vec{r} - \vec{r}'|$  with  $r$  in the denominator, we can not do so in the phase term of the exponential, since the latter is an oscillating function with range. Since  $\vec{k}$  is in the same direction as  $\vec{r}$  then the same spherical angles describe them both. Thus in spherical coordinates we have

$$\begin{aligned} x &= r \sin \theta \cos \phi, & k_x &= k \sin \theta \cos \phi, \\ y &= r \sin \theta \sin \phi, & k_y &= k \sin \theta \sin \phi, \\ z &= r \cos \theta, & k_z &= k \cos \theta. \end{aligned} \quad (2.81)$$

With these results Rayleigh's integral becomes

$$p(r, \theta, \phi) = -i\rho_0 ck \frac{e^{ikr}}{2\pi r} \iint_S \dot{w}(x', y', 0) e^{-i(k_x x' + k_y y')} dx' dy' \quad (2.82)$$

or, noting that the integrals here are Fourier transforms,

$$p(r, \theta, \phi) = -i\rho_0 ck \frac{e^{ikr}}{2\pi r} \mathcal{F}_{x'} \mathcal{F}_{y'} [\dot{w}(x', y', 0)]. \quad (2.83)$$

The final result is

$$p(r, \theta, \phi) = -i\rho_0 ck \frac{e^{ikr}}{2\pi r} \dot{W}(k_x, k_y, 0), \quad (2.84)$$

where  $k_x$  and  $k_y$  are given above in terms of spherical coordinates. This powerful formula states that the farfield of any planar source is determined from the two-dimensional Fourier transform of its normal velocity distribution as long as the direction of the farfield point is taken to be that of  $\vec{k}$ .

Most often what is plotted, when one asks for the farfield, is the directivity function. This is defined so as to remove the  $\exp(ikr)/r$  factor:

$$p(r, \theta, \phi) = \frac{e^{ikr}}{r} D(\theta, \phi) \quad (2.85)$$

with

$$D(\theta, \phi) = \frac{-i\rho_0 ck}{2\pi} \dot{W}(k_x, k_y, 0). \quad (2.86)$$

The directivity function has the units of Pascal-meters.

Equations (2.84) and (2.86) are quite significant. As we will demonstrate in the examples below, once the Fourier transform is computed for a given source distribution in a plane, these equations provide the directivity patterns for any frequency. Furthermore, these patterns can be constructed almost trivially using a procedure called the Ewald sphere construction.

Before we develop this construction, we present the farfield formula for vibrators with circular symmetry.

### 2.11.1 Vibrators with Circular Symmetry

For circular vibrators, such as a baffled drum head, the farfield radiation can be expressed in terms of a Hankel transform. If the vibration pattern of the vibrator is expressed as a function of polar coordinates,  $\dot{w}(x, y, z = 0) \rightarrow \dot{w}(\rho, \phi)$ , then we can use a Fourier series, Eq. (1.24), to represent the surface velocity:

$$\dot{w}(\rho, \phi') = \sum_{n=-\infty}^{\infty} \dot{w}_n(\rho) e^{in\phi'}. \quad (2.87)$$

The two-dimensional Fourier transform in rectangular coordinates in Eq. (2.83) can now be translated into polar coordinates with  $k_x = k_\rho \cos \phi$ ,  $k_y = k_\rho \sin \phi$ ,  $k_\rho \equiv k \sin \theta$ ,  $x' = \rho \cos \phi'$ , and  $y' = \rho \sin \phi'$ :

$$\begin{aligned} \mathcal{F}_{x'} \mathcal{F}_{y'} [\dot{w}(x', y', 0)] &= \sum_n \int_0^\infty \rho d\rho \dot{w}_n(\rho) \oint d\phi' e^{in\phi'} e^{-ik_\rho \rho (\cos \phi \cos \phi' + \sin \phi \sin \phi')} \\ &= \sum_n \int_0^\infty \rho d\rho \dot{w}_n(\rho) \oint d\phi' e^{-ik_\rho \rho \cos(\phi - \phi') + in\phi'}, \end{aligned}$$

where the integral over  $\phi'$  is written as  $\oint$  since it is circular spanning an interval of  $2\pi$ . To reduce this further we need an integral representation of the Bessel function,

$$J_n(z) = \frac{1}{2\pi} \int_{-\pi}^{\pi} e^{-iz \sin \xi + in\xi} d\xi, \quad (2.88)$$

and the substitution  $\phi - \phi' = \pi/2 - \xi$  to arrive at

$$\oint d\phi' e^{-ik_\rho \rho \cos(\phi - \phi') + in\phi'} = 2\pi e^{-in\pi/2} e^{in\phi} J_n(k_\rho \rho). \quad (2.89)$$

Finally, since the integral over  $\rho$  is an  $n$ th order Hankel transform given in Eq. (1.29),

$$\int_0^\infty \dot{w}_n(\rho) J_n(k_\rho \rho) \rho d\rho \equiv \mathcal{B}_n[\dot{w}_n(\rho)],$$

and we arrive at the final result:

$$\mathcal{F}_{x'} \mathcal{F}_{y'} [\dot{w}(x', y', 0)] = 2\pi \sum_n (-i)^n e^{in\phi} \mathcal{B}_n[\dot{w}_n(\rho)]. \quad (2.90)$$

Returning to Eq. (2.83), the farfield pressure for a vibrator with surface velocity expressed in polar coordinates becomes, with  $k_\rho = k \sin \theta$ ,

$$p(r, \theta, \phi) = \rho_0 c k \frac{e^{ikr}}{r} \sum_{n=-\infty}^{\infty} (-i)^{n+1} e^{in\phi} \mathcal{B}_n[\dot{w}_n(\rho)], \quad (2.91)$$

and the directivity pattern is given by

$$D(\theta, \phi) = \rho_0 c k \sum_{n=-\infty}^{\infty} (-i)^{n+1} e^{in\phi} \mathcal{B}_n[\dot{w}_n(\rho)]. \quad (2.92)$$

## 2.11.2 Ewald Sphere Construction

As a first example we will investigate the steady state radiation from a traveling wave on an infinite plate located in the plane  $z = 0$ . Let  $k_{x0}$  and  $k_{y0}$  be the supersonic wavenumbers (contained in the radiation circle) of the wave which has the form,

$$\dot{w}(x, y) = \dot{w}_0 e^{ik_{x0}x} e^{ik_{y0}y}. \quad (2.93)$$

Noting that  $\mathcal{F}_x[\exp(ik_{x0}x)] = 2\pi\delta(k_x - k_{x0})$  then

$$\dot{W}(k_x, k_y, 0) = 4\pi^2 \dot{w}_0 \delta(k_x - k_{x0}) \delta(k_y - k_{y0}), \quad (2.94)$$

and Eq. (2.86) yields the directivity function

$$D(\theta, \phi) = -2\pi i \dot{w}_0 \rho_0 c k \delta(k_x - k_{x0}) \delta(k_y - k_{y0}), \quad (2.95)$$

under the condition that

$$k_{x0} = k \sin \theta_0 \cos \phi_0, \quad (2.96)$$

$$k_{y0} = k \sin \theta_0 \sin \phi_0. \quad (2.97)$$

These conditions provide two equations to solve for the two unknown angles:

$$\begin{aligned} \sin \theta_0 &= \sqrt{k_{x0}^2 + k_{y0}^2}/k, \\ \tan \phi_0 &= k_{y0}/k_{x0}. \end{aligned}$$

Now a simple mapping procedure called the Ewald sphere construction procedure allows us to plot the directivity function on a hemisphere for any given source whose Fourier transform we know. The term Ewald sphere is borrowed from X-ray diffraction theory.<sup>7</sup> Figure 2.12 illustrates the concept for the example problem. In the figure  $k$  is the radius of the hemisphere so that the equatorial plane contains the radiation circle.

The Fourier transform of the source is plotted in the radiation circle making up the base of the hemisphere. In this case only a single delta function is plotted there located at  $(k_x, k_y) = (k_{x0}, k_{y0})$ . The amplitude (and phase) of the transform is then assigned

<sup>7</sup>A. Guiner (1963). *X-ray Diffraction*. Translated by Paul Lorrain and Dorothée Sainte-Marie Lorrain, San Francisco & London: W. H. Freeman & Co.

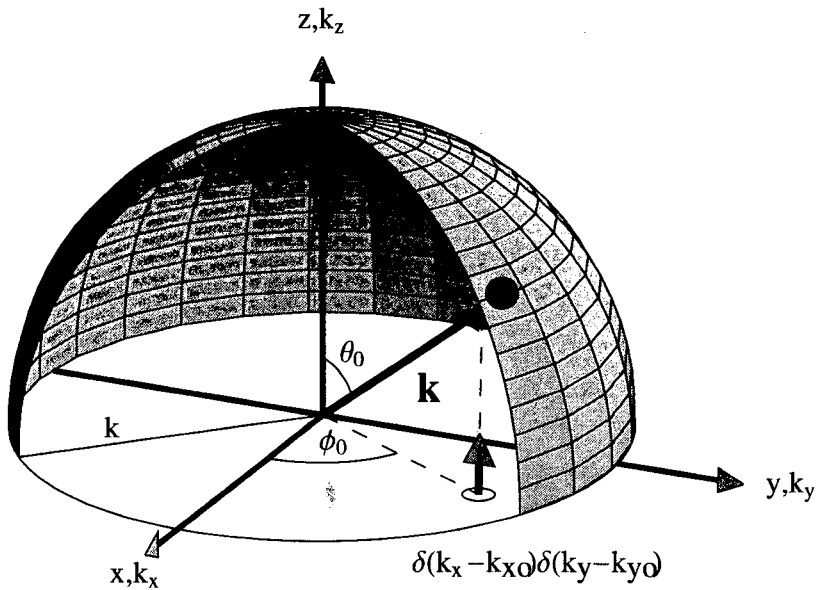


**Figure 2.12:** Construction of farfield in spherical coordinates using Ewald sphere construction.

to a point on the hemisphere determined by the vertical (upward) projection through the point to the hemisphere. This vertical projection satisfies the condition set up in Eq. (2.96) and Eq. (2.97) above. In this way the directivity pattern of the traveling wave is seen to be a delta function in the farfield at the spherical angles  $(\theta_0, \phi_0)$ , and zero at all other angles.

Another simple example is a point source located at the origin surrounded by an infinite rigid baffle. Thus,

$$\dot{w}(x, y, 0) = \delta(x)\delta(y),$$

and

$$\dot{W}(k_x, k_y, 0) = 1,$$

The projection of this covers the full Ewald sphere with a constant, unit amplitude. This constant directivity is verified by Eq. (2.86) since

$$D(\theta, \phi) = \frac{-i\rho_0 ck}{2\pi}; \quad (2.98)$$

a constant over all angles. As we expect the point source is omnidirectional.

### 2.11.3 A Baffled Square Piston

For the next example of the Ewald sphere construction we compute the farfield from a square piston vibrator with surface velocity

$$\dot{w}(x, y, 0) = \begin{cases} 1 & \text{if } -L/2 < x < L/2, \\ & -L/2 < y < L/2 \\ 0 & \text{otherwise.} \end{cases}$$

These conditions define the rectangle function, so that  $\dot{w}(x, y, 0) = \Pi(x/L)\Pi(y/L)$ .

The transform of this can be found using Eq. (1.41),

$$\dot{W}(k_x, k_y, 0) = L^2 \operatorname{sinc}(k_x L/2) \operatorname{sinc}(k_y L/2), \quad (2.99)$$

and the directivity function is, from Eq. (2.86),

$$D(\theta, \phi) = \frac{-i\rho_0 c k L^2}{2\pi} \operatorname{sinc}\left(\frac{kL}{2} \sin \theta \cos \phi\right) \operatorname{sinc}\left(\frac{kL}{2} \sin \theta \sin \phi\right). \quad (2.100)$$

The following figure, Fig. 2.13, provides a linear plot of the Fourier transform of the square piston using a three-dimensional plot. The value at the center is unity ( $\dot{W}/L^2$  is plotted) and the levels are greatest along the coordinate axes, decaying rapidly from the center. Along the diagonals the decay is most rapid.

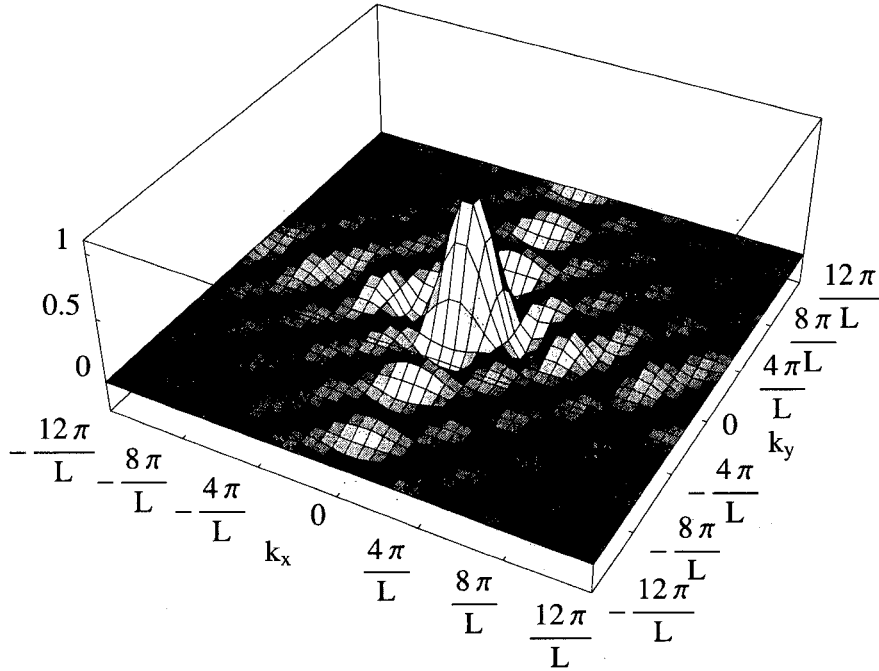


**Figure 2.13:** Surface plot of  $\operatorname{sinc}(k_x L/2) \operatorname{sinc}(k_y L/2)$ .

It is often desirable to plot the farfield on a dB scale, to show more dynamic range in the plot. Figure 2.14 is a contour plot of Eq. (2.99) using a logarithmic scale ( $20 \log_{10}[|\dot{W}|/L^2]$ ), cutoff at -40 dB. Ten contours are used to represent the region

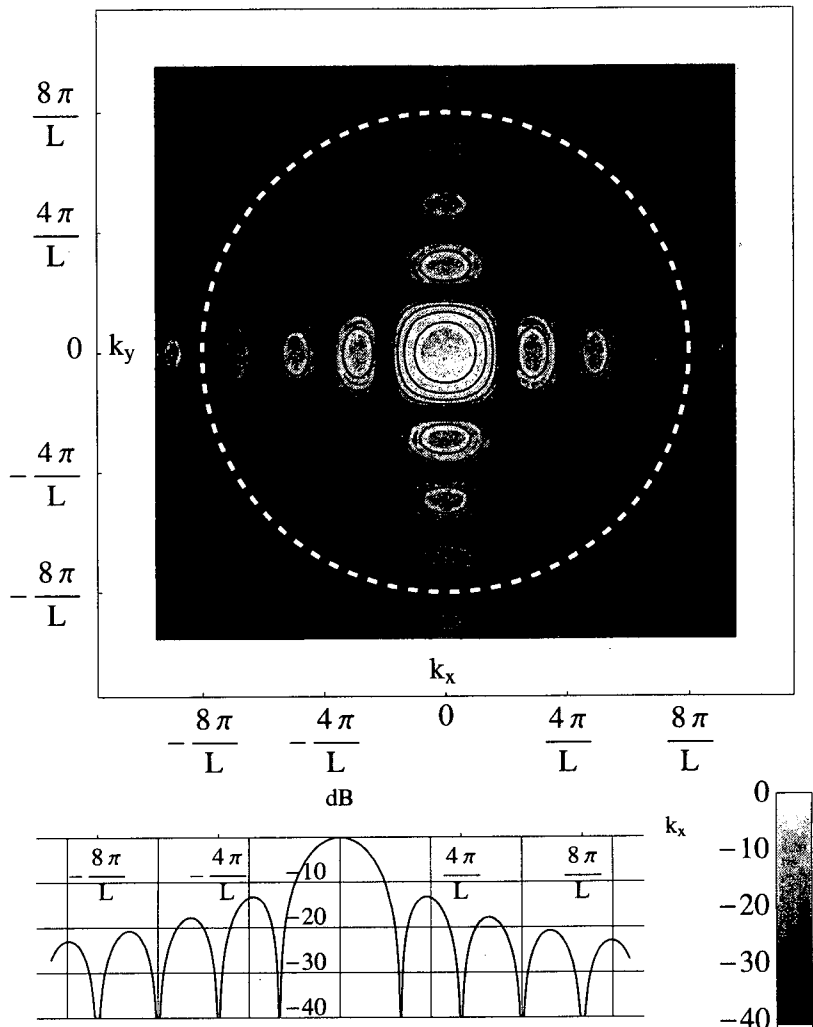


**Figure 2.14:** Logarithmic contour plot of the Fourier transform of square piston. The dashed circle has a radius  $k = 8\pi/L$ .

from  $-40$  to  $0$  dB, with a contour line every  $4$  dB. The gray scale plot indicates levels as shown in the key. The levels are distributed equally on the log scale. The bottom plot on the figure shows a horizontal slice through the center of the contour plot. The first sidelobe is at  $k_x L/2 = 3\pi/2$  and the level has dropped by  $-13.5$  dB from the maximum of the main lobe.

We can now use the Ewald sphere construction procedure to map out the farfield at any frequency using Fig. 2.14. In the following example we have chosen the frequency such that  $k = 8\pi/L$ . We draw a circle of this radius,  $k = 8\pi/L$ , on the  $k$ -space contour plot (Fig. 2.14). This circle is indicated by the dashed white circle. This circle serves as the equatorial base of the Ewald hemisphere shown in Fig. 2.15. A great semi-circle of that hemisphere is shown in the  $k_y = 0$  plane. We continue by projecting, as

indicated by the arrows, the values of the function, plotted on the base plane, vertically upwards to the hemisphere to determine the farfield directivity pattern. The values of the projections are plotted as a polar plot with a dB scale with the semi-circle as a base as shown in the figure. This polar plot above provides the levels of the farfield pressure in the corresponding direction (radially outward from the tips of the arrows). The conventional polar plot of the directivity is shown on the right in the figure for

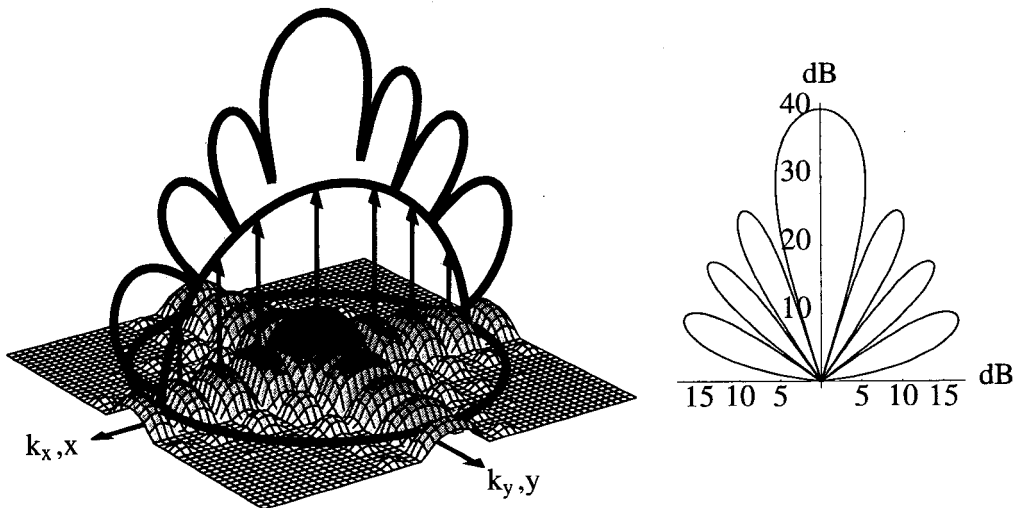


**Figure 2.15:** The Ewald sphere construction of the farfield from projection of Fig. 2.14 using a radius of  $k = 8\pi/L$ .

comparison. One can see that the main lobe, centered at the north pole, covers a fairly wide angle (about 35 degrees), and that the lowest levels correspond to the projected nulls in the surface plot below.

It is easy now to sketch directivity patterns for other frequencies by returning to Fig. 2.14 and drawing a circle for the desired frequency. We can see that at very low frequencies (small radius) there is very little variation in the transform in the circle so that the farfield would be nearly omnidirectional. Whereas at  $k = 8\pi/L$  the farfield will have three side lobes, as already shown in Fig. 2.15.

It is interesting to consider the limit as the square plate becomes infinite, since it should provide the same result as before; we expect a delta function directivity pattern to occur. This fact is illustrated in Fig. 2.14 if we make  $L$  large keeping  $k$  fixed. The function contracts towards the center, concentrating to a spot at the center in the limit. Indeed, as a result of Eq. (1.36),

$$\lim_{L \rightarrow \infty} L \operatorname{sinc}(k_x L/2) = \pi \delta(k_x). \quad (2.101)$$

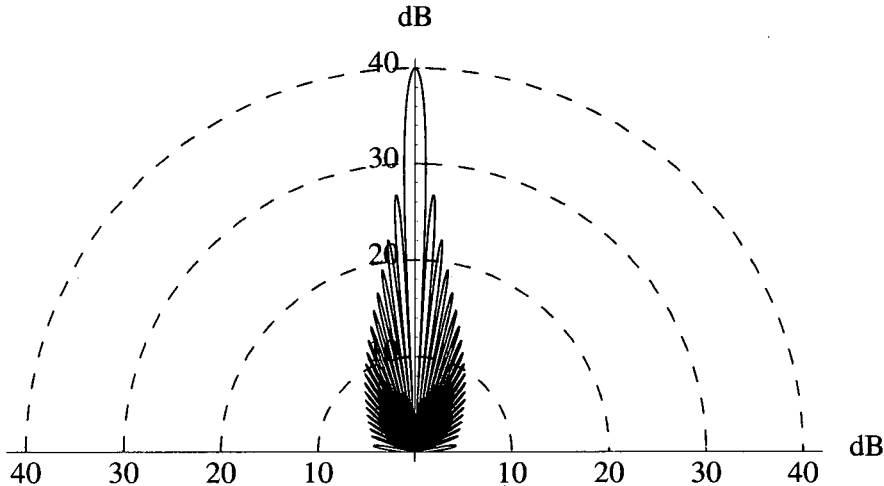


**Figure 2.16:** Directivity pattern of square plate along  $x$  axis for 20 wavelengths across length,  $k = 40\pi/L$ .

Thus the directivity pattern becomes a delta function located at  $k_x = 0$ , with infinite pressure at normal ( $\theta = 0$ ) and zero pressure at any other angle.

The same delta function directivity occurs if, instead of increasing  $L$ , we increase frequency. Figure 2.16 plots a high frequency case,  $k = 40\pi/L$ . It shows that the piston is very directive, approaching a delta function in directivity. In the Ewald sphere construction this case corresponds to a radiation circle five times the radius shown in Fig. 2.14.

#### 2.11.4 Baffled Square Plate with Traveling Wave

The example above was for a vibrator with no variation in velocity across its face. We will now see that vibrators with complicated vibration patterns can be studied easily from a knowledge of the piston results. To illustrate this we choose the simplest example, a square plate with a traveling wave vibration pattern in the  $x$  direction. The velocity on the surface is given by

$$\dot{w}(x, y, 0) = \begin{cases} \dot{w}_0 e^{ik_{x_0}x} & \text{if } -L/2 < x < L/2, \\ 0 & \text{otherwise.} \end{cases}$$

This is a somewhat unrealistic vibrator, since there are no waves traveling in the negative  $x$  direction, but mathematically simple.

We construct the Fourier transform by writing the surface velocity using the rectangle function of Section 1.6. This introduces the effect of the baffle. Thus

$$\dot{W}(k_x, k_y, 0) = \dot{w}_0 \int_{-\infty}^{\infty} \Pi(y/L) e^{-ik_y y} dy \int_{-\infty}^{\infty} \Pi(x/L) e^{ik_{x_0}x} e^{-ik_x x} dx.$$

The first integral is just  $L \operatorname{sinc}(k_y L/2)$  as before. The second integral is recognized as a product of two spatial functions, and thus we can use the  $k$ -space convolution theorem,

Eq. (1.15). The Fourier transform of  $e^{ik_{x0}x}$  is  $2\pi\delta(k_x - k_{x0})$ , given by Eq. (1.36), so that

$$\dot{W}(k_x, k_y, 0) = \dot{w}_0 L^2 \operatorname{sinc}(k_y L/2) (\operatorname{sinc}(k_x L/2) * \delta(k_x - k_{x0})).$$

The convolution with a delta function, Eq. (1.37), yields

$$\dot{W}(k_x, k_y, 0) = \dot{w}_0 L^2 \operatorname{sinc}(k_y L/2) \operatorname{sinc}((k_x - k_{x0})L/2). \quad (2.102)$$

From Eq. (2.96) then

$$\operatorname{sinc}[(k_x - k_{x0})L/2] = \operatorname{sinc}[kL/2(\sin \theta \cos \phi - \sin \theta_0 \cos \phi_0)]. \quad (2.103)$$

This result is similar to the square piston except that the main lobe in the  $x$  direction has been shifted off the normal to an angle given by  $k_{x0} = k \sin \theta_0$ . As long as  $k_{x0}$  is supersonic we can see that the Ewald construction provides a shifted main lobe and side lobes, with the main lobe pointing in the direction of  $\theta_0$ . Figure 2.17 presents the case for  $k_{x0} = k/2$ , or  $\theta_0 = 30$  degrees and  $\phi_0 = 0$ . Note that  $\phi = \pi$  is in the second quadrant of the plot. The phase velocity of the piston wave is  $c_{x0} = 2c$ , twice the velocity of sound in the fluid.

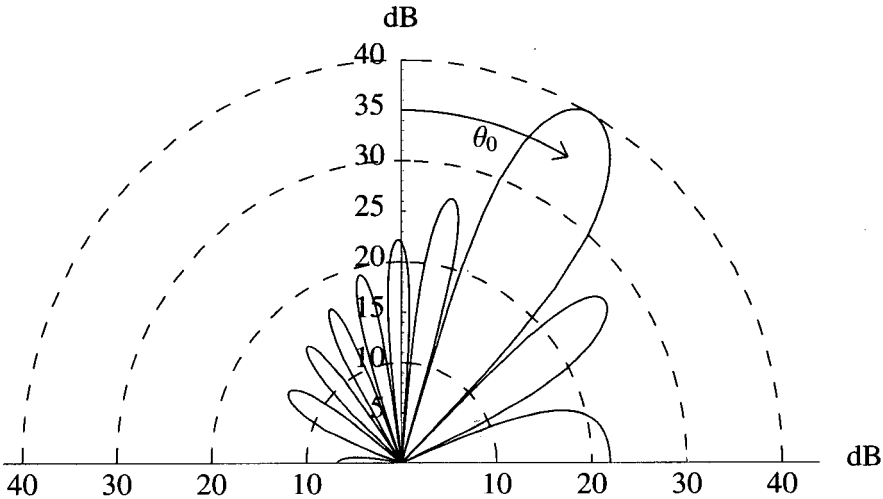


**Figure 2.17:** Traveling wave on baffled plate, for  $k_{x0} = k/2$  and  $k = 30/L$ .

If the traveling wave is just sonic so that  $k_{x0} = k$  (the phase velocity of the wave,  $c_{x0} = c$ ), we expect that the main lobe will now lie in the  $(x, y)$  plane. This condition represents beaming parallel to the plate. Figure 2.18 illustrates this case for  $k = 30/L$ .

The progression of the main lobe towards the horizon, as shown in Figs 2.17 and 2.18 indicates that as the wave traveling on the plate becomes subsonic, this main lobe will drop below the horizon. However, one can see that the side lobes remain above, radiating into the farfield. Thus, the subsonic wave is able to radiate to the farfield unlike the case of the infinite plate discussed in Section 2.7. This is an important phenomenon related to the truncation of the traveling wave at the baffle. We will discuss this in much more detail later when we encounter edge and corner modes of plate radiators.

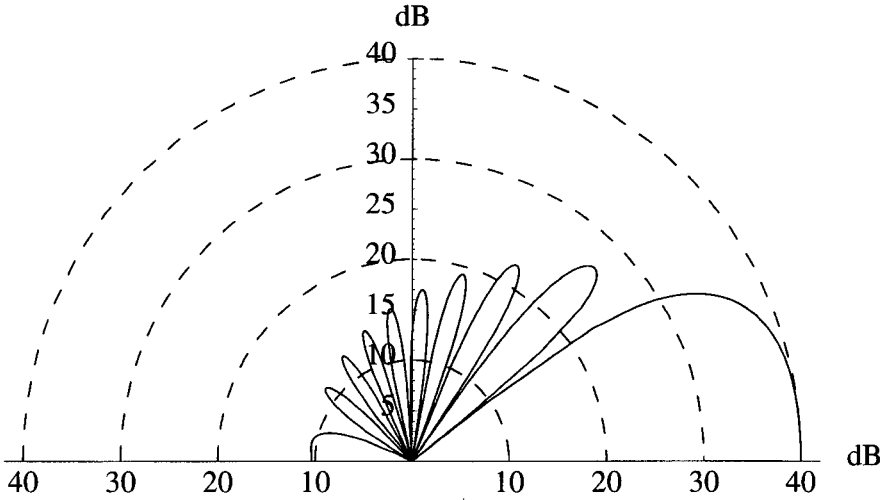


**Figure 2.18:** Traveling wave on baffled plate illustrating beaming in the horizontal plane,  $k_{x0} = k$  and  $k = 30/L$ .

### 2.11.5 Baffled Circular Piston

The vibration of a baffled circular piston of radius  $a$  located in the  $z = 0$  plane is defined by

$$\dot{w}(r, \phi) = \dot{w}(r) = \begin{cases} \dot{w}_0 & \text{if } 0 \leq r \leq a \\ 0 & \text{otherwise.} \end{cases}$$

The farfield radiation follows directly from Eq. (2.92) with  $n = 0$ :

$$\begin{aligned} D(\theta, \phi) &= -i\rho_0 ck \int_0^\infty \dot{w}(r) J_0(k_r r) r dr \\ &= -i\rho_0 ck \dot{w}_0 \int_0^a J_0(k_r r) r dr, \end{aligned}$$

where the link to the farfield is given by  $k_r = k \sin \theta$ . The indefinite integral over the Bessel function is well known,

$$\int J_0(x) x dx = x J_1(x), \quad (2.104)$$

so that

$$\int_0^a J_0(k_r r) r dr = \frac{a}{k_r} J_1(k_r a), \quad (2.105)$$

and thus

$$D(\theta, \phi) = -i\rho_0 c k a^2 \dot{w}_0 \frac{J_1(k_r a)}{k_r a}.$$

Given  $\pi a^2 \dot{w}_0 = Q_h$  (the volume velocity of the piston) then

$$D(\theta, \phi) = \frac{-i\rho_0 c k Q_h}{\pi} \frac{J_1(ka \sin \theta)}{ka \sin \theta}. \quad (2.106)$$

An example of the directivity pattern for a circular piston is shown in Fig. 2.19 where the logarithm of  $D$  is plotted for  $ka = 10$ . The maximum on the polar axis is set arbitrarily at 40 dB. Two side lobes arise at this value of  $ka$ . Using the Ewald sphere construction one can visualize  $D(\theta, \phi)$  at any frequency from the logarithmic plot of  $J_1(x)/x$  shown in Fig. 2.20.

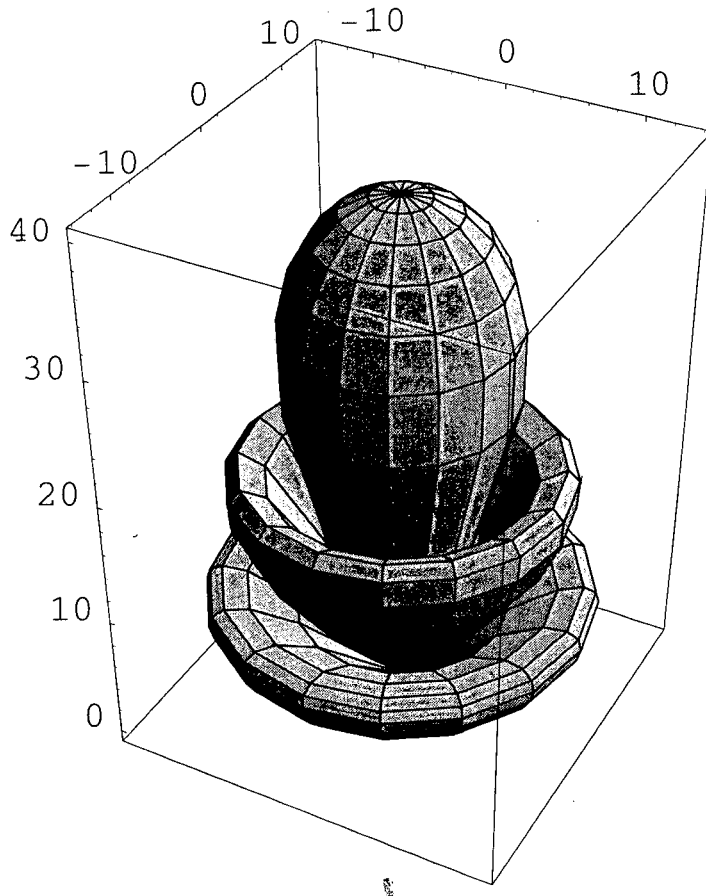


**Figure 2.19:** Logarithm of the directivity function for a circular piston,  $20\log_{10}(D)$  for  $ka = 10$ .

### 2.11.6 First Product Theorem for Arrays

We now derive the first product theorem which states: *the directivity pattern of an array of  $N$  identical (size and shape) radiators is equal to the product of the directivity pattern of one of the radiators times the transform of an array of  $N$  baffled point sources positioned at the centers of the original radiators (now removed) with the same relative amplitude and phases as the original radiators.*

To prove the first product theorem, let  $D_0(\theta, \phi)$  be the directivity pattern of one of the radiators in the array located, however, at the origin. Equation (2.86) shows that this pattern is proportional to  $Q_1 \dot{W}(k_x, k_y, 0)$ , the Fourier transform of the normal velocity distribution  $Q_1 \dot{w}(x, y, 0)$  across one radiator and its baffle. The other radiators

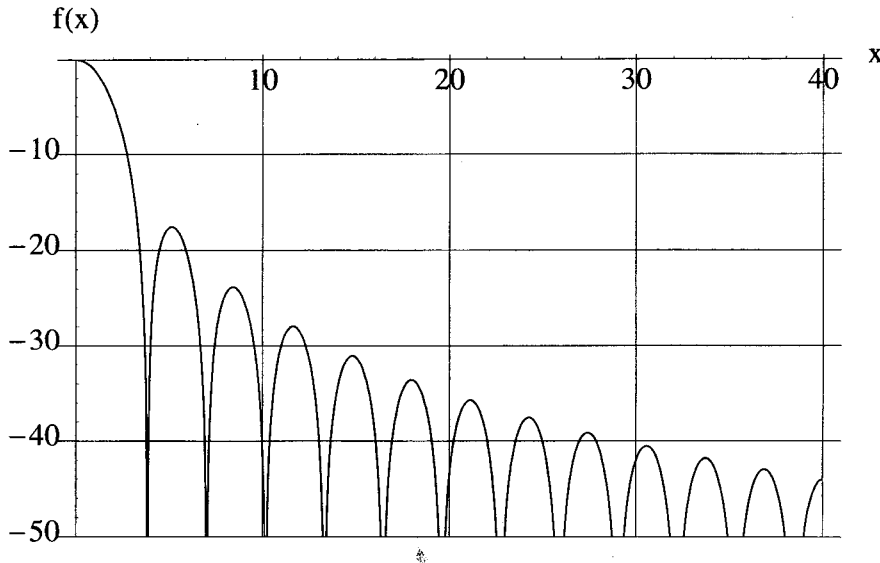


**Figure 2.20:** Logarithmic plot of  $f(x) = 20\log_{10}(|2J_1(x)/x|)$  which can be used to visualize the directivity function for  $ka < 40$ .

are replaced by the baffle.  $Q_1$  is the complex amplitude of one radiator. If we shift this radiator in the  $x$  and  $y$  directions by an amount  $(x_n, y_n)$ , and let it have a different amplitude of vibration,  $Q_n$ , then the velocity of the shifted radiator is  $Q_n \dot{w}(x-x_n, y-y_n, 0)$  and the directivity is (by the shift theorem)  $Q_n \dot{W}(k_x, k_y, 0) e^{-ik_x x_n} e^{-ik_y y_n}$ . If we consider a collection of  $N$  of these radiators, all identical in geometry then by superposition the farfield pressure would be

$$D(\theta, \phi) = \frac{-i\rho_0 ck}{2\pi} \dot{W}(k_x, k_y, 0) \sum_{n=1}^N Q_n e^{-ik_x x_n} e^{-ik_y y_n}. \quad (2.107)$$

Referring back to Section 2.10.1 on page 37, we recognize  $Q_n e^{-ik_x x_n} e^{-ik_y y_n}$  as the transform of a point source with strength  $Q_n$  located at the point  $(x_n, y_n)$ , that is,  $\delta(x - x_n)\delta(y - y_n)$ . Thus,

$$\sum_{n=1}^N Q_n e^{-ik_x x_n} e^{-ik_y y_n},$$

represents the transform of a sum of point sources of complex strengths given by  $Q_n$  located at the positions of the original, physically identical radiators. Equation (2.107) represents a statement of the **first product theorem**: the directivity pattern of an array of like vibrators is the product of the directivity pattern of one of the radiators (with unit amplitude) with the sum of  $N$  point sources located at the positions of the original  $N$  radiators. This completes the proof of the first product theorem.

### Example: Two Baffled Square Pistons

Consider two identical square pistons located on the  $x$  axis and separated by a distance  $d$ , as shown in Fig. 2.21. Assume that they are vibrating 180 degrees out of phase with

respect to one another but with equal amplitudes. Thus we set  $Q_1 = 1$  and  $Q_2 = -1$ . If  $D_0$  is the directivity pattern of a square piston of width  $L$ , centered on the origin.

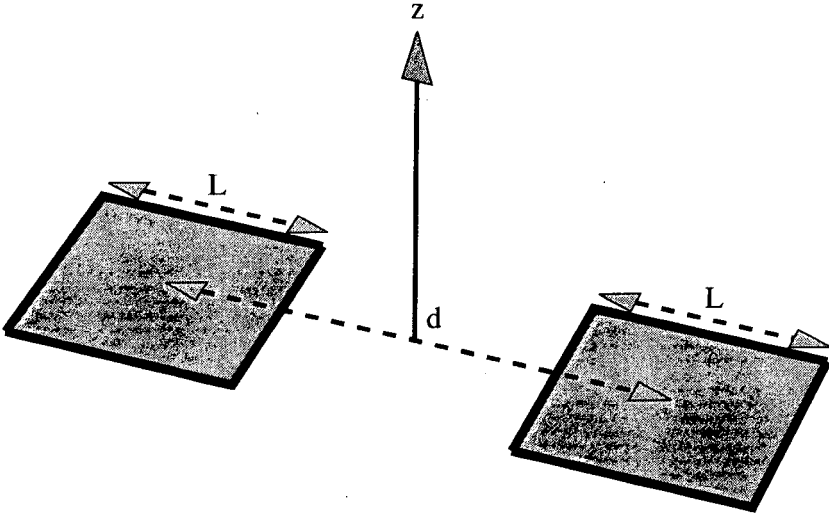


**Figure 2.21:** Two baffled square pistons on the  $x$  axis, each of length  $L$  and separated by a distance  $d$ .

The first product theorem takes the form

$$D(\theta, \phi) = D_0(\theta, \phi)(e^{ik_x d/2} - e^{-ik_x d/2}),$$

since the point sources are located at  $x = \pm d/2$ ,  $y = 0$ . Thus

$$D(\theta, \phi) = 2iD_0(\theta, \phi) \sin(k_x d/2)$$

and since the directivity pattern of a square piston centered at the origin, Eq. (2.99), is

$$D_0(\theta, \phi) = \frac{-i\rho_0 ckL^2}{2\pi} \operatorname{sinc}(k_x L/2) \operatorname{sinc}(k_y L/2),$$

then

$$\begin{aligned} D(\theta, \phi) &= \frac{\rho_0 ckL^2}{\pi} \operatorname{sinc}(k_x L/2) \operatorname{sinc}(k_y L/2) \sin(k_x d/2) \\ &= \frac{\rho_0 ckL^2}{\pi} \operatorname{sinc}(kL/2 \sin \theta \cos \phi) \sin(kd/2 \sin \theta \cos \phi) \operatorname{sinc}(kL/2 \sin \theta \sin \phi). \end{aligned} \quad (2.108)$$

The directivity pattern of the single piston is modulated by the sine term with the amount of modulation depending on the distance between the pistons. When  $d$  is small (pistons overlapping) the opposing motions of the pistons cancel and the radiation is nearly extinguished. At the angle of maximum radiation from the single piston ( $\theta = 0$ ), the dipole pair has a null for any  $d$  and  $k$ .

## 2.12 Radiated Power

The total power radiated into a half-space from planar radiators is given by the normal acoustic intensity integrated over the area of the vibrating region. For baffled radiators this region,  $S$ , is finite, covering only the non-baffled area, otherwise the area  $S$  is infinite. From Eq. (2.17), with  $ds = dx dy$  we have

$$\Pi(\omega) = 1/2 \iint_S \operatorname{Re} [p(x, y, 0) \dot{w}^*(x, y, 0)] ds. \quad (2.109)$$

Inserting the angular spectrum representations (see Eq. (2.51)),

$$p(x, y, 0) = \frac{1}{4\pi^2} \int_{-\infty}^{\infty} \int_{-\infty}^{\infty} P(k_x, k_y, 0) e^{i(k_x x + k_y y)} dk_x dk_y$$

and

$$\dot{w}^*(x, y, 0) = \frac{1}{4\pi^2} \int_{-\infty}^{\infty} \int_{-\infty}^{\infty} \dot{W}^*(k'_x, k'_y, 0) e^{-i(k'_x x + k'_y y)} dk'_x dk'_y,$$

and the delta function relation (see Eq. (1.5))

$$\frac{1}{4\pi^2} \int_{-\infty}^{\infty} \int_{-\infty}^{\infty} e^{i(k_x - k'_x)x} e^{i(k_y - k'_y)y} dx dy = \delta(k_x - k'_x) \delta(k_y - k'_y) \quad (2.110)$$

into Eq. (2.109), yields

$$\Pi(\omega) = \frac{1}{8\pi^2} \operatorname{Re} \left[ \int_{-\infty}^{\infty} \int_{-\infty}^{\infty} P(k_x, k_y, 0) \dot{W}^*(k_x, k_y, 0) dk_x dk_y \right].$$

Using Eq. (2.61) with  $z = z' = 0$ ,

$$P(k_x, k_y, 0) = \frac{\rho_0 c k}{k_z} \dot{W}(k_x, k_y, 0),$$

the equation for power becomes,

$$\Pi(\omega) = \frac{\rho_0 c k}{8\pi^2} \operatorname{Re} \left( \int_{-\infty}^{\infty} \int_{-\infty}^{\infty} \frac{|\dot{W}(k_x, k_y, 0)|^2}{\sqrt{k^2 - k_x^2 - k_y^2}} dk_x dk_y \right). \quad (2.111)$$

If  $S_r$  is the area inside and including the radiation circle defined by

$$\int_{S_r} dk_x dk_y \equiv \int_{-k}^k dk_y \int_{-\sqrt{k^2 - k_y^2}}^{\sqrt{k^2 - k_y^2}} dk_x, \quad (2.112)$$

then, since the integrand is imaginary outside of  $S_r$ , we can rewrite this integral restricting the limits of the integration:

$$\Pi(\omega) = \frac{\rho_0 c k}{8\pi^2} \iint_{S_r} \frac{|\dot{W}(k_x, k_y, 0)|^2}{\sqrt{k^2 - k_x^2 - k_y^2}} dk_x dk_y. \quad (2.113)$$

Equation (2.113) provides a means of computing the power radiated by a source from a knowledge of the angular spectrum of its normal surface velocity. As we have seen before, only the part of the angular spectrum within the radiation circle radiates to the farfield, and thus only this part contributes to the integrand in Eq. (2.113).

There is a very interesting counterpart to Eq. (2.113) in the space domain, but is less well-known and seems to have been first provided by Bouwkamp:<sup>8</sup>

$$\Pi(\omega) = \frac{\rho_0 c k}{4\pi} \iint_S \iint_{S'} \dot{w}(x', y', 0) \frac{\sin(kR)}{R} \dot{w}^*(x, y, 0) ds ds', \quad (2.114)$$

where  $R \equiv |\vec{r} - \vec{r}'|$  is defined in the same way as in Rayleigh's integrals (Section 2.10) and  $ds' = dx' dy'$  is integrated over the infinite surface  $S'$ .

To prove this relationship consider the following. Equation (2.111) can be written as

$$\Pi(\omega) = \frac{\rho_0 c k}{8\pi^2} \int_{-\infty}^{\infty} \int_{-\infty}^{\infty} |\dot{W}(k_x, k_y, 0)|^2 \operatorname{Re}\left(\frac{1}{k_z}\right) dk_x dk_y.$$

Inserting  $e^{i(k_x x + k_y y)} \Big|_{x=y=0}$  into the integrand,

$$\Pi(\omega) = \frac{\rho_0 c k}{8\pi^2} \int_{-\infty}^{\infty} \int_{-\infty}^{\infty} \dot{W}(k_x, k_y, 0) \dot{W}^*(k_x, k_y, 0) \operatorname{Re}\left(\frac{1}{k_z}\right) e^{i(k_x x + k_y y)} dk_x dk_y \Big|_{x=y=0},$$

where the exponential has been added to make the integral look like an inverse Fourier transform (evaluated at the origin). This integral has the form

$$\mathcal{I} = \mathcal{F}_x^{-1} \mathcal{F}_y^{-1} [\dot{W} \{ \dot{W}^* \operatorname{Re}(1/k_z) \}] \Big|_{x=y=0},$$

where

$$\Pi(\omega) = \frac{\rho_0 c k}{2} \mathcal{I}.$$

Using the inverse Fourier transform of the convolution theorem, Eq. (1.19), we have

$$\mathcal{I} = \dot{w}(x, y, 0) \ast \ast \left( w^*(-x, -y, 0) \ast \ast \mathcal{F}_x^{-1} \mathcal{F}_y^{-1} [\operatorname{Re}(1/k_z)] \right),$$

where we have used the following to derive the inverse transform of  $\dot{W}^*$ :

$$\begin{aligned} \frac{1}{4\pi^2} \iint \dot{W}^*(k_x, k_y) e^{i(k_x x + k_y y)} dk_x dk_y &= \left( \frac{1}{4\pi^2} \iint \dot{W}(k_x, k_y) e^{ik_x(-x) + ik_y(-y)} dk_x dk_y \right)^* \\ &= \dot{w}^*(-x, -y, 0). \end{aligned}$$

The inverse transform of  $1/k_z$  is found from Weyl's integral with  $z = r' = 0$  (Eq. (2.74) and Eq. (2.70)):

$$-i \frac{e^{ikr}}{2\pi r} = \mathcal{F}_x^{-1} \mathcal{F}_y^{-1} \left[ \frac{1}{k_z} \right]. \quad (2.115)$$

<sup>8</sup>C. J. Bouwkamp (1970). "Theoretical and Numerical Treatment of Diffraction Through a Circular Aperture," IEEE Trans. Antennas Propag., **AP-18**, pp. 152–176.

To determine the inverse transform of  $\text{Re}[1/k_z]$  we need to draw upon a theorem about Fourier transforms.<sup>9</sup>  $f(x)$  can be split unambiguously into an even and odd function,

$$f(x) = e(x) + o(x) \quad (2.116)$$

where  $e$  and  $o$  are even and odd functions, respectively. Its transform  $F(k_x)$  is then

$$F(k_x) = E(k_x) + O(k_x), \quad (2.117)$$

where  $E$  and  $O$  are even and odd functions in transform space. It is straightforward to show, using

$$\text{Re} \left[ \frac{-ie^{ikr}}{2\pi r} \right] = \frac{\sin kr}{2\pi r},$$

that

$$\text{Re}[E(k_x)] = \mathcal{F}_x[\text{Re}(e(x))], \quad (2.118)$$

$$\text{Im}[E(k_x)] = \mathcal{F}_x[\text{Im}(e(x))]. \quad (2.119)$$

The same result can be applied to two-dimensional even functions and for the inverse Fourier transform. Thus, since  $k_z$  is even in  $k_x$  and  $k_y$ , Eq. (2.115) can be written as

$$\text{Re} \left( -i \frac{e^{ikr}}{2\pi r} \right) = \mathcal{F}_x^{-1} \mathcal{F}_y^{-1} \left[ \text{Re} \left( \frac{1}{k_z} \right) \right], \quad (2.120)$$

so that

$$\mathcal{I} = \dot{w}(x, y, 0) * * \left( \dot{w}^*(-x, -y, 0) * * \frac{\sin(kr)}{2\pi r} \right) \Big|_{x=y=0}, \quad (2.121)$$

where  $r = \sqrt{x^2 + y^2}$ . This is essentially the final result, although the convolutions need to be written out in order to compare with Eq. (2.114). To help in the untangling of the multiple convolutions we write the one-dimensional equivalent in general terms,

$$f(x) * \{g(x) * h(x)\} \equiv f(x) * \int dx' g(x') h(x - x') \equiv f(x) * q(x),$$

where

$$q(x) \equiv \int dx' g(x') h(x - x').$$

Thus, remembering that the result of the convolutions is a function of  $x$  only,

$$\begin{aligned} f(x) * \{g(x) * h(x)\} &\equiv f(x) * q(x) \equiv \int dx'' f(x'') q(x - x'') \\ &= \int dx'' f(x'') \int dx' g(x') h(x - x'' - x'). \end{aligned} \quad (2.122)$$

Finally, returning to the expression for  $\mathcal{I}$  we have

$$\mathcal{I} = \int_{-\infty}^{\infty} \int_{-\infty}^{\infty} dx'' dy'' \int_{-\infty}^{\infty} \int_{-\infty}^{\infty} dx' dy' w(x'', y'', 0) w^*(-x', -y', 0) \frac{\sin(k\bar{R})}{2\pi\bar{R}} \Big|_{x=y=0}$$

<sup>9</sup>R. N. Bracewell (1978). *The Fourier Transform and Its Application*. McGraw-Hill, New York, 2nd ed., p. 14.

where  $\bar{R} = \sqrt{(x - x'' - x')^2 + (y - y'' - y')^2}$ . Therefore, noting that substituting  $x'$  for  $-x'$  and  $y'$  for  $-y'$  does not change the value of the integrals, the final result for the radiated power is

$$\Pi(\omega) = \frac{\rho_0 ck}{4\pi} \int_{-\infty}^{\infty} \int_{-\infty}^{\infty} dx'' dy'' \int_{-\infty}^{\infty} \int_{-\infty}^{\infty} dx' dy' w(x'', y'', 0) w^*(x', y', 0) \frac{\sin(kR')}{R'}, \quad (2.123)$$

where  $R' = \sqrt{(x' - x'')^2 + (y' - y'')^2}$ . This completes the proof of Eq. (2.114).

### 2.12.1 Low Frequency Expansion

This formula, Eq. (2.114), is extremely useful in deriving a low frequency series expression for the power radiated from a planar vibrator.<sup>10</sup> We can expand  $\sin(kR)/R$  in a MacLaurin series

$$\sin(kR)/R = \sum_{m=0}^{\infty} \frac{k^{2m+1}}{(2m+1)!} (-1)^m [(x - x')^2 + (y - y')^2]^m. \quad (2.124)$$

Furthermore, we can expand the term  $[(x - x')^2 + (y - y')^2]^m$  using the binomial theorem,

$$[(x - x')^2 + (y - y')^2]^m = \sum_{l=0}^m \binom{m}{l} (x - x')^{2m-2l} (y - y')^{2l}, \quad (2.125)$$

where

$$\binom{m}{l} \equiv \frac{m!}{l!(m-l)!}. \quad (2.126)$$

With a little effort we finally arrive at

$$\begin{aligned} \Pi(\omega) &= \frac{\rho_0 c}{4\pi} \sum_{m=0}^{\infty} \sum_{l=0}^m \sum_{p=0}^{2m-2l} \sum_{q=0}^{2l} \frac{k^{2m+2}}{(2m+1)!} \binom{m}{l} \binom{2m-2l}{p} \binom{2l}{q} \\ &\quad \times [(\frac{\partial}{\partial k_x})^{2m-2l-p} (\frac{\partial}{\partial k_y})^{2l-q} \dot{W}^*(k_x, k_y, 0)] \\ &\quad \times [(\frac{\partial}{\partial k_x})^p (\frac{\partial}{\partial k_y})^q \dot{W}(k_x, k_y, 0)] \Big|_{k_x=k_y=0}. \end{aligned} \quad (2.127)$$

In particular, for example, the low frequency limit has one term ( $m = 0$ ) yielding

$$\Pi_0 = \frac{\rho_0 ck^2}{4\pi} |\dot{W}(0, 0, 0)|^2. \quad (2.128)$$

The low frequency power can be related to the volume flow of the radiator,  $Q_h$ , by recognizing that the forward transform is

$$\dot{W}(0, 0, 0) = \iint \dot{w}(x, y, 0) dx dy \equiv Q_h, \quad (2.129)$$

<sup>10</sup>E. G. Williams (1983). "A series expansion of the acoustic power radiated from planar sources", J. Acoust. Soc. Am., **73**, pp. 1520–1524.

so that Eq. (2.128) becomes

$$\Pi_0 = \frac{\rho_0 c k^2}{4\pi} |Q_h|^2. \quad (2.130)$$

## 2.13 Vibration and Radiation from an Infinite Point-driven Plate

Mathematical models of some simple vibrating structures are invaluable in the application of NAH to practical vibration/radiation problems. These models help in the understanding of  $k$ -space and its physical significance. Outside of NAH these models are essential for understanding the vibration and radiation from more complex physical structures. Point driven structures occur quite often in practice. To gain some understanding of the radiation fields we study the infinite plate excited at a point with a known force. We present the equation of motion of a vibrating plate without derivation since this is not within the scope of this text.

Let  $w(x, y, 0)$  be the normal displacement of the plate and let a point force excite the plate at the origin. The differential equation for the plate motion which must be solved is of fourth order. Let the plate be driven by a point force of magnitude  $F$  at the point  $(x, y, z) = (0, 0, 0^-)$  and be loaded with the acoustic fluid on the top side  $z = 0^+$ , with a vacuum on the bottom side. If  $p_a(x, y, t)$  is the pressure of the fluid acting on the plate, then

$$D \left( \frac{\partial^4 w}{\partial x^4} + 2 \frac{\partial^4 w}{\partial x^2 \partial y^2} + \frac{\partial^4 w}{\partial y^4} \right) + \rho_s h \frac{\partial^2 w}{\partial t^2} = F(t) \delta(x) \delta(y) - p_a(x, y, t), \quad (2.131)$$

where  $D$  is the flexural rigidity of the plate given by

$$D = \frac{Eh^3}{12(1-\nu^2)}, \quad (2.132)$$

$E$  is Young's modulus,  $\nu$  is Poisson's ratio,  $h$  is the thickness of the plate and  $\rho_s$  is the density of the plate. For convenience we will need Skudrzyk's plate constant<sup>11</sup>  $\alpha$  which we will use later:

$$\alpha \equiv \left( \frac{D}{\rho_s h} \right)^{1/4} = \left( \frac{Eh^2}{12\rho_s(1-\nu^2)} \right)^{1/4}. \quad (2.133)$$

The plate equation of motion is almost never solved in the time domain. If one assumes that the time dependence is given as usual by  $e^{-i\omega t}$  then Eq. (2.131) becomes (where  $w$  and  $p_a$  are functions of  $\omega$  now)

$$D \left( \frac{\partial^4 w}{\partial x^4} + 2 \frac{\partial^4 w}{\partial x^2 \partial y^2} + \frac{\partial^4 w}{\partial y^4} \right) - \rho_s h \omega^2 w = F(\omega) \delta(x) \delta(y) - p_a(x, y). \quad (2.134)$$

---

<sup>11</sup>Eugen Skudrzyk (1968). *Simple and Complex Vibratory Systems*. The Pennsylvania State University Press, University Park, PA.

Since the point drive at the origin dictates circular symmetry we can write the equation of motion in polar coordinates with the transformation

$$\begin{aligned} x &= r \cos \phi \\ y &= r \sin \phi \\ x^2 + y^2 &= r^2. \end{aligned}$$

Note that we are using  $r$  instead of  $\rho$  here, and the context of the development should prevent any confusion with the definition of  $r$  used up to now. Given that the normal displacement  $w(x, y) \rightarrow w(r)$  the equation of motion becomes

$$D \left( \frac{d^2}{dr^2} + \frac{d}{r dr} \right)^2 w - \rho_s h \omega^2 w = F(\omega) \frac{\delta(r)}{2\pi r} - p_a(r), \quad (2.135)$$

where the shorthand notation is used for the derivatives:

$$\left( \frac{d^2}{dr^2} + \frac{d}{r dr} \right)^2 \equiv \left( \frac{d^2}{dr^2} + \frac{d}{r dr} \right) \left( \frac{d^2}{dr^2} + \frac{d}{r dr} \right).$$

To simplify the solution we assume light fluid loading,  $p_a(r) \approx 0$ , so that the pressure term in Eq. (2.135) can be ignored. The solution to the resulting equation is well known. It is obtained by use of the Hankel transform pair, Section 1.4. That is,

$$W(k_r) \equiv \int_0^\infty w(r) J_0(k_r r) r dr, \quad (2.136)$$

and

$$w(r) = \int_0^\infty W(k_r) J_0(k_r r) k_r dk_r \equiv \mathcal{B}^{-1}[W(k_r)]. \quad (2.137)$$

We will find in Chapter 4 (from Eqs (4.13) and (4.17)) that

$$\left( \frac{d^2}{dr^2} + \frac{d}{r dr} \right) J_0(k_r r) = -k_r^2 J_0(k_r r).$$

Thus applying the differential operators to Eq. (2.137) yields

$$\begin{aligned} \left( \frac{d^2}{dr^2} + \frac{d}{r dr} \right) w(r) &= \int_0^\infty W(k_r) \left( \frac{d^2}{dr^2} + \frac{d}{r dr} \right) J_0(k_r r) k_r dk_r \\ &= \int_0^\infty W(k_r) (-k_r^2) J_0(k_r r) k_r dk_r \end{aligned}$$

which, written in shorthand, is

$$\mathcal{B}^{-1}[-k_r^2 W(k_r)] = \frac{d^2 w(r)}{dr^2} + \frac{1}{r} \frac{dw(r)}{dr}.$$

Inverting this equation (writing as a forward transform) yields

$$\int_0^\infty \left( \frac{d^2 w(r)}{dr^2} + \frac{1}{r} \frac{dw(r)}{dr} \right) J_0(k_r r) r dr = -k_r^2 W(k_r),$$

so that the Hankel transform of Eq. (2.135) leads to the simple result:

$$W(k_r) = \frac{F(\omega)}{2\pi D(k_r^4 - k_f^4)}, \quad (2.138)$$

where  $k_f$  is the free wavenumber of the plate,

$$k_f = (m_s \omega^2 / D)^{1/4}, \quad (2.139)$$

and  $m_s = \rho_s h$  is the mass per unit area of the plate. The normal velocity is

$$\dot{W}(k_r) = \frac{-i\omega F}{2\pi D(k_r^4 - k_f^4)}. \quad (2.140)$$

Note that the free wavenumber of the plate is dispersive, depending on  $\sqrt{\omega}$ . The dispersion equation is simply, using Eq. (2.133),

$$k_f = \frac{\sqrt{\omega}}{\alpha}. \quad (2.141)$$

The inverse Hankel transform of Eq. (2.138), provides the solution for the displacement:

$$w(r) = \frac{F}{2\pi D} \int_0^\infty \frac{J_0(k_r r)}{(k_r^4 - k_f^4)} k_r dk_r. \quad (2.142)$$

This integral can be solved by using contour integration and residue evaluation. Towards that end we extend the integral to  $-\infty$  by noting that (Eq. (4.20))

$$\begin{aligned} J_0(x) &= \frac{1}{2} H_0^{(1)}(x) + \frac{1}{2} H_0^{(2)}(x) \\ &= \frac{1}{2} H_0^{(1)}(x) - \frac{1}{2} H_0^{(1)}(-x), \end{aligned} \quad (2.143)$$

since  $H_0^{(1)}(-x) = -H_0^{(2)}(x)$ . Equation (2.142) becomes

$$w(r) = \frac{F}{4\pi D} \int_{-\infty}^\infty \frac{H_0^{(1)}(k_r r)}{(k_r^4 - k_f^4)} k_r dk_r. \quad (2.144)$$

The important point regarding the contour integration is the fact that the residues are determined from the zeros of the denominator of Eq. (2.144), that is, the poles of the  $k$ -space velocity (Eq. (2.140)). Generally the poles are related to the wave types which are free to travel on the structure, being independent of the forcing function driving the plate. In this case the poles are given by  $k_r^4 - k_f^4 = 0$  which has the four solutions  $k_r = \pm k_f$  and  $k_r = \pm ik_f$ .

Recall that from residue theory at each of the simple poles  $x_0$

$$\oint F(x) dx = 2\pi i R(x_0),$$

where the residue  $R(x_0) = \lim_{x \rightarrow x_0} [(x - x_0)F(x)]$ . Using this fact with the poles  $k_r = k_f$  and  $k_r = ik_f$  within the closed contour, and  $\dot{w} = -i\omega w$ , Eq. (2.144) becomes,

$$\dot{w}(r) = \frac{F}{8\alpha^2 m_s} \left[ H_0^{(1)}(k_f r) - H_0^{(1)}(ik_f r) \right],$$

where  $\alpha$  was given in Eq. (2.133). The second solution,  $H_0^{(1)}(ik_f r)$  is equivalent to a MacDonald function (Eq. (4.34)):

$$H_0^{(1)}(ik_f r) = \frac{-2i}{\pi} K_0(k_f r) \quad (2.145)$$

so that the complete solution in physical space has the form

$$\dot{w}(r) = \frac{F}{8\alpha^2 m_s} \left[ H_0^{(1)}(k_f r) + \frac{2i}{\pi} K_0(k_f r) \right]. \quad (2.146)$$

Equation (2.143) indicates that at  $r = 0$  the term in the square bracket above is unity (since  $J_0(0) = 1$ ) so that

$$\dot{w}(0) = F/(8\alpha^2 m_s). \quad (2.147)$$

The Hankel function provides the free wave solution, a cylindrical wave traveling outward from the origin, and the decaying MacDonald function provides the flexural nearfield. Whereas the Hankel function is complex, the MacDonald function is purely real. Figure 2.22 is a plot of the imaginary part of the traveling wave solution,  $H_0^{(1)}(k_f r)$ ,

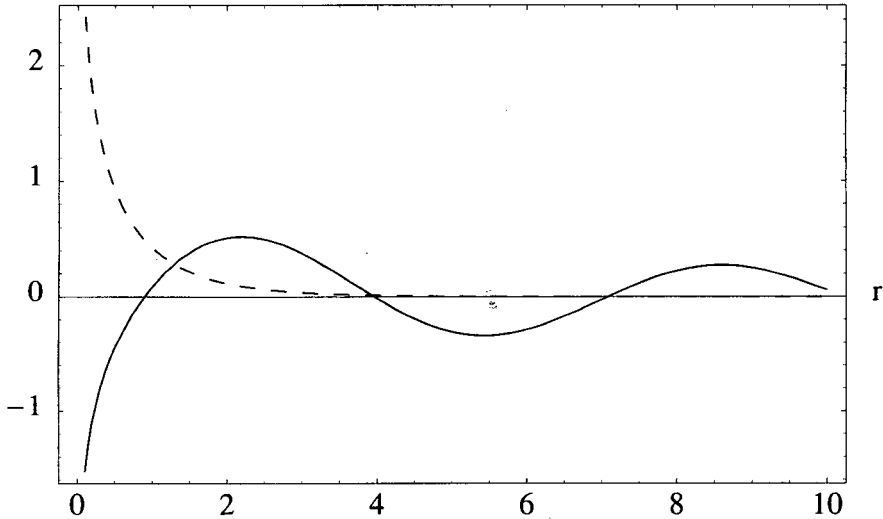


**Figure 2.22:** Traveling wave solution,  $\text{Im}[H_0(k_f r)]$  (solid line) compared to flexural wave nearfield,  $K_0(k_f r)$  (dashed line) for  $k_f = 1$ . The nearfield exists only close to the drive-point. Both curves blow up at  $r = 0$ .

compared with the flexural nearfield,  $K_0(k_f r)$ . The asymptotic versions of these two functions (Eqs (4.22) and (4.39)) clearly indicate the wave types:

$$H_0^{(1)}(k_f r) \rightarrow \sqrt{\frac{2}{\pi k_f r}} e^{i(k_f r - \pi/4)}, \quad (2.148)$$

and

$$K_0(k_f r) \rightarrow \sqrt{\frac{\pi}{2k_f r}} e^{-k_f r}, \quad (2.149)$$

both valid for large values of  $k_f r$ .

The plate solution also provides a very useful structural formula, given in Eq. (2.147); the drive-point impedance of a plate is

$$Z_p \equiv F/\dot{w}(0) = 8\alpha^2 m_s. \quad (2.150)$$

Associated with the free wavenumber is the phase velocity of the flexural (bending) wave defined through

$$k_f = \omega/c_b. \quad (2.151)$$

Thus Eq. (2.141) leads to

$$c_b = \alpha\sqrt{\omega}. \quad (2.152)$$

Note that the bending wave phase velocity  $c_b$  is dispersive since it depends on frequency.

### 2.13.1 Farfield Radiation

The farfield directivity pattern is determined from Eq. (2.140) and the Ewald sphere construction process, Section 2.11.2. To obtain the farfield we saw in Section 2.11.1 that we must make the replacement,  $k_r = k \sin \theta$ . Thus the pressure in the farfield is

$$p(r, \theta, \phi) = \frac{-i\rho_0 ck}{2\pi} \frac{e^{ikr}}{r} \dot{W}(k_r) = \frac{-i\rho_0 ck}{2\pi} \frac{e^{ikr}}{r} \dot{W}(k \sin \theta). \quad (2.153)$$

The  $k$ -space velocity  $\dot{W}(k_r)$  is plotted in Fig. 2.23. It is interesting to note that the  $k$ -space velocity is infinite when the radial wavenumber equals the free wavenumber in the plate. This forms a circle in  $k$ -space, representing a locus of possible values for the free, flexural waves traveling in the plate. If the radiation circle,  $k_r = k$ , is located outside of this free wavenumber circle,  $k > k_f$  (supersonic free wavenumber), then we can see that the dominant plate radiation is at a polar angle  $\theta_0$  given by

$$\sin \theta_0 = k_f/k.$$

The farfield pressure is infinite at  $\theta = \theta_0$ . The radiation pattern is circumferentially symmetric, since  $\dot{W}$  is independent of angle.

We can write the  $k$ -space normal velocity in partial fraction form,

$$\dot{W}(k_r) = \frac{-i\omega F}{2\pi D(k_r^4 - k_f^4)} = \frac{-i\omega F}{2\pi D k_f^2} \left[ \frac{1}{(k_r^2 - k_f^2)} - \frac{1}{(k_r^2 + k_f^2)} \right]. \quad (2.154)$$

The radiation from the plate consists of two similar terms, differing by a minus sign. Each of these terms represents a wave type. The first term corresponds to a diverging wave from the origin of the plate, and the second to an exponentially decaying wave; as we have seen, the inverse Hankel transform results in  $H_0^{(1)}(k_r r)$  and  $H_0^{(1)}(ik_r r)$  for each of these terms, respectively. Thus returning to Fig. 2.23 we see that a traveling

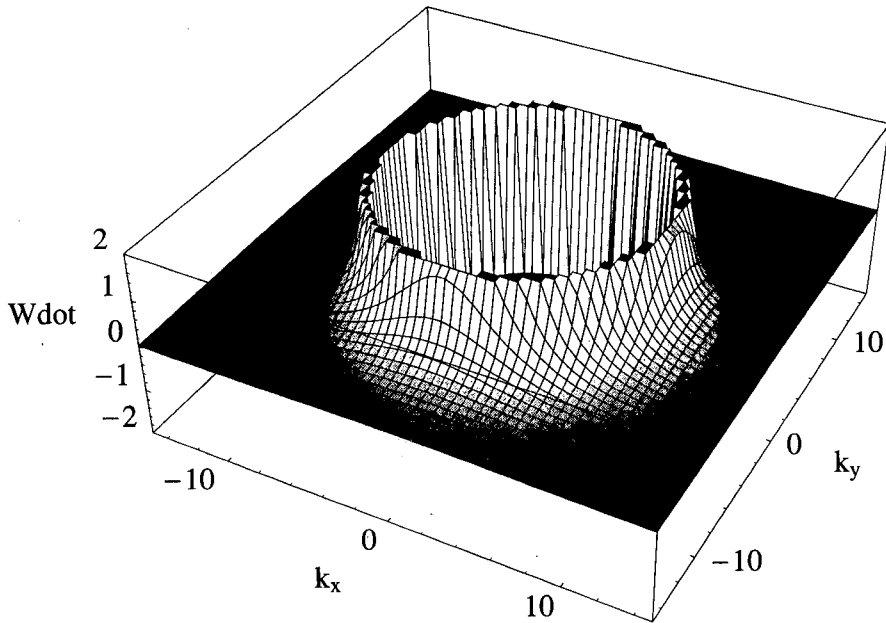


**Figure 2.23:**  $k$ -space diagram for an infinite, point-driven plate. The  $k$ -space velocity is infinite when  $k_r = k_f$  as indicated by the circle.

wave solution produces more than just a delta function in  $k$ -space, as was the case with plane waves (Eq. (2.95)). The circle in the figure is not a delta function due to the fact that it is spread in  $k_r$  with a drop off in amplitude given by  $1/(k_r^4 - k_f^4)$ . This spread is due partly to the outgoing wave and partly due to the flexural nearfield of the plate located around the driver. This flexural nearfield is a local distortion of the plate at the drive-point; as though the driver were punching through the plate. As we can see by referring back to Fig. 2.22, this local distortion is much like a spread delta function in physical space. Thus it must have a broad spectrum in  $k$ -space with a corresponding broad directivity pattern in the farfield.

For the case  $k_f > k$  (subsonic free wave on the plate) the radiation circle is located inside the free wavenumber circle in Fig. 2.23; we have the situation shown in Fig. 2.24. Drawing the radiation circle in this figure, say at  $k = 10$ , indicates that the plate still radiates to the farfield and that the directivity pattern of the plate has a maximum amplitude at  $\theta = \pi/2$ . The level of the pressure radiated to the farfield is small, however, compared to the supersonic wave case. As  $k \rightarrow 0$  we can see from Eq. (2.154), since  $k_r = k \sin \theta$ , that the contributions of the traveling and nearfield waves are about equal, each varying as  $1/k_f^2$ .

The frequency at which  $k = k_f$ , when the radiation circle falls on the peak of the  $k$ -space velocity, is called the coincidence frequency. In this case the bending wave speed  $c_b$  just equals the speed of sound in the fluid. The peak in directivity occurs on the horizon. As has been discussed above, at frequencies below the coincidence frequency the plate is a poor radiator ( $k_f$  is subsonic). At frequencies above coincidence the plate radiates very efficiently ( $k_r$  is supersonic).

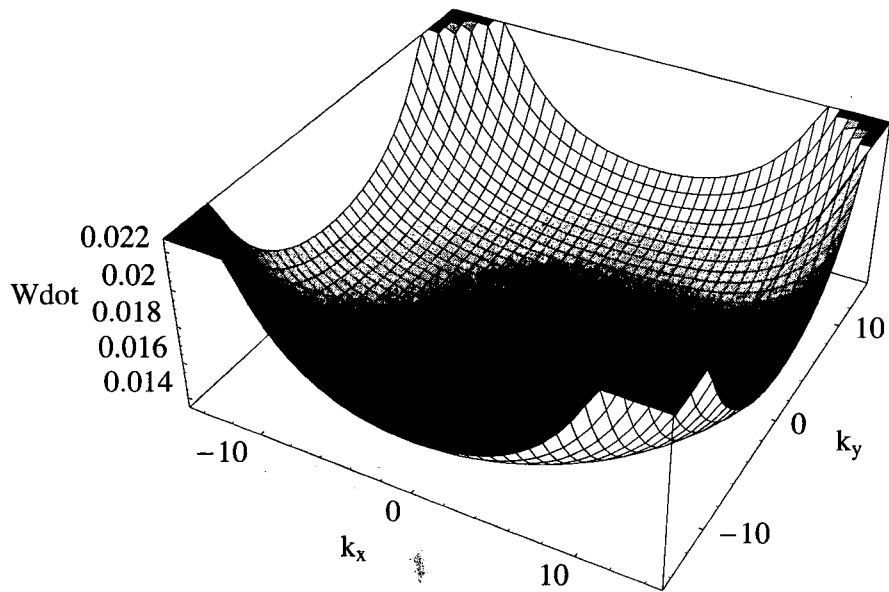


**Figure 2.24:**  $k$ -space diagram of the magnitude of the  $k$ -space surface velocity for an infinite, point-driven plate with radiation circle inside of free wavenumber circle.

The coincidence frequency  $f_c$  is given by  $\alpha\sqrt{\omega_c} = c$  or

$$f = c^2/(2\pi\alpha^2). \quad (2.155)$$

As an example of the coincidence frequency consider a 2 inch steel plate with  $E = 19.5 \times 10^{10}$  newtons/m<sup>2</sup>,  $\nu = 0.28$  and  $\rho_s = 7700$  kg/m<sup>3</sup>. Figure 2.25 is a plot of  $c_b$  as a function of frequency. The coincidence frequencies for the 2 inch plate in water and in air are 4.5 kHz and 240 Hz, respectively. As can be seen, the coincidence frequency is higher for the thinner plate.

## 2.14 Vibration and Radiation of a Finite, Simply Supported Plate

The finite vibrating plate represents a more realistic source than the infinite one. The vibration problem is of interest because it provides an introduction to normal modes, and the resulting expansion using orthogonal functions (normal modes) to solve the vibration problem for arbitrary excitation. The corresponding radiation problem provides an introduction to edge and corner mode radiation which occurs due to the finite boundaries in the problem. Furthermore, we introduce concepts of radiation impedance and radiation efficiency and write them in terms of normal modes.

The literature on finite plates is vast, and is reviewed extensively in a book by Leissa.<sup>12</sup> The way the plate is supported along its boundaries is crucial to its vibration

<sup>12</sup>A. W. Leissa (1969). *Vibration of Plates*. NASA SP-160. Office of Technology Utilization, National Aeronautics and Space Administration, Washington, D.C.

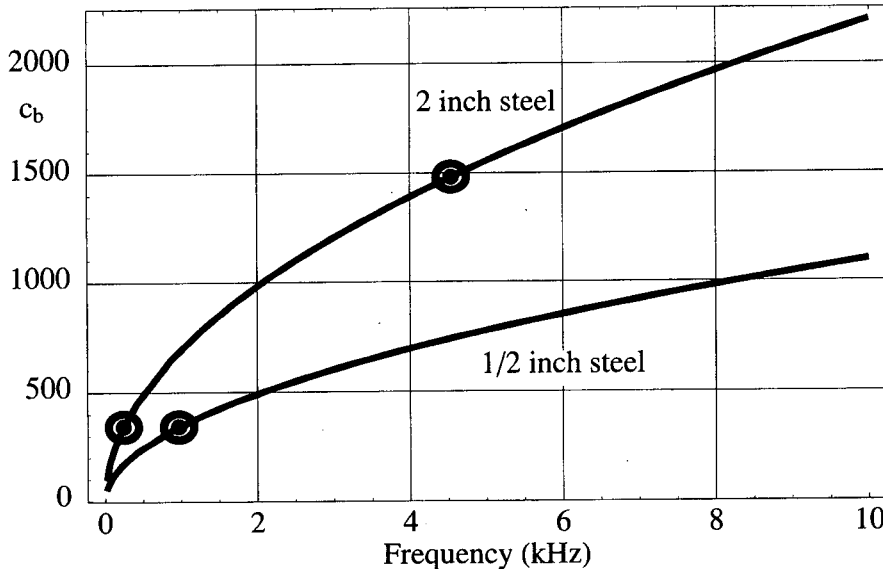


**Figure 2.25:** Bending wave speed in 2 inch and 1/2 inch steel plates. The circles indicate the coincidence frequencies for sound speed in water (1481 m/s) and air (343 m/s).

and radiation. To determine its radiation the plate is almost always surrounded by an infinite, rigid plane baffle, otherwise the problem is intractable.

We will consider here only one particular type of boundary support, called the simply supported boundary condition, because it leads to a simple solution which can be used to illuminate important concepts.

First we present the homogeneous equation of motion in the frequency domain of the plate along with the boundary condition at the edges. The plate is rectangular of length  $L_x$  and width  $L_y$ . The origin of the coordinate system is located at the lower left corner of the plate. The equation of motion is the same as the infinite plate:

$$D \left( \frac{\partial^4 w}{\partial x^4} + 2 \frac{\partial^4 w}{\partial x^2 \partial y^2} + \frac{\partial^4 w}{\partial y^4} \right) - \rho_s h \omega^2 w = 0, \quad (2.156)$$

which is often written as

$$\nabla^4 w(x, y, \omega) - k_f^4 w(x, y, \omega) = 0 \quad (2.157)$$

where  $\nabla^4 = (\frac{\partial^2}{\partial x^2} + \frac{\partial^2}{\partial y^2})^2$  and the bending wavenumber is  $k_f = (\rho_s h \omega^2 / D)^{1/4}$ , the same as the infinite plate. The simply supported boundary condition implies a knife edge support where the plate can not move in the  $z$  direction but is free to rotate about this support. The first boundary condition implies that  $w(x, y) = 0$  along the boundary and the second that the bending moment vanishes along the edges. The moments anywhere in the plate are related to the plate displacement:<sup>13</sup>

$$M_x = -D \left( \frac{\partial^2 w}{\partial x^2} + \nu \frac{\partial^2 w}{\partial y^2} \right), \quad (2.158)$$

<sup>13</sup>E. Skudrzyk (1968). *Simple and Complex Vibratory Systems*. The Pennsylvania State University Press, University Park, PA.

$$M_y = -D\left(\frac{\partial^2 w}{\partial y^2} + \nu \frac{\partial^2 w}{\partial x^2}\right). \quad (2.159)$$

The simply supported boundary condition is

$$\begin{aligned} w(x, y) &= M_x(x, y) = 0, & x &= 0, \text{ and } L_x, \\ w(x, y) &= M_y(x, y) = 0, & y &= 0, \text{ and } L_y, \end{aligned} \quad (2.160)$$

which leads to the conclusion,

$$\begin{aligned} \frac{\partial^2 w(x, y)}{\partial x^2} &= 0, & x &= 0, \text{ and } L_x, \\ \frac{\partial^2 w(x, y)}{\partial y^2} &= 0, & y &= 0, \text{ and } L_y. \end{aligned} \quad (2.161)$$

In proceeding with the solution to Eq. (2.157) we can not use Fourier transforms as we did with the infinite plate because the equation of motion is specified over a limited area. Consider the following set of modes:

$$\Phi_{mn}(x, y) = \frac{2}{\sqrt{L_x L_y}} \sin(m\pi x/L_x) \sin(n\pi y/L_y), \quad n = 1, 2, 3 \dots, \quad m = 1, 2, 3 \dots \quad (2.162)$$

They satisfy the boundary conditions, Eq. (2.161), and also the equation of motion, Eq. (2.157), as long as

$$(m\pi/L_x)^2 + (n\pi/L_y)^2 = k_f^2. \quad (2.163)$$

The infinite set of functions given by Eq. (2.162), the modes of the plate, represent a set of orthonormal functions; they satisfy the very important relations,

$$\begin{aligned} \int_0^{L_x} \int_0^{L_y} \Phi_{mn}(x, y) \Phi_{pq}(x, y) dx dy &= 0 \quad \text{if } m \neq p, \text{ or } n \neq q \\ &= 1 \quad \text{if } m = p, \text{ and } n = q. \end{aligned} \quad (2.164)$$

Figure 2.26 shows the spatial variation of the first nine modes for a simply supported square plate. The orthogonality of the modes is actually guaranteed by the theory of partial differential equations, and similar sets of orthogonal modes exist for other boundary conditions, although it is more difficult to write down expressions for them. This same theory<sup>14</sup> guarantees that the modes form a complete set. We will use Eq. (2.164) to solve for the response of the plate when it is driven by external forces.

The eigenvalue equation given by Eq. (2.163) relates the modes to the frequency of vibration since, by Eq. (2.141),  $k_f = \sqrt{\omega}/\alpha$ . Thus for each mode  $(m, n)$  there corresponds an eigenfrequency  $\omega_{mn}$  given by the equation,

$$\omega_{mn} = \alpha^2 [(m\pi/L_x)^2 + (n\pi/L_y)^2]. \quad (2.165)$$

Only at this eigenfrequency, however, is this mode a solution to the equation of motion.

<sup>14</sup>Discovered by Sturm and Liouville in 1836 and 1837. See B. Diprima (1977). *Elementary Differential Equations and Boundary Value Problems*. Wiley and Sons, New York, 3rd ed., pp. 531–541.

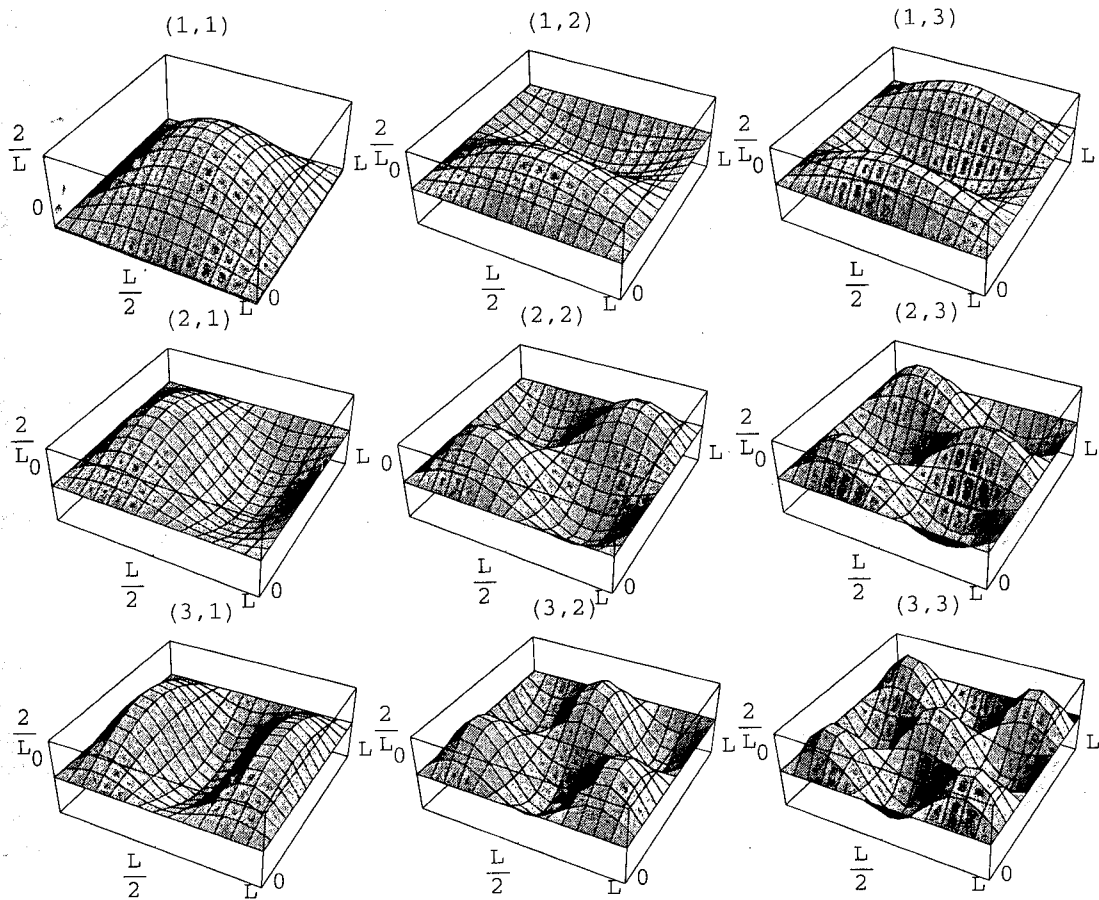


**Figure 2.26:** Some of the orthonormal modes,  $\Phi_{mn}(x, y)$ , of a simply supported plate. At the top of each mode is the  $(m, n)$  index corresponding to it.

Now we are in a position to formulate the solution for the point excited, simply-supported rectangular plate. If the point source is of magnitude  $F$  and is located at the point  $(x_0, y_0)$ , then the equation of motion is (see Eq. (2.131))

$$\nabla^4 w(x, y, \omega) - k_f^4 w(x, y, \omega) = \frac{1}{D} [F(\omega) \delta(x - x_0) \delta(y - y_0) - p_a(x, y, \omega)], \quad (2.166)$$

where  $p_a$  is the loading (forces) due to the fluid. Note that, if we assume that the plate is in an infinite rigid baffle,  $p_a$  can be expressed in terms of the displacement by using Rayleigh's integral, Eq. (2.75):

$$p(x, y, \omega) = \frac{-\omega^2 \rho_0}{2\pi} \int_{-\infty}^{\infty} \int_{-\infty}^{\infty} w(x', y', \omega) \frac{e^{ik|\vec{r}-\vec{r}'|}}{|\vec{r}-\vec{r}'|} dx' dy'.$$

This makes Eq. (2.166) an integral-differential equation. When the fluid is light, such as air,  $p_a$  can be ignored unless  $\rho_s h$  is very small (as in a tympanic membrane). We proceed to study the rectangular plate with negligible fluid loading.

One of the most common tools for solving problems of this type is to use the fact that the orthonormal modes form a complete set for the specified boundary condition, which means that any displacement on the plate can be expressed as a sum of these modes with appropriate weighting coefficients. Thus we postulate a solution of Eq. (2.166) of the form

$$w(x, y, \omega) = \sum_{m=1}^{\infty} \sum_{n=1}^{\infty} A_{mn}(\omega) \Phi_{mn}(x, y). \quad (2.167)$$

The solution requires three steps:

- (1) We insert this solution into Eq. (2.166),
- (2) multiply both sides by  $\Phi_{pq}(x, y)$  and
- (3) integrate over the surface of the plate and use Eq. (2.164).

This will result in an equation for the unknown coefficients  $A_{mn}(\omega)$ , which together with Eq. (2.167) provide the final solution.

Implementing these three steps leads to the solution

$$w(x, y, \omega) = -\frac{F}{\rho_s h} \sum_{m=1}^{\infty} \sum_{n=1}^{\infty} \frac{\Phi_{mn}(x_0, y_0) \Phi_{mn}(x, y)}{\omega^2 - \omega_{mn}^2}. \quad (2.168)$$

In the process of obtaining this equation we used

$$D \nabla^4 \Phi_{mn}(x, y) = \rho_s h \omega_{mn}^2 \Phi_{mn}(x, y),$$

which resulted from the fact that the modes are solutions of the homogeneous equation, Eq. (2.157), when  $\omega^2 = \omega_{mn}^2$ .

Actually the procedure leading to Eq. (2.168) is very general, and can be used for vibrating systems in general, whenever the modes of the system can be identified. Note that the amplitude of each mode in Eq. (2.168) is given by that mode evaluated at the excitation point  $(x_0, y_0)$ . This leads to the familiar notion that when the force is located on a nodal line for a mode, that mode is not excited. For example, if the force were located at the center of the plate only odd-odd ( $m$  and  $n$  odd) modes would be excited. In general, however, almost all the modes of the plate are excited at any frequency.

When the driving frequency of the force, which we recall is given by  $F(\omega)e^{-i\omega t}$ , equals the eigenfrequency (resonance frequency) of a mode, the denominator vanishes and the response becomes infinite. These frequencies are the resonances of the plate. The response is finite, however, if damping is added to the plate by making Young's modulus  $E$  complex. As a result  $\omega_{mn}$  becomes complex, since it depends upon  $\sqrt{E}$ , and the denominator of Eq. (2.168) no longer has any real zeros.

Equation (2.168) leads to an equation for the transfer mobility (ratio of velocity over excitation force)  $Y(\omega)$  of the plate:

$$Y(\omega) \equiv \frac{-i\omega w}{F} = \frac{i\omega}{\rho_s h} \sum_{m=1}^{\infty} \sum_{n=1}^{\infty} \frac{\Phi_{mn}(x_0, y_0) \Phi_{mn}(x, y)}{\omega^2 - \omega_{mn}^2}. \quad (2.169)$$

When  $x = x_0$  and  $y = y_0$  this equation leads to the drive-point mobility. The transfer mobility provides the Green function for the plate when we put  $F = 1$ .

### 2.14.1 Rectangular Plate with Fluid Loading

Before we consider the radiation from the simply-supported plate, we look briefly at the vibration when the plate is fluid loaded. The integral-differential equation was provided by Eq. (2.166). One can still attempt to solve this equation using the in vacuo modes, a technique that is sometimes used in the literature. Of course the in vacuo modes are not the real modes of the system, and the theory of partial differential equations does not provide us with a formulation which even proves that normal modes exist in this system. This is a subject of continuing debate.

One can proceed with the three step solution provided above and obtain a result cast in terms of coupled in vacuo modes, as has been done by Davies.<sup>15</sup> Another solution technique was provided by Lax<sup>16</sup> which is quite a bit easier to use on a computer. In the latter case the solution is obtained without fluid loading, using the sum of the in vacuo modes as outlined above. This is the zero order solution,  $w^{(0)}(x, y)$ . Using this solution  $p_a$  can be approximated using Rayleigh's integral, and Eq. (2.166) solved again to obtain a first order solution,  $w^{(1)}(x, y)$ . This process is continued until convergence is obtained.

### 2.14.2 Radiation from Rectangular Plates: Radiation Impedance and Efficiency

Since the vibration of a point-driven plate can be expressed as summations of the in vacuo normal modes, we will study the radiation from a single mode first. This is particularly important when the plate is driven near a resonance frequency corresponding to one of the modes, since the vibration is then dominated by a single normal mode. Also we will present some very basic concepts of plate radiation; radiation efficiency, radiation impedance and the concept of edge and corner mode radiation. We will assume throughout that the plate is in an infinite, rigid baffle.

The real part of the radiation impedance is called the radiation resistance and is defined for the  $(m, n)$ th mode of the plate as

$$R_{mn}(\omega) \equiv \Pi(\omega) / \frac{1}{2} \left\langle |\dot{w}_{mn}|^2 \right\rangle, \quad (2.170)$$

where the spatial average of the square of surface velocity is defined by

$$\left\langle |\dot{w}_{mn}|^2 \right\rangle \equiv \frac{1}{L_x L_y} \int_0^{L_x} \int_0^{L_y} |\dot{w}_{mn}(x, y)|^2 dx dy. \quad (2.171)$$

The radiation efficiency is defined in general by

$$S \equiv \frac{\Pi}{\Pi_0} \equiv \frac{\Pi}{\frac{1}{2} \rho_0 c L_x L_y \left\langle |\dot{w}|^2 \right\rangle}, \quad (2.172)$$

<sup>15</sup>H. G. Davies (1969). "Acoustic Radiation from Fluid Loaded Rectangular Plates," MIT, TR71476-1, December.

<sup>16</sup>M. Lax (1944). "The Effect of Radiation on the Vibrations of a Circular Diaphragm," J. Acoust. Soc. Am., **16**, pp. 5-13.

where  $\Pi_0 \equiv \frac{1}{2}\rho_0 c L_x L_y \langle |\dot{w}|^2 \rangle$  is the power radiated by the area  $L_x L_y$  of an infinite plate vibrating as an infinite rigid piston with a velocity amplitude given by the average square velocity  $\langle |\dot{w}_{mn}|^2 \rangle$ . This follows from the fact that for a plane wave,  $p = \rho_0 c \dot{w}$ , and thus  $I = \frac{1}{2}\rho_0 c |\dot{w}|^2$  and  $\Pi_0 = \int I dA = \frac{1}{2}\rho_0 c L_x L_y \langle |\dot{w}|^2 \rangle$ . Thus it follows, if  $S_{mn}$  is the radiation efficiency of mode  $(m, n)$ , that

$$S_{mn} = \frac{R_{mn}}{\rho_0 c L_x L_y} = \frac{\Pi}{\frac{1}{2}\rho_0 c L_x L_y \langle |\dot{w}_{mn}|^2 \rangle}. \quad (2.173)$$

Radiation efficiency eliminates the dependence on the panel size. A radiation efficiency of unity is considered 100% efficient (compared with a plane wave).

For a single normal mode of plate vibration  $\Phi_{mn}(x, y)$  given in Eq. (2.162) the velocity of the plate is, from Eq. (2.167),

$$\dot{w}_{mn}(x, y) = -i\omega A_{mn} \Phi_{mn}(x, y), \quad (2.174)$$

and the spatial average of the square of the velocity is

$$\langle |\dot{w}_{mn}|^2 \rangle = \omega^2 \langle |A_{mn} \Phi_{mn}|^2 \rangle = \frac{\omega^2 |A_{mn}|^2}{L_x L_y},$$

since the mode is orthonormal. The radiation efficiency is then

$$S_{mn} = \frac{\Pi}{\frac{1}{2}\omega^2 |A_{mn}|^2 \rho_0 c}, \quad (2.175)$$

where  $\Pi$  is the power radiated from the mode.

We now compute the power radiated by a normal mode. We will approach this computation by determining the farfield pressure of a mode and using the following formula for the power:

$$\Pi(\omega) = \int_0^{2\pi} \int_0^{\pi/2} \frac{|p(r, \theta, \phi, \omega)|^2}{2\rho_0 c} r^2 \sin \theta d\theta d\phi. \quad (2.176)$$

Note the integrand is simply the power per unit area through a hemisphere of radius  $r$ .

To determine the farfield pressure we return to Eq. (2.84), with  $\dot{W}(k_x, k_y)$  the Fourier transform of the modal velocity,  $k_x = k \sin \theta \cos \phi$ , and  $k_y = k \sin \theta \sin \phi$ . Thus we must evaluate the Fourier transform of Eq. (2.174):

$$\dot{W}(k_x, k_y) = -i\omega \mathcal{F}_x \mathcal{F}_y [A_{mn} \Phi_{mn}(x, y)].$$

Using Eq. (2.162) and taking Fourier transforms yields

$$\dot{W}(k_x, k_y) = -i\omega 4mn\pi^2 \sqrt{L_x L_y} A_{mn} \left[ \frac{(-1)^m e^{-ik_x L_x} - 1}{(k_x L_x)^2 - (m\pi)^2} \right] \left[ \frac{(-1)^n e^{-ik_y L_y} - 1}{(k_y L_y)^2 - (n\pi)^2} \right], \quad (2.177)$$

so that the farfield pressure becomes (remember that  $k_x$  and  $k_y$  are functions of  $\theta$  and  $\phi$ )

$$p(r, \theta, \phi) = -\omega^2 \rho_0 \frac{e^{ikr}}{r} 2mn\pi \sqrt{L_x L_y} A_{mn} \left[ \frac{(-1)^m e^{-ik_x L_x} - 1}{(k_x L_x)^2 - (m\pi)^2} \right] \left[ \frac{(-1)^n e^{-ik_y L_y} - 1}{(k_y L_y)^2 - (n\pi)^2} \right]. \quad (2.178)$$

With a bit of algebra we obtain the radiation efficiency of a mode in an infinite baffle:

$$S_{mn} = \frac{64k^2 L_x L_y}{\pi^6 m^2 n^2} \int_0^{2\pi} \int_0^{\pi/2} \left( \frac{\{\cos\}(\frac{k_x L_x}{2}) \{\cos\}(\frac{k_y L_y}{2})}{[(k_x L_x/m\pi)^2 - 1][(k_y L_y/n\pi)^2 - 1]} \right)^2 \sin \theta d\theta d\phi. \quad (2.179)$$

In this expression cosine is used when the integer  $m$  or  $n$  is odd, and sine when it is even. This expression can not be simplified any further and we must turn to computer evaluation. Calculations by Wallace<sup>17</sup> are shown in Figs 2.27 and 2.28 for the radiation efficiency of various normal modes.

First consider the radiation efficiency of the  $(m, n) = (1, 1)$  mode whose shape is shown on the top left of Fig. 2.26. Its radiation efficiency is shown in Fig. 2.27 plotted against  $\gamma$  where, using Eq. (2.163) ( $k_f$  is the free bending wavenumber),

$$\gamma = k / \sqrt{(m\pi/L_x)^2 + (n\pi/L_y)^2} = k/k_f. \quad (2.180)$$

Thus  $\gamma$  is a measure of the coincidence frequency; when  $\gamma < 1$  the mode is below coincidence and when  $\gamma > 1$  it is above. The latter condition implies strong radiation. The radiation efficiency in Fig. 2.27 confirms this. We can see that all the modes reach 100% efficiency at and above coincidence. In fact, close to  $\gamma = 1$  the efficiency is greater than 1, reaching values of 2 and sometimes 3.

To understand how the plate reaches efficiencies greater than one, we consider the radiation impedance of an infinite plate. Equation (2.45) in Section 2.7 indicates that the pressure above an infinite plate vibrating in a normal mode is infinite at the coincidence frequency,  $k_{z0} = 0$ . An infinite pressure implies that the radiation resistance must also be infinite at coincidence; this results from the fact that the surface velocity is finite (and non-zero), so that when the plate pushes against this infinite resistance an infinite pressure is produced. Of course, in a physical experiment the plate would be loaded by this resistance and its velocity would be diminished as a result. Under the same conditions the radiation efficiency of a *finite* plate is no longer infinite, but still reaches values greater than one as reflected in Fig. 2.27. Put in other terms, the radiation impedance used in the denominator of Eq. (2.175) is finite, always given by  $\rho_0 c$ , so that when the radiation impedance of the actual mode is greater than this, efficiencies larger than unity occur.

The frequency region below coincidence is very important and an extremely interesting region. This is especially true for plates in water, because the coincidence frequency is much higher and thus this region (see Fig. 2.25) covers a broader range of frequencies. It becomes clear from studying Figs 2.27 and 2.28 (from Wallace) that at low frequencies

<sup>17</sup>C. E. Wallace (1972). "Radiation Resistance of a Rectangular Panel", J. Acoust. Soc. Am., **51**, pp. 946–952.

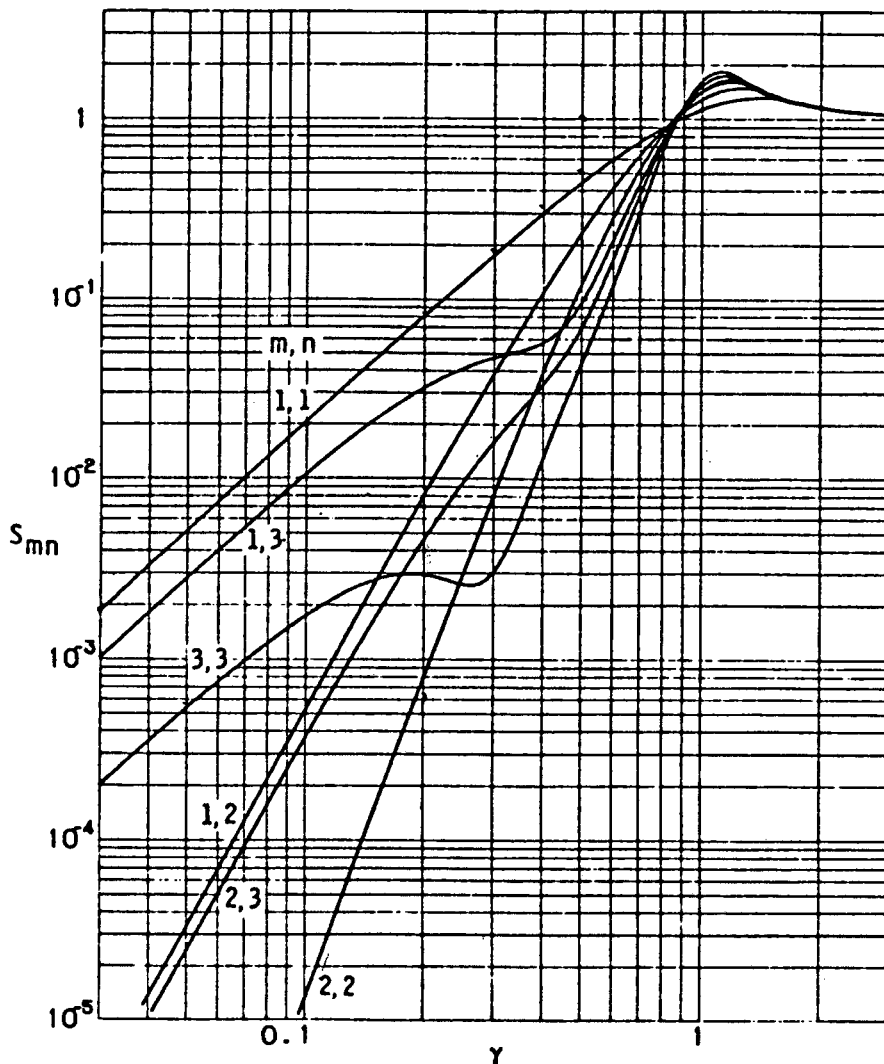


**Figure 2.27:** Radiation efficiency for the low-numbered modes of a square plate (from Wallace).

the efficiencies are quite different for different modes. We now attempt to explain in some depth the nature of the radiation efficiencies in this region.

We turn to some pioneering work by Gideon Maidanik.<sup>18</sup> In this work he classified the modes of a simply supported baffled panel as edge, corner and surface modes, depending on where the wavenumbers of the modes fall in  $k$ -space. The surface mode (supersonic condition) occurs when the wavenumbers of the mode fall inside the radiation circle,  $k_x = m\pi/L_x < k$  and  $k_y = n\pi/L_y < k$ ; an edge mode when one of these wavenumbers is greater than  $k$ ; and a corner mode when both these wavenumbers are greater than  $k$ . The latter two represent subsonic wave cases. Figure 2.29 illustrates

<sup>18</sup>G. Maidanik (1962). "Response of Ribbed Panels to Reverberant Acoustic Fields", J. Acoust. Soc. Am., **34**, pp. 809–826.

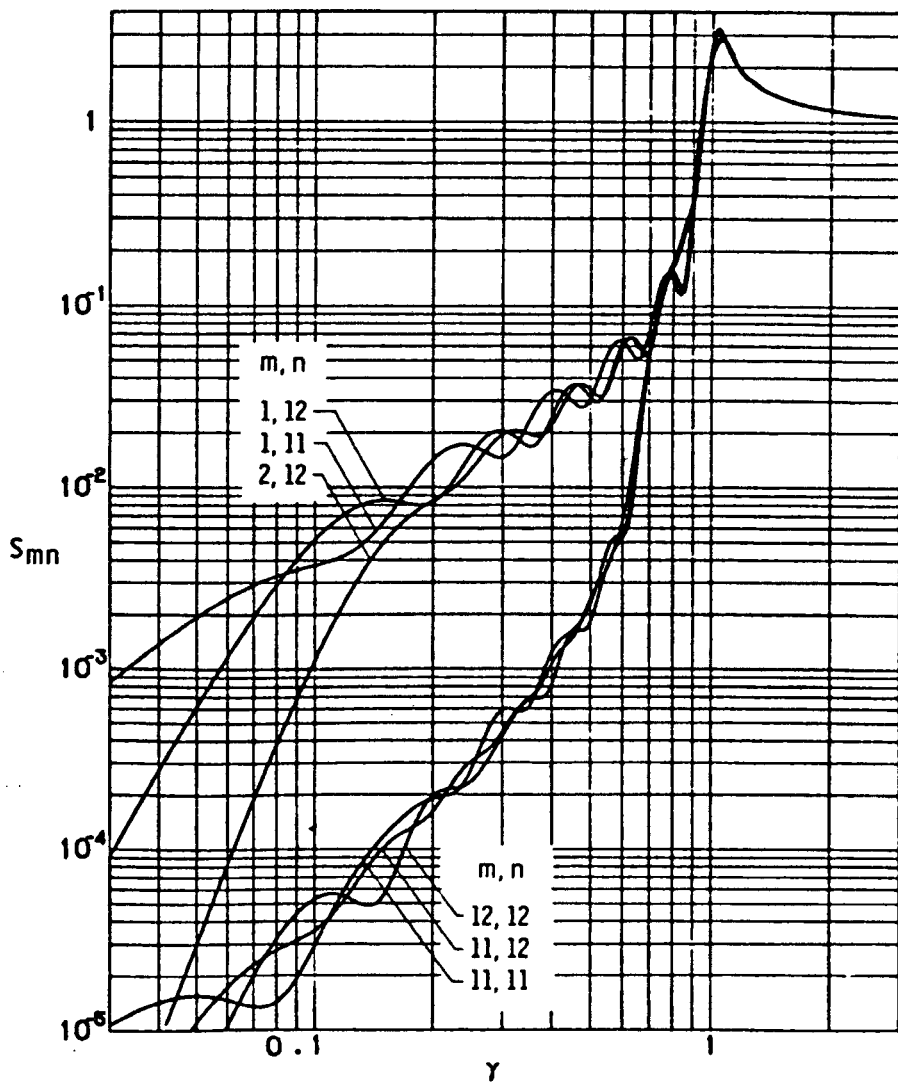


**Figure 2.28:** Radiation efficiency for the typical high-numbered modes of a square plate (from Wallace).

the definitions.

To understand the physical significance of this classification scheme we must consider the mutual interaction of adjacent regions of surface velocity for a normal mode. Consider Fig. 2.30. This figure represents the  $\Phi_{36}$  mode. We want to determine the mutual effects of two adjacent cells as shown on the right in the figure. Assume that these two cells are isolated in an infinite baffle and that they are small in dimensions compared to an acoustic wavelength. By the first product theorem from Section 2.11.6 we can replace these cells by two point sources at the centers; the farfield is the product of the farfield of the point sources and the directivity pattern of one of the cells. Since the cell is assumed small compared with a wavelength, the directivity pattern of a cell is nearly omnidirectional and can be ignored.

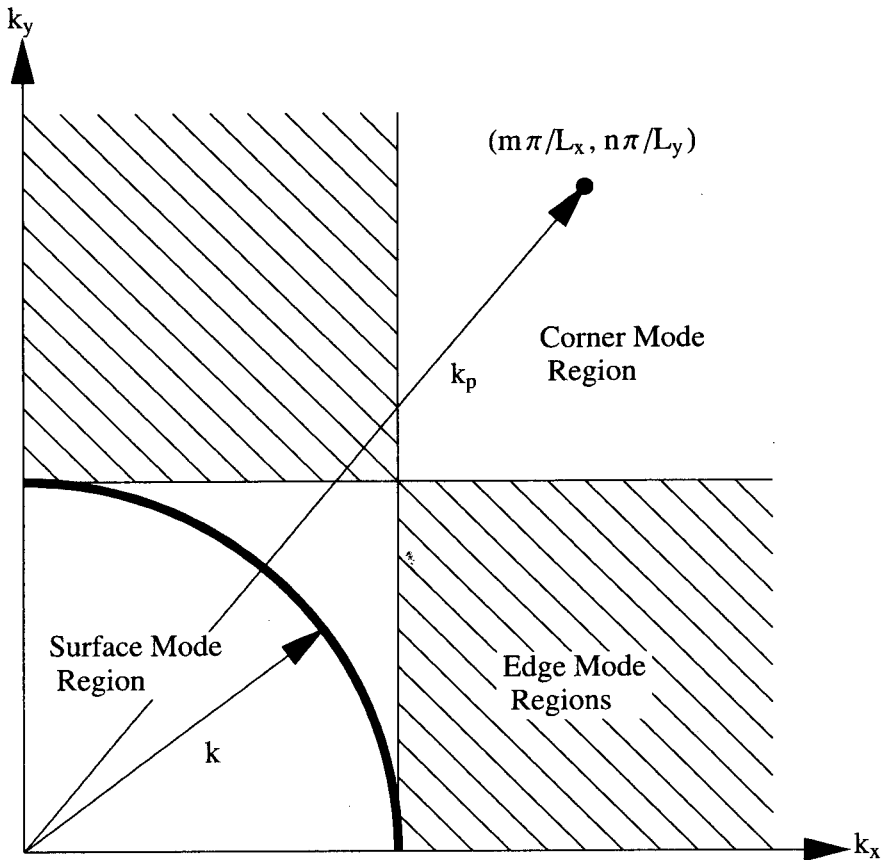


**Figure 2.29:** Radiation classification of normal modes of a simply supported plate.

The power radiated into the half-space by one of these point sources from Eq. (2.130) ( $Q_h = 1$ ) is just

$$\Pi_1 = \frac{\rho_0 c k^2}{4\pi}.$$

The power radiated by both can easily be computed using Eq. (2.114) with

$$\dot{w}(x, y, 0) = \delta(x)\delta(y - b) \pm \delta(x)\delta(y), \quad (2.181)$$

where the positive cell is located a distance  $b$  above the negative cell (minus sign in the second term). The case where both cells are positive is included for completeness and is represented by the positive instead of the negative sign in the second term. The double integral over  $S'$  in Eq. (2.114) is

$$\iint_{S'} \dot{w}(x', y', 0) \frac{\sin(kR)}{kR} dx' dy' = \frac{\sin(k\sqrt{x^2 + (y-b)^2})}{\sqrt{x^2 + (y-b)^2}} \pm \frac{\sin(k\sqrt{x^2 + y^2})}{\sqrt{x^2 + y^2}}.$$

The double integral over  $S$  in Eq. (2.114), using the results above, becomes

$$\Pi(\omega) = \frac{\rho_0 c k^2}{4\pi} \left[ 2(1 \pm \frac{\sin(kb)}{kb}) \right] = 2\Pi_1(1 \pm \frac{\sin(kb)}{kb}). \quad (2.182)$$

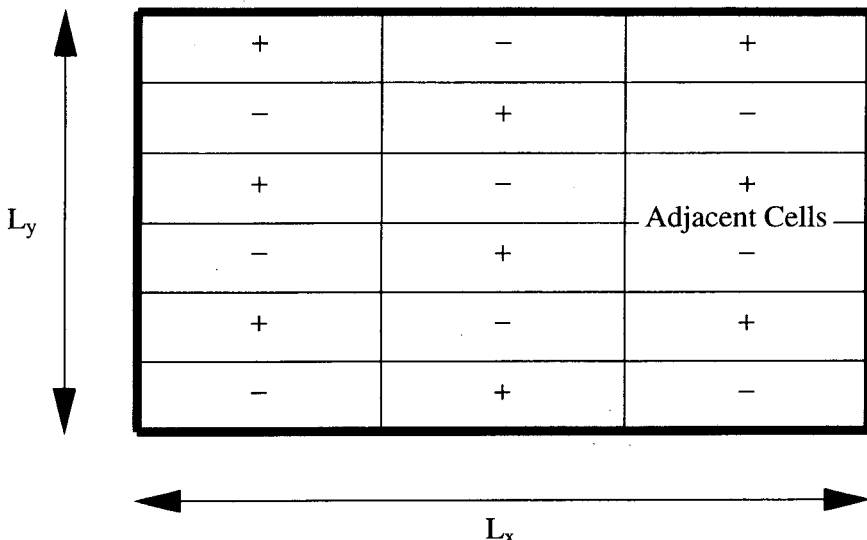


**Figure 2.30:** Surface velocity for a  $m = 3$ ,  $n = 6$  normal mode. Adjacent cells shown on the right used to compute the mutual radiation impedance between them.

Although not relevant to this discussion we note that when the two point sources are in phase with each other the power radiated is four times that of one of them, if they are located very close to one another ( $kb \ll 1$ ). This is a well known result and is due to the increase in the radiation resistance from the presence of the second source. However, if the two sources are separated by more than an acoustic wavelength the sinc term is small and the total power radiated is increased only by a factor of 2. The two sources do not “see” each other, and radiate independently.

We see a similar circumstance with the adjoining cells of opposing sign (using the minus sign in the second term of Eq. (2.182)); when they are far apart, the power is also increased by a factor of 2. When the sources are  $\lambda/4$  apart the power radiated, however, is *reduced* by 36%. At  $\lambda/8$  the power is down to 10%. As  $b$  tends towards zero the power radiated goes to zero. This is a statement of the hydrodynamic short circuit which occurs when two sources vibrate out of phase close to one another. We now apply this argument to various normal modes of the simply supported plate to derive the radiation classification scheme.

Consider first the effect of adjacent cell cancellation in a mode vibrating at a frequency so that the wavenumbers of the mode are within the region labeled as a corner mode in Fig. 2.29. In this case the separation distance between the centers of adjacent cells in both the  $x$  and  $y$  directions is less than  $\lambda/2$  since  $k_p > k$ . In the limit (separations much less than a wavelength) the result of the cancellation of adjacent cells is to leave four regions at the corners which have no corresponding sources to cancel. This is shown in Fig. 2.31. Of course, as the frequency increases for the same mode shape the cancellation across nodal lines becomes less complete. The power radiated by this mode is similar to the power radiated from four point sources located at the corners of the plate. Due to cancellations the mode radiates inefficiently.

In the next figure, Fig. 2.32, we illustrate the case of an edge mode. Reference to

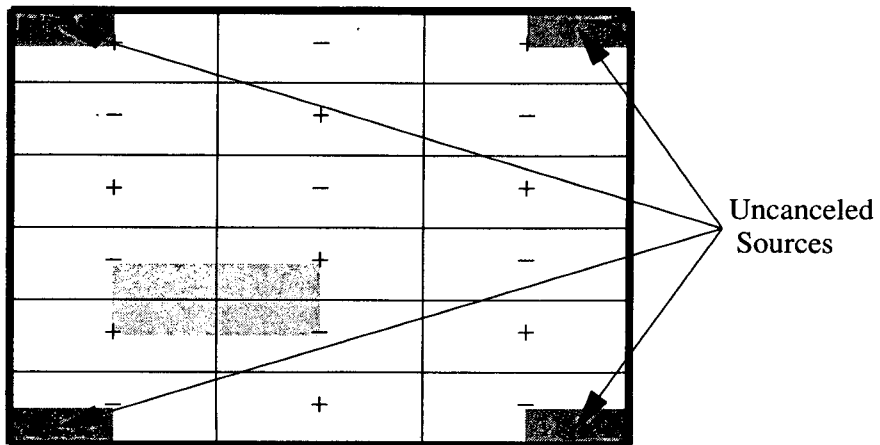


**Figure 2.31:** Example of a corner mode. All adjacent regions (one shown in light gray) cancel. Only the four corner regions are left uncanceled.

Fig. 2.29 indicates that this is a mode with adjacent cells in one direction separated by less than a half wavelength, whereas the cells in the other direction are separated by more than a half wavelength. Thus adjacent cells in the latter direction do not cancel one another. In this example the wavelength in the vertical direction is much larger

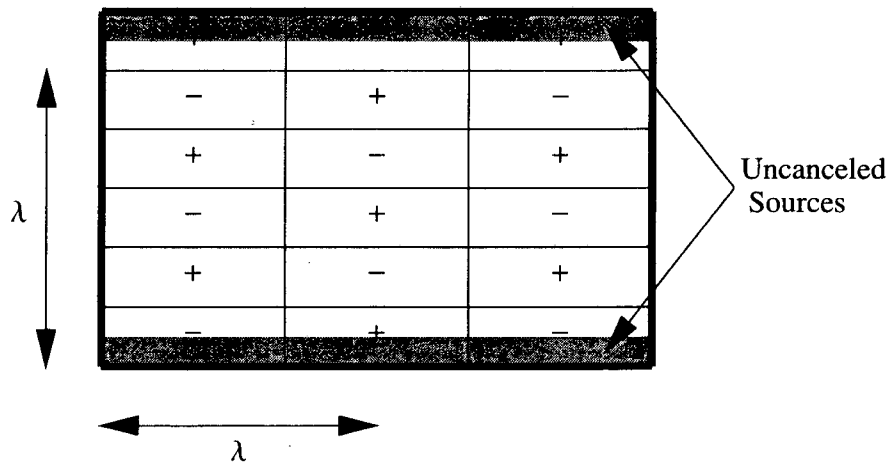


**Figure 2.32:** Example of an edge mode. Adjacent vertical regions cancel one another, but the horizontal regions on the edge no longer cancel leaving two strips uncanceled.

than the separation between nodal lines. This is not the case in the horizontal direction, where  $\lambda < \lambda_m$ ,  $\lambda_m = 2\pi/k_m$ . Thus cancellation occurs vertically but not horizontally. The power radiated from this mode is similar to the power radiated by two baffled horizontal strips. This radiator is more efficient than the edge mode due to the larger radiating area of the strips versus the four corners.

The third kind of radiation classification is called the surface mode. In this case no adjacent regions cancel and the whole area of the plate radiates to the farfield. The

mode wavelengths in each direction are each greater than the fluid wavelength, and each cell radiates independently.

Now we return to the corner mode and consider the low frequency limit. When the largest dimension of the plate is less than  $\lambda/2$ , all eigenmodes are corner modes. We must consider the fact that the distance between the corner regions, in the low frequency limit,\* is much less than a wavelength, and thus they are coupled through their mutual radiation resistances, an effect we studied above in reference to Eq. (2.182). There are three cases to consider which depend on the evenness or oddness of the mode. These cases are illustrated in Fig. 2.33. The odd-odd mode combination, illustrated

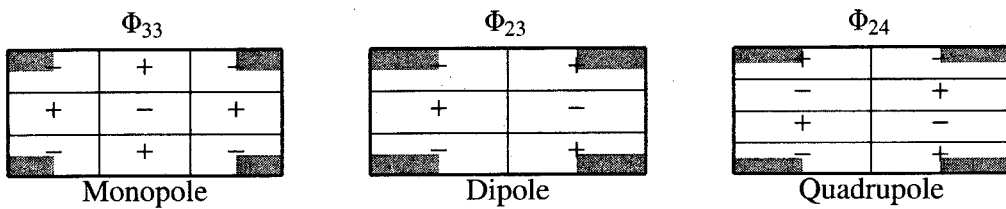


**Figure 2.33:** Low frequency limits for the radiation classification of normal modes.

with a (3,3) mode in the figure results in four positive corner regions which interfere constructively to produce monopole-like radiation which has

$$\Pi(\omega) \propto k^2. \quad (2.183)$$

The even-odd (or odd-even) mode combination shown in the center figure is two horizontal dipoles adding constructively in the vertical direction and thus have

$$\Pi(\omega) \propto k^4. \quad (2.184)$$

In this case note that  $1 - \sin(kb)/kb \approx (kb)^2/6$  so that Eq. (2.182) leads to a  $k^4$  dependency. The last case, with an even-even mode combination, is two dipoles placed in opposition to one another, destructively interfering in both directions. This combination is known as a quadrupole and its frequency dependence is

$$\Pi(\omega) \propto k^6 \quad (2.185)$$

and thus is the least efficient of the three combinations. In view of Eq. (2.182), the product of two factors like  $1 - \sin(kb)/kb$  occurs and results in the product of two  $k^2$  dependencies, one for each coordinate direction leading to a  $k^6$  dependency.

We can now return to Figs 2.27 and 2.28 and view the radiation efficiencies in the light of what we have just learned. For example, in Fig. 2.27 we can clearly see that for  $\gamma < 0.1$ , the radiation efficiencies of the (1,1), (1,3) and (3,3) monopole modes are the highest; the (1,2) and (2,3) dipole modes are next; and the (2,2) quadrupole mode is the least efficient. The slopes of the curves indicate the  $k$  dependence.

In the middle frequency region below the coincidence frequency we see that since the panel is square, then the (1,3) will correspond to an edge mode, whereas the (3,3) mode must be a corner mode. The efficiency curves verify the fact that the edge mode

is more efficient than the corner mode (by about a factor of ten in this case). The same holds true for the modes shown in Fig. 2.28. Here the (11,11), (11,12) and (12,12) modes are corner modes (since the panel is square), and the (1,11), (1,12) and (2,12) modes are edge modes. In the region  $0.1 < \gamma < 0.6$  the edge modes are nearly 100 times more efficient. In the region  $\gamma < 0.1$  the (1,11), (1,12) and (2,12) modes reach their low frequency limits of monopole, dipole and quadrupole, respectively.

Returning to the point-driven, simply supported plate and having gained an understanding of how the individual normal modes radiate, we apply these ideas to the general solution, Eq. (2.168), which demands a sum over all the normal modes. Figure 2.34 illustrates the spectrum of modes for the point-driven case. The array of dots

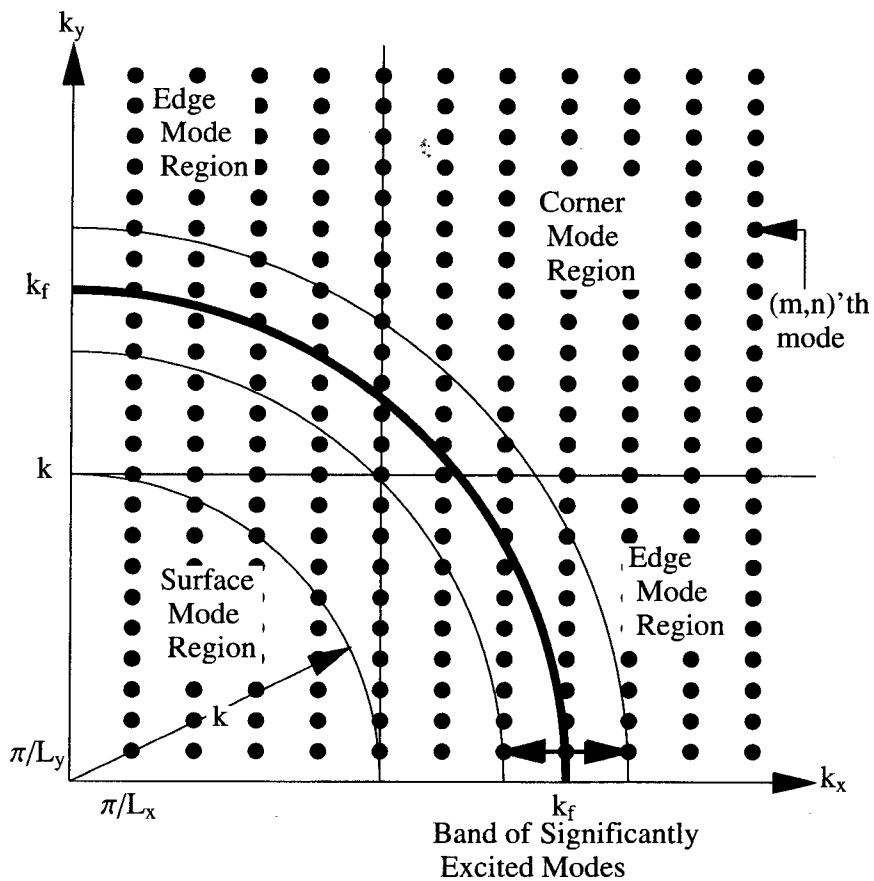


**Figure 2.34:**  $k$ -space diagram with eigenmodes displayed as dots. The circular ring is a region in which the amplitudes of the excited modes are the largest. The plate is excited at the frequency  $\omega$ ,  $k = \omega/c$  and  $k < k_f$ .

represent the individual modes. A quarter circle representing the resonance condition,  $\omega = \omega_{mn}$ , is shown which has a radius given by the flexural wavenumber,  $k_f = \sqrt{\omega/\alpha}$ . This radius corresponding to the condition in which the denominator of Eq. (2.168) vanishes. A second quarter circle with radius  $k = \omega/c$  is shown. The frequency is chosen so that the resonance modes of the plate are subsonic. The annulus region shown, drawn with somewhat arbitrary width, represents the modes which are strongly excited, since

their resonance frequencies are close to the resonance circle. As Eq. (2.168) implies, all modes are excited as long as  $\Phi_{mn}(x_0, y_0)$  is non-zero (which can be obtained if the point drive is very close to a corner of the plate). Figure 2.34 indicates that all three radiation classes exist at the same time. Each dot in the figure represents an excited mode. Thus corner, edge and surface modes are all excited. It is a curious, and perhaps remarkable, fact that the low order modes (the surface modes) are excited above their individual coincidence frequencies ( $\gamma > 1$  so they are very efficient radiators). However, their amplitudes of excitation are very small due to  $\omega^2 - \omega_{mn}^2$  in the denominator. On the other hand the resonant modes are strongly excited since  $\omega^2 - \omega_{mn}^2$  is close to zero, but are very inefficient radiators.

Finally, we note that if damping is added to the plate ( $\omega_{mn}$  becomes complex) the resonance amplitudes are no longer infinite and the relative amplitudes of the low order surface modes are greater. How much of a role they actually play in the radiation from the plate remains an interesting and unanswered question.

## 2.15 Supersonic Intensity

Supersonic intensity is an outgrowth of Fourier acoustics with tremendous utility for sound source localization. It was first introduced in 1996 in applications to source localization on cylinders.<sup>19</sup> Supersonic intensity is a powerful tool, yet simple in its derivation, which we present in this section.

The supersonic intensity is built from the supersonic plane wave components of the velocity and pressure, the latter defined by

$$p^{(s)}(x, y, z) \equiv \frac{1}{4\pi^2} \iint_{S_r} P(k_x, k_y, z) e^{ik_x x} e^{ik_y y} dk_x dk_y, \quad (2.186)$$

where  $S_r$  is the area in the radiation circle; the integration is over values of  $k_x$  and  $k_y$  such that  $k_x^2 + k_y^2 \leq k^2$ . The superscript  $s$  indicates a supersonic quantity. Similarly the supersonic normal surface velocity is

$$\dot{w}^{(s)}(x, y, z) \equiv \frac{1}{4\pi^2} \iint_{S_r} \dot{W}(k_x, k_y, z) e^{ik_x x} e^{ik_y y} dk_x dk_y. \quad (2.187)$$

The supersonic intensity (normal component) is defined in the same way as the total normal intensity, Eq. (2.16):

$$\Pi^{(s)} \equiv I^{(s)}(x, y, z) \equiv \frac{1}{2} \operatorname{Re}[p^{(s)}(x, y, z) \dot{w}^{(s)}(x, y, z)^*]. \quad (2.188)$$

Eliminating the subsonic plane wave components from the intensity, eliminates the circulation of power flow which arises from the beating of the subsonic and supersonic plane wave components near vibrating structures with subsonic flexural waves.

The credibility of the concept of supersonic intensity lies in the fact that power is conserved. That is the total (real) power passing through the plane at  $z = \text{constant}$  is

<sup>19</sup>Earl G. Williams (1995). "Supersonic acoustic intensity", J. Acoust. Soc. Am., **97**, pp. 121–127.

identical to the supersonic power which passes through that plane. That is,

$$\iint_{-\infty}^{\infty} I^{(s)}(x, y, z_0) dx dy = \iint_{-\infty}^{\infty} \frac{1}{2} \operatorname{Re}[p(x, y, z_0) \dot{w}(x, y, z_0)] dx dy, \quad (2.189)$$

where  $p$  and  $\dot{w}$  are the nonfiltered fields.

The proof of this is quite simple. Expanding  $p^{(s)}$  and  $\dot{w}^{(s)}$  in their Fourier transforms, the left hand side of Eq. (2.189) becomes

$$\begin{aligned} \Pi^{(s)}(\omega) &= \frac{1}{2} \operatorname{Re} \left[ \frac{1}{(4\pi^2)^2} \iint_{-\infty}^{\infty} \iint_{S_r} \iint_{S'_r} P(k_x, k_y, z) \dot{W}(k'_x, k'_y, z)^* \right. \\ &\quad \times e^{i(k_x - k'_x)x} e^{i(k_y - k'_y)y} dx dy dk_x dk_y dk'_x dk'_y \Big]. \end{aligned}$$

The integral over  $x$  and  $y$  yields  $4\pi^2 \delta(k_x - k'_x) \delta(k_y - k'_y)$  (see Eq. (1.36)) so that the right hand side collapses to a double integral. From Eq. (2.61) we have

$$P(k_x, k_y, z) = \frac{\rho_0 c k}{k_z} \dot{W}(k_x, k_y, z),$$

so that

$$\Pi^{(s)}(\omega) = \frac{1}{8\pi^2} \iint_{S_r} \operatorname{Re} \left[ \frac{\rho_0 c k}{k_z} \right] |\dot{W}(k_x, k_y, z)|^2 dk_x dk_y.$$

This result is identical to Eq. (2.113), an expression for the total real power passing through the  $(x, y)$  plane. Thus  $\Pi^{(s)}(\omega) = \Pi(\omega)$  and power is conserved. To show the utility of the supersonic intensity for source localization, we turn to an example.

### 2.15.1 Supersonic Intensity for a Point Source

The concept of supersonic intensity, and its ability to locate the regions on a structure which radiate to the farfield, is clarified by considering a point source in an infinite baffle. Let the source plane be located at  $z = 0$ . The source has a strength given by its volume flow  $Q_h$  of Eq. (2.76) which in polar coordinates must be

$$\dot{w}(\rho) = \frac{Q_h}{2\pi} \frac{\delta(\rho)}{\rho}, \quad (2.190)$$

since  $Q_h \equiv \iint \dot{w}(x, y) dx dy$ . From Eq. (2.85) for an axisymmetric source we have

$$\dot{W}(k_x, k_y) = 2\pi \mathcal{B}[\dot{w}(\rho)] = Q_h. \quad (2.191)$$

Following the definition, Eq. (2.187), the supersonic surface velocity is

$$w^{(s)}(x, y) = \frac{Q_h}{4\pi^2} \iint_{S_r} e^{ik_x x} e^{ik_y y} dk_x dk_y.$$

Transforming to polar coordinates and using Eq. (2.89) yields

$$\dot{w}^{(s)}(x, y) = \frac{Q_h}{2\pi} \int_0^k J_0(k_\rho \rho) k_\rho dk_\rho = \frac{k Q_h}{2\pi} \frac{J_1(k\rho)}{\rho}, \quad (2.192)$$

where we have used the indefinite integral relation

$$\int J_0(x)x dx = xJ_1(x). \quad (2.193)$$

Similarly, following the definition of the supersonic pressure, Eq. (2.186), in the plane  $z = 0$ , along with Eq. (2.61) on page 34 with  $z = z'$ , we have

$$\begin{aligned} p^{(s)}(x, y) &= \frac{1}{4\pi^2} \iint_{S_r} P(k_x, k_y) e^{ik_x x} e^{ik_y y} dk_x dk_y \\ &= \frac{\rho_0 c k}{4\pi^2} \iint_{S_r} \frac{W(k_x, k_y)}{k_z} e^{ik_x x} e^{ik_y y} dk_x dk_y. \end{aligned}$$

Again transforming to polar coordinates and using Eq. (2.89) we find

$$p^{(s)}(x, y) = \frac{Q_h \rho_0 c k}{2\pi} \int_0^k \frac{J_0(k\rho)}{\sqrt{k^2 - k_\rho^2}} k_\rho dk_\rho.$$

The integral is given in tables:<sup>20</sup>

$$\int_0^1 \frac{J_0(\gamma x)}{\sqrt{1-x^2}} x dx = \frac{\sin \gamma x}{\gamma x},$$

so that finally

$$p^{(s)}(x, y) = \frac{Q_h \rho_0 c k^2}{2\pi} \frac{\sin k\rho}{k\rho}. \quad (2.194)$$

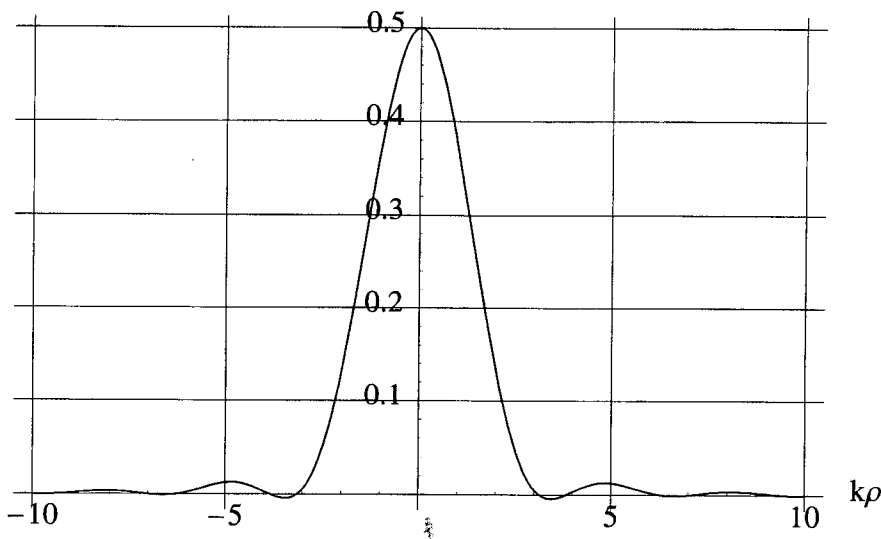
The supersonic pressure follows a sinc function. Following Eq. (2.188) we have for the normal supersonic intensity,

$$I^{(s)}(x, y) = \frac{Q_h^2 \rho_0 c k^2}{8\pi^2} \frac{J_1(k\rho) \sin(k\rho)}{\rho^2}. \quad (2.195)$$

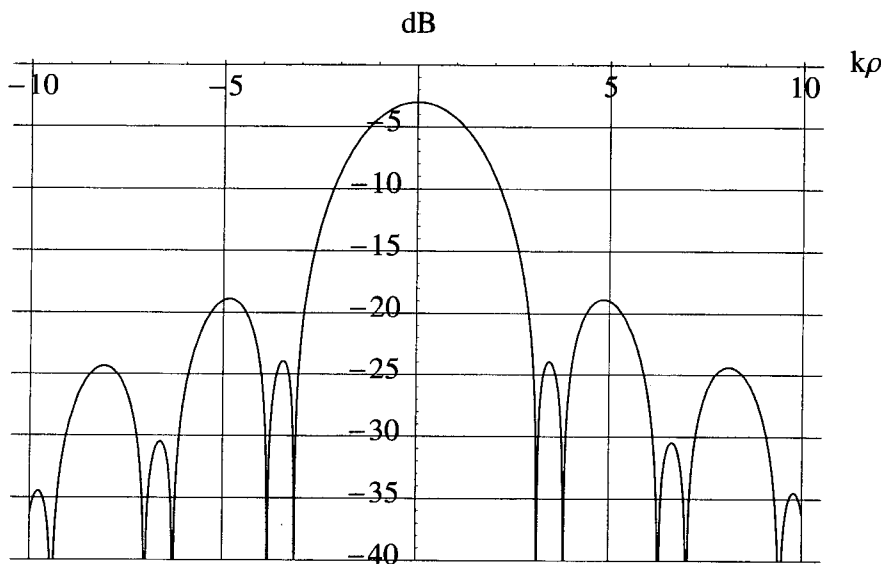
Figure 2.35 is a plot of  $J_1(k\rho) \sin(k\rho)/(k\rho)^2$ , the spatial variation of the supersonic intensity over the plane. Note that there are almost no negative values and the side lobes are small in level. To show the side lobe levels better, Fig. 2.36 is a dB plot. The first major side lobe is 16 dB below the main peak. The small sidelobes between the larger ones are the small regions where the intensity is negative.

Figure 2.36 clarifies the assertion that the supersonic intensity localizes the sources on a vibrating structure, identifying the location of the “hot spots” which radiate to the farfield. Even though  $I^{(s)}$  spreads over the whole plane, it is mainly confined to an area  $\lambda/2$  on either side of the actual location of the point source. The side lobes are an inevitable phenomena of the sharp cutoff at  $k_\rho = k$ , which produces ringing in real space. Certainly, using a taper on this cutoff, a technique which we will study in detail

<sup>20</sup>I. S. Gradshteyn and I. M. Ryzhik (1965). *Tables of integrals, series and products*, Academic Press, New York and London.



**Figure 2.35:** Plot of  $\frac{J_1(k\rho) \sin(k\rho)}{(k\rho)^2}$ . Note the regions of negative intensity are almost nonexistent, and the side lobes are small.



**Figure 2.36:** Logarithmic plot of Fig. 2.35:  $10 \log_{10} \left| \frac{J_1(k\rho) \sin(k\rho)}{(k\rho)^2} \right|$  to show more clearly the side lobe levels.

in Chapter 3, would suppress the side lobe levels even more. We will not, however, pursue this any further here.

To demonstrate that the total power is conserved we calculate

$$\Pi^{(s)} = \frac{Q_h^2 \rho_0 c k^2}{8\pi^2} \int_0^\infty \int_0^{2\pi} \frac{J_1(k\rho) \sin(k\rho)}{\rho^2} \rho d\rho d\phi = \frac{Q_h^2 \rho_0 c k^2}{4\pi},$$

having used the relation<sup>21</sup>

$$\int_0^\infty \frac{J_1(k\rho) \sin(k\rho)}{\rho} d\rho = 1. \quad (2.196)$$

This is identical to Eq. (2.130) and thus power is conserved. We now consider an example for a vibrating plate.

### 2.15.2 Supersonic Intensity of a Mode of a Simply Supported Plate

Consider a normal mode of a simply-supported, baffled square plate of dimensions  $(L_x, L_y)$ . The modes are given by Eq. (2.162) and for this example we choose  $m = 11$ ,  $n = 9$ , and  $L_x = L_y = 2$ . Figure 2.37 shows the mode shape using a density plot, with white and black indicating maximum positive and negative values, respectively. The region of the baffle is shown surrounding the plate. The legend indicates the cor-

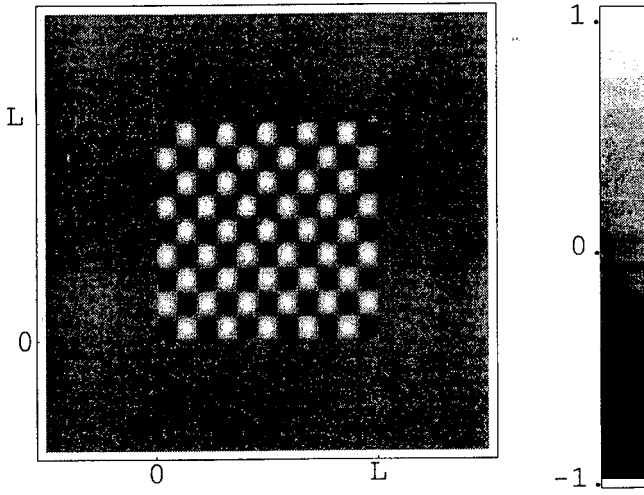


**Figure 2.37:** Mode shape shown in grey scale for a  $m = 11$ ,  $n = 9$  mode of a square plate,  $\Psi_{mn}(x, y) = \sin(11\pi x/L_x) \sin(9\pi y/L_y)$ .  $k = 6$  and  $L = L_x = L_y = 2$ . The baffle is shown surrounding the plate.

responding levels of vibration. We assume that this mode is forced into excitation at a frequency such that  $k = 6$ . The actual eigenfrequency for this mode is irrelevant since we are not considering any of the elastic details and we are interested only in the radiation. However, this mode corresponds to a free wavenumber,  $k_f = 22.3$  (Eq. (2.163)), and  $\gamma = k/k_f = 0.27$  (Eq. (2.180)). Thus the plate is excited below coincidence and according to the radiation classification of Fig. 2.29 a corner mode exists.

The pressure on the plate and baffle is computed using Rayleigh's integral, Eq. (2.61). Fourier transforms of the resulting pressure and specified velocity (mode shape) provide the integrands for Eqs (2.186) and (2.187). These equations are then used to compute the supersonic intensity, using Eq. (2.188), for this mode. The result is shown in

<sup>21</sup>Gradshteyn and Ryzhik, *Tables of integrals, series and products*.

Fig. 2.38. Note that the intensity is positive throughout. One of the beneficial aspects

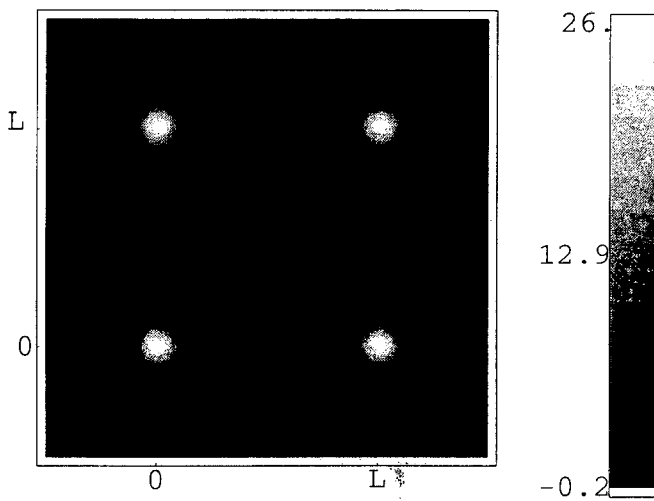


**Figure 2.38:** Supersonic intensity for the normal mode shown in Fig. 2.37. The intensity is only positive, with black near zero level. White indicates maximum level and locates the regions of the plate which radiate to the farfield.

of the supersonic intensity is the removal of the circulating power flow. Furthermore, the largest levels of intensity ( $\text{watts}/\text{m}^2$ ), shown in white, localize the regions on the plate which radiate to the farfield. Note that the sources are the four corner regions of the plate, perfectly consistent with the theory of mode classification presented in Section 2.14.2, in which this mode is classified as a corner mode, depicted in Fig. 2.31.

The power radiated by each identified source is easily obtained by computing the surface integral over the source region, so that if  $S_s$  is the area identified as a source (such as one of the corner regions in Fig. 2.38, then the power radiated from the source is

$$\Pi_s = \iint_{S_s} I^{(s)}(x, y) dx dy.$$

One can divide the plate into radiating regions. The conservation of power, Eq. (2.191), guarantees that the sum of all the powers from all the regions must equal the actual power radiated.

As a point of comparison, Fig. 2.39 is a plot of the actual normal intensity on the surface, which includes all the subsonic waves. We note that it is positive and negative throughout, which arises from the beating of subsonic and supersonic plane waves and indicates circulation of the intensity vector. The actual source regions which radiate to the farfield are not as evident, although the four corners have the largest levels.

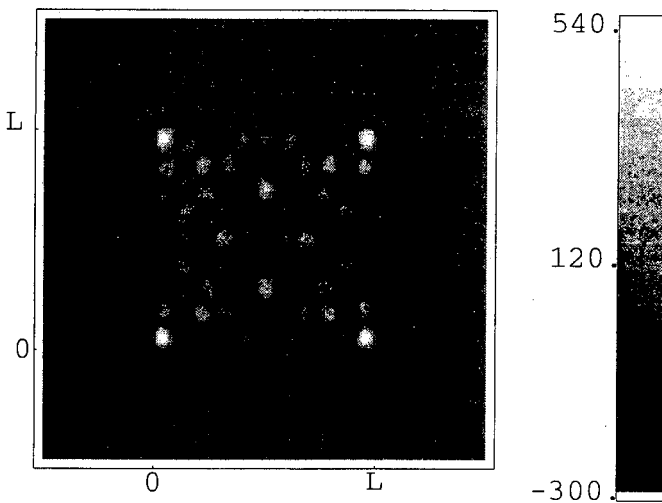


**Figure 2.39:** Normal acoustic intensity for the normal mode shown in Fig. 2.37. The intensity is both positive (white) and negative (black), indicating circulating intensity flow. The source regions are not evident.

## Problems

- 2.1** A baffled ring is vibrating with constant velocity  $w_0$  over its surface. Given that the inner radius is  $a$  and the outer radius is  $b$  find the formula for the farfield directivity pattern,  $D(\theta, \phi)$ .
- 2.2** An infinite plate in the  $z = 0$  plane in an infinite half-space is vibrating with a normal surface velocity,  $\eta(x, y) = \eta_0 \sin(3\pi x/L) \sin(6\pi y/L)$ .
- In terms of  $L$ , what is the distance between the nodal lines in the  $x$  and  $y$  directions.
  - Solve for the pressure field in the half space  $z \geq 0$ .
  - What does the farfield pressure look like if  $k = 8\pi/L$ ?
  - What does the farfield pressure look like if  $k = 3\pi/L$ ?
- 2.3** Consider a baffled, rectangular piston of dimensions  $L_x$  and  $L_y$  in the  $x$  and  $y$  directions, respectively. The velocity on its surface is  $\dot{w}_0$ .
- Write the equation for the  $k$ -space surface velocity,  $\dot{W}(k_x, k_y, 0)$ .
  - Write the equation for the directivity function,  $D(\theta, \phi)$ .
  - Use the Ewald construction along with Fig. 2.8 to sketch out the directivity function for the case  $L_x = 3L_y$  at the normalized frequency  $kL_x/2 = 15$ . Your sketch should make clear the difference in directivity in the  $x$  and  $y$  directions.
- 2.4** Let  $n$  baffled point sources all of equal strength be spaced at intervals of  $d$  along the *negative*  $x$  axis with the first source located at the origin.

- (a) Find the directivity function,  $D(\theta, \phi)$ . Hint: Note that

$$(1 + e^{ia} + e^{2ia} + \cdots + e^{(n-1)ia}) = \frac{1 - e^{nia}}{1 - e^{ia}},$$

and your final form should be written mostly in terms of sin functions.

- (b) Write an equation for the locations of the maxima of the directivity pattern. At what frequency is the first sidelobe maximum in the  $x, y$  plane?
- (c) Keeping the distance between the first and last elements constant ( $nd = L = \text{constant}$ ), take the limit as  $n \rightarrow \infty$  and write the expression for the directivity pattern. This is called a continuous line array.

**2.5** The formula for radiated power was given by Eq. (2.113)

$$\Pi(\omega) = \frac{\rho_0 c k}{8\pi^2} \iint_{S_r} \frac{|\dot{W}(k_x, k_y, 0)|^2}{\sqrt{k^2 - k_x^2 - k_y^2}} dk_x dk_y.$$

Convert this integral to polar coordinates,  $k_x, k_y \rightarrow k_\rho, \psi$  and use the relationship between the farfield and the  $k$ -space velocity to show that

$$\Pi(\omega) = \frac{1}{2\rho_0 c} \iint |rp(r, \theta, \phi)|^2 \sin \theta d\theta d\phi.$$

**2.6** Evaluate the differentiation with respect to  $z$  in

$$\frac{\partial}{\partial z} \left[ \frac{e^{ik|\vec{r} - \vec{r}'|}}{|\vec{r} - \vec{r}'|} \right]$$

where

$$|\vec{r} - \vec{r}'| = \sqrt{(x - x')^2 + (y - y')^2 + (z - z')^2}.$$

What difference do you obtain if you differentiate with respect to  $z'$  instead of  $z$ ?

**2.7** Equation (2.67) presented Rayleigh's second integral formula which provides a means of computing the pressure given the pressure in a different plane. That is

$$p(x, y, z) = -\frac{1}{2\pi} \int_{-\infty}^{\infty} \int_{-\infty}^{\infty} p(x', y', 0) \frac{\partial}{\partial z} \left[ \frac{e^{ik|\vec{r} - \vec{r}'|}}{|\vec{r} - \vec{r}'|} \right] dx' dy'. \quad (2.197)$$

His first formula, Eq. (2.75) provided a means to compute the pressure given the normal velocity. However, he did not present a formula to compute the normal velocity. Using Eq. (2.197) and Euler's equation, derive an integral formula for  $\dot{w}(x, y, z)$ .

**2.8** Given the following formula,

$$-2\pi \frac{\partial p(x, y, z)}{\partial z} = \int_{-\infty}^{\infty} \int_{-\infty}^{\infty} p(x', y', 0) \frac{\partial^2}{\partial z^2} \left[ \frac{e^{ik|\vec{r} - \vec{r}'|}}{|\vec{r} - \vec{r}'|} \right] dx' dy',$$

and use the fact that  $\frac{e^{ik|\vec{r}-\vec{r}'|}}{|\vec{r}-\vec{r}'|}$  satisfies the *homogeneous* wave equation (Eq. (2.13) of the notes) when  $r \neq r'$ , to derive the differential-integral equation given by Bouwkamp:<sup>22</sup>

$$\frac{\partial p(x, y, z)}{\partial z} = \frac{1}{2\pi} \left[ k^2 + \frac{\partial^2}{\partial x^2} + \frac{\partial^2}{\partial y^2} \right] \int_{-\infty}^{\infty} \int_{-\infty}^{\infty} p(x', y', 0) \left[ \frac{e^{ik|\vec{r}-\vec{r}'|}}{|\vec{r}-\vec{r}'|} \right] dx' dy'.$$

- 2.9** The phase gradient method of acoustic intensity measurement was presented in 1968.<sup>23</sup> The formula for the steady-state intensity presented was

$$\vec{I} = \frac{1}{2\rho_0 ck} |p|^2 \vec{\nabla} \Theta_p,$$

where

$$p(x, y, z) = |p| e^{i\Theta_p(x, y, z)}.$$

Derive his formula starting with the definition of intensity

$$\vec{I} = \frac{1}{2} \text{Re}[p \vec{v}^*]$$

using the fact that

$$\vec{\nabla} p(x, y, z) = p(x, y, z) \vec{\nabla} [\log_e(p(x, y, z))].$$

Mechel's formula provides an important fact about the phase of the pressure field. It must increase in the direction of energy flow.

- 2.10** The wavelengths of a plane/evanescent wave in the  $x, y, z$  directions, respectively, are

$$\lambda_x = 1/3, \quad \lambda_y = \infty, \quad \lambda_z = 1/2.$$

- (a) What are the corresponding wavenumbers,  $k_x, k_y, k_z$ , in  $x, y, z$  directions?
  - (b) What are the trace velocities  $c_x, c_y, c_z$ ?
  - (c) Determine the direction of the wave in spherical coordinates.
  - (d) What is the frequency,  $f$ , for this wave in terms of the speed of sound,  $c$ ?
- 2.11** Two plane/evanescent waves traveling in an infinite half-space ( $z \geq 0$ ) are given with  $k_x = \pm 2k$ , and  $k_y = 0$ , that is,

$$p(x, y, 0) = P_0 (e^{i2kx} + e^{-i2kx}) e^{-i\omega t}.$$

Write down the expression for  $p(x, y, z)$ .

- 2.12** Given a baffled point source at  $(x_0, y_0)$ , that is,

$$\dot{w}(x, y, 0) = Q_0 \delta(x - x_0) \delta(y - y_0).$$

Write the expression for the pressure in the  $z = 0$  plane,  $p(x, y, 0)$ .

<sup>22</sup>C. J. Bouwkamp (1954), "Diffraction Theory", Rep. Progr. Phys., **17**, pp. 35–100.

<sup>23</sup>F. P. Mechel (1968). Proceedings of the ICA, Tokyo.

**2.13** Given a point source at the origin with pressure field

$$p(x, y, z) = p_0 e^{ikR} / R,$$

where  $R = \sqrt{x^2 + y^2 + z^2}$ , compute the vector velocity,  $\vec{v}(x, y, z)$  on the  $x$  axis ( $y = z = 0$ ).

**2.14** The normal intensity in the  $z = 0$  plane is given by

$$I_z(x, y, 0) = \frac{\Pi(x/L_x)\Pi(y/L_y)}{x^2y^2},$$

where  $\Pi(x/L_x)$  and  $\Pi(y/L_y)$  are rectangular window functions. Find the total power,  $\Pi(\omega)$  (unfortunately the same symbol as the rectangular window), crossing the  $z = 0$  plane in the  $+z$  direction.

**2.15** Let the pressure in the  $z = 0$  plane be given by

$$p(x, y, 0) = p_0 \delta(x - x_0) \delta(y - y_0).$$

- (a) Compute the angular spectrum,  $P(k_x, k_y, 0)$ .
- (b) Find  $P(k_x, k_y, z)$ , in the infinite, source-free half-space,  $z \geq 0$ ,
- (c) Find the angular spectrum of the normal velocity,  $\dot{W}(k_x, k_y, z)$ .
- (d) Make a rough sketch of  $|\dot{W}(k_x, k_y, z)|$  in terms of  $k$  along the  $k_x$  axis ( $k_y = 0$ ), where  $-\infty < k_x < +\infty$ . Include rough sketches when  $z \rightarrow \infty$  and when  $z \rightarrow 0$ .
- (e) Compute the power,  $\Pi(\omega)$ , radiated into the infinite half-space in terms of  $k$ .

**2.16** Sketch the farfield over a complete hemisphere given the Fourier transform on the right of the function on the left. Note that  $\rho = \sqrt{x^2 + y^2}$  and  $k_\rho = \sqrt{k_x^2 + k_y^2}$  as usual and  $\kappa$  is a constant. Consider two cases: (a) when the acoustic wavenumber  $k = 2\kappa$  and (b)  $k = \kappa/2$ . Considering the fact that the function on the left represents the normal velocity of an infinite membrane, discuss the meaning of the answer obtained for case (b).

**2.17** In the following problem we are going to simulate a nearfield holography measurement of a baffled point source, located at the origin in the  $z = 0$  plane and given by  $\dot{w}(x, y, 0) = Q_0 \delta(x) \delta(y)$ . The simulated pressure measurement is made in the plane  $z = z_h$ . Assume that the “measurement” is perfect, over an infinite aperture with infinitesimally close measurement points. The measured pressure is

$$p(x, y, z_h) = \frac{-iQ_0\rho_0 ck}{2\pi} \frac{e^{ikR}}{R},$$

with  $R = \sqrt{x^2 + y^2 + z_h^2}$ . Following the holographic reconstruction equation, Eq. (3.4),

- (a) determine the Fourier transform of the pressure,  $P(k_x, k_y, z_h)$ ,

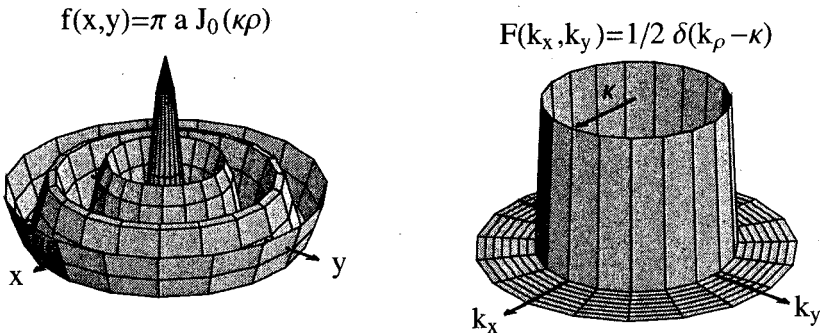


**Figure 2.40:** A Bessel function and its Fourier transform.

- (b) multiply by the inverse velocity propagator,  $G$ , and
- (c) apply a rectangular  $k$ -space window to the “data” given by

$$\Pi(k_x/(2k_c))\Pi(k_y/(2k_c))$$

and do the inverse Fourier transforms to arrive at an algebraic expression for the reconstructed velocity,  $\tilde{w}(x, y, 0)$ . You should be able to do the integrations.

- (d) Discuss the difference between the reconstructed velocity,  $\tilde{w}(x, y, 0)$ , and the actual velocity,  $w(x, y, 0) = Q_0\delta(x)\delta(y)$ .

**2.18** (Challenge problem) Starting with the Rayleigh integral,

$$p(\vec{r}, \omega) = \frac{-i\omega\rho_0}{2\pi} \int_{-\infty}^{\infty} \int_{-\infty}^{\infty} \dot{w}(\vec{r}', \omega) \frac{e^{i\omega|\vec{r}-\vec{r}'|/c}}{|\vec{r}-\vec{r}'|} dx' dy',$$

where  $\vec{r} = (x, y, z)$  and the dependence upon  $\omega$  has been written explicitly, use Fourier transforms and their associated relationships given in Chapter 1 to derive the time-domain version of Rayleigh’s integral given by

$$p(\vec{r}, t) = \frac{\rho_0}{2\pi} \frac{\partial}{\partial t} \int_{-\infty}^{\infty} \int_{-\infty}^{\infty} dx' dy' \int_{-\infty}^{\infty} dt' \dot{w}(x', y', 0, t') \frac{\delta(t - t' - |\vec{r} - \vec{r}'|/c)}{|\vec{r} - \vec{r}'|}.$$

**2.19** Show that Eq. (2.162) satisfies Eq. (2.156) and that Eq. (2.163) results.

**2.20** Using Eq. (2.164), verify that the normal modes given in Eq. (2.162) are orthonormal.

**2.21** Derive the result shown in Eq. (2.177).

**2.22** Derive Eq. (2.168) following the three steps specified in the text.

# Chapter 3

## The Inverse Problem: Planar Nearfield Acoustical Holography

### 3.1 Introduction

Acoustical holography, the predecessor of NAH, appeared in the mid 1960s.<sup>1</sup> Acoustical holography, however, is only an approximation to the inverse problem of reconstructing sound fields. This inverse problem backtracks the pressure field in space and time towards the sources. Only source details greater than the acoustic wavelength can be retrieved in this procedure. Nearfield acoustical holography, which appeared in 1980,<sup>2</sup> provides a rigorous solution, however, to the inversion resulting in an almost unlimited resolution in the reconstruction. When evanescent waves are present (such as plate vibrator sources which contain subsonic waves), an essential requirement for this increased resolution is the measurement of the sound field very close to the sources of interest. This latter fact leads to prefixure of the term “nearfield” to acoustical holography to arrive at the name NAH.

NAH reconstructs not only the pressure but also the three components of the fluid velocity as well as the acoustic intensity vector. The practical implementation of the theory requires the materials presented in the previous chapters. The regularization of the inverse problem is naturally based in  $k$ -space analysis, which we have taken care to present in sufficient detail in Chapter 2 so that the reader will be well positioned to understand NAH.

This chapter deals with planar NAH, the stepping stone to other geometries. Because of its great speed, the implementation of the theory is based on the DFT (discrete Fourier transform) and the FFT (fast Fourier transform).

<sup>1</sup>B. P. Hildebrand and B. B. Brenden (1974). *An Introduction to Acoustical Holography*. Plenum Press, New York.

<sup>2</sup>E. G. Williams and J. D. Maynard (1980), “Holographic Imaging without the wavelength resolution limit,” Phys. Rev. Lett., **45**, pp. 554–557.

## 3.2 Overview of the Theory

In Section 2.9 on the angular spectrum we found that given knowledge of the pressure on a plane we could determine the pressure and vector velocity on any other plane in a source-free medium. In other words, if the acoustic sources are confined to the half space  $z \leq z_s$ , and if the pressure is known on a plane  $z = z_h \geq z_s$  then the pressure on any other plane is given (through the angular spectrum) as

$$P(k_x, k_y, z) = P(k_x, k_y, z_h) e^{ik_z(z-z_h)}, \quad (3.1)$$

as was presented in Eq. (2.54). Similarly, the vector velocity was determined by Eq. (2.59) and, in particular, the normal velocity was (Eq. (2.61))

$$\dot{W}(k_x, k_y, z) = \frac{k_z}{\rho_0 c k} e^{ik_z(z-z_h)} P(k_x, k_y, z_h) = G(k_x, k_y, z - z_h) P(k_x, k_y, z_h), \quad (3.2)$$

where

$$G(k_x, k_y, z - z_h) \equiv \frac{k_z}{\rho_0 c k} e^{ik_z(z-z_h)}. \quad (3.3)$$

$G$  is called the velocity propagator. In these formulas  $z$  and  $z_h$  play critical roles. When  $z \geq z_h$  the solution is a forward problem, as provided by the Rayleigh integrals, and  $G$  is a forward propagator. However, when  $z < z_h$  the solution is an inverse problem. In other words, if the field is measured in the plane  $z = z_h$ , then the solution for the pressure in a plane closer to the sources determines what the pressure must have been there before it reached the measurement plane.  $G$  is then the inverse velocity propagator. This is an inverse problem.

The Rayleigh integrals do not provide an inverse solution. They can only provide the pressure *radiated* from the sources. Nearfield acoustical holography provides a solution to the inverse problem, as we will see below.

Nearfield acoustical holography (NAH) was first proposed by Williams and Maynard in 1980.<sup>3</sup> Its major attraction is its solution to the inverse problem, that is the reconstruction of the surface velocity field on plate radiators from a measurement of the pressure in a parallel plane at a small distance from the plate. Let the plane  $z = z_h$  be the measurement plane, and  $z = z_s$  be the surface of the vibrator. NAH provides the relationship

$$p(x, y, z_h) \Rightarrow \dot{w}(x, y, z_s),$$

where  $z_h \geq z_s$ . From what we have learned about the angular spectrum we can formulate the solution very easily. The mathematics behind NAH is summarized in the single statement:

$$\dot{w}(x, y, z_s) = \mathcal{F}_x^{-1} \mathcal{F}_y^{-1} \left[ \mathcal{F}_x \mathcal{F}_y [p(x, y, z_h)] G(k_x, k_y, z_s - z_h) \right]. \quad (3.4)$$

Using the convolution theorem, Eq. (1.20) on page 4, then the statement is rewritten as

$$\dot{w}(x, y, z_s) = p(x, y, z_h) * * g_v^{-1}(x, y, z_s - z_h) \quad (3.5)$$

---

<sup>3</sup>Williams and Maynard, "Holographic Imaging without the Wavelength Resolution Limit".

where we have defined the inverse velocity propagator,

$$\begin{aligned} g_v^{-1}(x, y, z_s - z_h) &\equiv \mathcal{F}_x^{-1} \mathcal{F}_y^{-1} [G(k_x, k_y, z_s - z_h)] \\ &= \mathcal{F}_x^{-1} \mathcal{F}_y^{-1} \left[ \frac{k_z}{\rho_0 c k} e^{ik_z(z_s - z_h)} \right], \end{aligned} \quad (3.6)$$

consistent with the definition given in Eq. (2.70).

In words, Eq. (3.4) states:

- (1) measure the pressure  $\rightarrow p(x, y, z_h)$ ,
- (2) compute its angular spectrum  $\rightarrow P(k_x, k_y, z_h)$ ,
- (3) multiply by the inverse propagator  $G(k_x, k_y, z_s - z_h) \rightarrow W(k_x, k_y, z_s)$ ,
- (4) compute the inverse transforms  $\rightarrow w(x, y, z_s)$ .

Because NAH solves an inverse problem, the mathematical solution must be approached with some caution to assure that the solution is unique and stable.<sup>4</sup> That is, straightforward implementation of Eq. (3.4) will lead to disaster! How this equation must be modified to avoid disaster is the springboard for the NAH technique.

### 3.3 Presentation of Theory for a One-Dimensional Radiator

To understand all the details for the implementation of NAH for the general planar geometry, we will present the theory assuming that the measured field only depends on  $x$  and  $z$  and is independent of  $y$ . This is called a one-dimensional planar radiator. In no way does this compromise our understanding of the full two-dimensional problem, for we will see that it is trivial to make the extrapolation to this case once we have gained the knowledge from the one-dimensional case.

Given a one-dimensional plate vibrator located in the plane  $z = z_s$ , the measured pressure in the plane  $z = z_h$  where  $z_h \geq z_s$  is of the form

$$p(x, y, z_h) \rightarrow p(x, z_h),$$

that is, the pressure is independent of  $y$ . Given this pressure measurement, we develop the solution for the normal surface velocity in the source plane at  $z = z_s$ . First we obtain the angular spectrum so that we can backpropagate the field to the plate surface at  $z = z_s$ :

$$\mathcal{F}_x \mathcal{F}_y [p(x, z_h)] = 2\pi P(k_x, k_y, z_h) \delta(k_y), \quad (3.7)$$

where the Dirac delta function arises from the transform over  $y$ . Because of the delta function the following occurs in the inverse Fourier transform in  $k_y$  (carrying out the

---

<sup>4</sup>Some precise mathematical details are given in G. C. Sherman (1967). "Integral-transform formulation of Diffraction", J. Opt. Soc. Am. **55**, pp. 1490–1498.

$\mathcal{F}_y^{-1}$  operation in Eq. (3.4)):

$$\begin{aligned} \frac{1}{2\pi} \int_{-\infty}^{\infty} P(k_x, k_y, z_h) G(k_x, k_y, z_s - z_h) 2\pi \delta(k_y) e^{ik_y y} dk_y = \\ = P(k_x, 0, z_h) G(k_x, 0, z_s - z_h). \end{aligned} \quad (3.8)$$

In other words, the one-dimensional vibrator is equivalent to evaluating the angular spectrum and the velocity propagator at  $k_y = 0$ . This is not surprising since this case corresponds to an infinite wavelength in the  $y$  direction. Thus the holographic process given in Eq. (3.4) does not depend on transforms in  $y$  and the reconstruction equation becomes

$$\dot{w}(x, z_s) = \mathcal{F}_x^{-1} [\mathcal{F}_x[p(x, z_h)] G(k_x, 0, z_s - z_h)]. \quad (3.9)$$

Of particular importance in Eq. (3.9) is the inverse velocity propagator  $G$  (from Eq. (3.3)):

$$G(k_x, 0, z_s - z_h) = \frac{k_z}{\rho_0 c k} e^{-ik_z(z_h - z_s)}. \quad (3.10)$$

Here we are presented with our first difficulty, caused by the exponential in this equation. Since  $k_y = 0$  for the one-dimensional problem,  $k_z$  is defined by  $k_z = \sqrt{k^2 - k_x^2}$  within the radiation circle and by  $k_z = i\sqrt{k_x^2 - k^2} = ik'_z$  outside of it. In the latter case  $k_x$  is subsonic and we have seen in Section 2.8 (Eq. (2.49)) that this leads to exponentially decaying sound fields. However, since we are solving the inverse problem, then we are backpropagating the field, a process which reverses the sign of the exponent producing a rising exponential. In this case the exponential in Eq. (3.10) leads to

$$e^{-ik_z(z_h - z_s)} = e^{k'_z(z_h - z_s)},$$

which multiplies the measured pressure angular spectrum  $P(k_x, 0, z_h)$ . As  $k_x$  increases to infinity the inverse propagator  $G$  becomes infinite.

In order for the product  $G(k_x, 0, z_s - z_h)P(k_x, 0, z_h)$  to remain finite we must assume that the angular spectrum of the pressure drops off at a faster rate with  $k_x$  compared with the rising rate of the propagator. This is in fact guaranteed by the angular spectrum relationship for subsonic waves

$$P(k_x, 0, z_h) = P(k_x, 0, z_s) e^{-k'_z(z_h - z_s)}. \quad (3.11)$$

The exponential decay in this equation balances the increase in the inverse propagator, Eq. (3.10), so that the backpropagation of the sound field is well behaved.

For the experimental problem, however,  $p(x, y, z_h)$  is a measured quantity and its angular spectrum is not computed analytically, but through the application of a numerical Fourier transform. As one might imagine, spatial noise in the measurement has a strong likelihood of completely destroying this delicate cancellation process.